ARGESIM Report AR 10

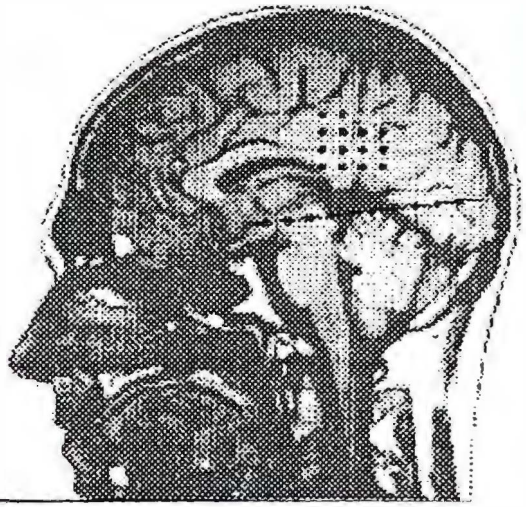

Proceedings

Brain Modelling

TU-BioMed Symposium 1998

Frank Ratty, ed.

ISBN print 978-3-901608-10-0
ISBN ebook 978-3-901608-94-0
DOI 10.11128/arep.10
ARGESIM Publisher

-9

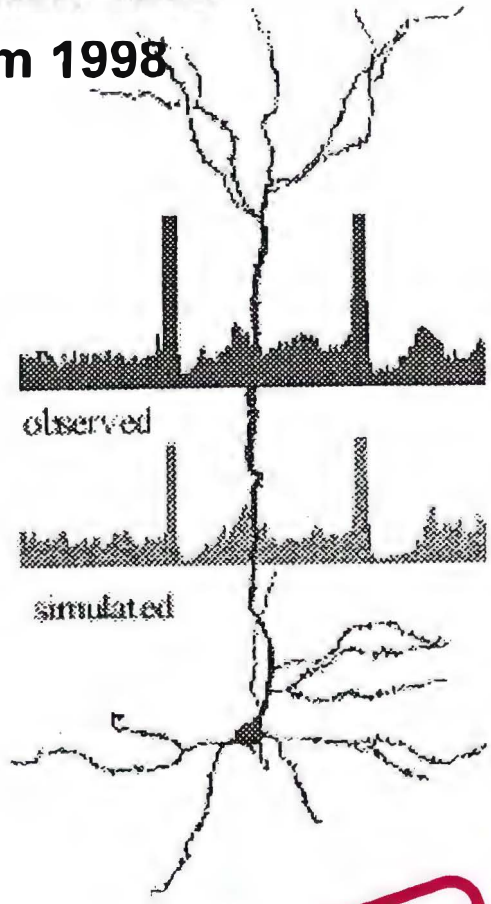

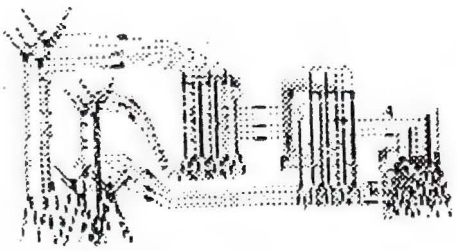

ARGESIM Report

ARGESIM Report

ARGESIM Report

ARGESIM Report AR 10
ISBN print 978-3-901608-10-0, 1998
ISBN ebook 978-3-901608-94-0, 2021
DOI 10.11128/arep.10

ARGESIM Reports
Series Editor: Prof. Dr. F. Breitenecker

ARGE Simulation News (ARGESIM)
c/o Vienna University ofTechnology
Wiedner Hauptstraße. 8-10, A-1040 Vienna,
Austria Tel: +43-1-58801-5386, -5374 Fax:
+43-1-587421 l Email: info@argesim.org
WWW: http://www.argesim.org

TABLE OF CONTENTS

Brain Modelling - today

BRAIN MODELLING - today, this is a broad field between the disciplines. On one hand we are interested to explore the biophysical laws that describe the molecular events - and such questions go down to the level of quantum physics, an example is given by GUSTAV BERNROIDER in his contribution on *Quantum neurodynamics and its relation to cognition and consciousness*. At the next level of scaling the gating mechanisms at the ionic channels are very important for information processing and data distribution. Noise influence will be of great importance in order to detect weak signals and sometimes stochastic resonance is believed to accomplish real wonder - beyond the laws of physics, compare DONATELLA PETRACCHI - *Neural encoding: what stochastic resonance cannot do and what possibly it could do*, or ILLE GEBESHUBER and coworkers' *Stochastic resonance in the inner ear: the effects of endogenious transduction channel noise and stereociliary thermal motions on the human hearing threshold in various frequency bands* where it is demonstrated that nature tries to make profit from everything it can catch even when it is the thermal noise, which - up to now - was assumed to perform the border for sensory detection.

Nonlinear effects dominate the reactions at the level of the single neuron. Computational neuroscience is a new quickly expanding field that uses the powerful computers that are now available to simulate the reactions along the complicated shapes of neural elements. One technique is presented by FRANK RATTAY: *Simulation of neural excitation with compartment models*. This method is very useful to study the influences of membrane compositions on the reactions of a target neuron. We should be aware of the fact that changes of ion channels concerning types and densities are responsible for the individual behavior of functional neural subunits like initial segment, node and internode etc. Worldwide there are rather few investigations to simulate complete neurons or even soma-axon combinations. Examples are given by ALEXANDER STAENKE & Co *Spike Propagation in Aplysia Neurons* and by VINCENT STÜGER & Co *Modeling the electrical excitation of the mammalian auditory nerve*. Furthermore, the compartment model technique (which was already used by the early investigators like HODGKIN & HUXLEY in order to simulate neural signaling) can also be used in related fields - as demonstrated by MARTIN REICHEL & Co in the contribution *Computer simulation of denervated muscle by skin electrodes*. Another technical application that was developed by FRANK RATTAY from compartment modeling is to investigate *The contribution of a single neuron to the EEG signal and an attempt to explain the cochleogram*.

The EEG signal as it reflects the activities of a great number of neurons is rather difficult to interpret. MARIKE ESSL tries to analyze with mathematical tools simulated signals: *Simulation of EEG signals with autoregressive models* and OLIVER FILZ & Co investigate in Properties of Interhemispheric EEG Coherence during Sleep. HERBERT BAUER demonstrates that the EEG is able to show cognitive functions in his contribution on *Slow Potential Topography and Cognitive Anatomy.*

Furthermore, the nonlinear theory is applied to brain dynamics in CLAUDIA MONGINI & Co's contribution on *Non-linear dynamics and biological neuronal ensembles: application of Chaos Theory to analysis and modelling.*

But even the simplest neural nets as for example the touch reflex need a lot of nonlinear mathematics to be simulated. This is demonstrated by RICHARDSON NAVES LEAO and coworkers in *A Flexor and Crossed Extensor Reflexes Model using Neural Networks.* In this contributions artificial neural network techniques are shown to be nowadays a powerful tool in control technique. This means that - in spite of the fact that we currently are far away from a complete understanding of our brain - we use in technical applications methods that are copied from biology. However, the artificial neural nets still have essential shortcomings compared to the biological ones - that is demonstrated by ALICE MLADENKA & Co in *Biological and Artificial Neural Nets: A comparison.*

One fact that is not considered in artificial neural nets is the temporal component. Compartment models as introduced in the beginning are high above the molecular level. Nevertheless up to thousands of nonlinear differential equations that describe the membrane along a single neuron do not allow to simulate the temporal influence even in small nets of biological neurons. A new method to simulate biological neural nets is proposed by PETER SLOWIK & Co in *A novel neurosimulator to predict propagation of information in neuronal systems.* This program takes care on the traveling time of a neural impulse from his point of generation until to the synaptic contacts and with a rather simple method for calculating the traveling times it is possible to simulate the biological way of data processing in small neural nets about thousand times quicker compared to the compartment model approach.

Frank Rattay

Vienna, February 27, 1998

Simulation of Neural Excitation with Compartment Models

Frank Rattay
TU-BioMed Vienna University of Technology
Email: frattay@email.tuwien.ac.at

Introduction

A breakthrough in our understanding of the physics of neural signals which propagate as membrane voltage along the nerve fiber (axon) was achieved by the ingenious work of Hodgkin and Huxley (1952). To explore the complicated gating mechanism of the ion channels a long non-insulated wire was used as stimulating electrode, and thereby every part of the neural membrane had to react in the same way, i.e. propagation of signals was prevented. Refinements of their method as well as the application of patch clamp techniques (Neher and Sakmann, 1976) supply us with models for different neural cell membranes. With such models reliable prediction of membrane voltage V as a function of time is possible for arbitrary stimulating currents (comp. Rattay 1990,1993; Belluzzi and Sacchi 1991, DeSchutter and Bower 1994 or Staenke et al. this volume). The main equation has always the same form: One part of the stimulating current resulting from synaptic inputs or from an inserted electrode is used to load the capacity C of the cell membrane and the other part passes through the ion channels, i.e.

$$I_{stimulus} = C_m \frac{dV}{dt} + I_{ion}$$

and the velocity of voltage change becomes

$$\frac{dV}{dt} = \left[-I_{ion} + I_{stimulus}\right] / C_m \quad (1),$$

where the ion currents I_{ion} are calculated from appropriate membrane models. Usually, the membrane models are formulated for $1cm^2$ of cell membrane and the currents in eqn. (1) become current densities.

A positive stimulating current applied at the inside of an axon or at any other part of a neuron will cause an increase of V according to eqn. (1) if the membrane has been in the resting state before. In order to generate a spike this positive stimulus current has to be strong enough to reach threshold voltage. Threshold voltage causes many of the voltage sensitive sodium channels to open, and by sodium current influx (from the sodium rich extracellular fluid) the voltage increases to an action potential without the need of further stimulating support. A negative stimulating current applied at the inside will cause hyperpolarization (Fig. 1A, B).

Fig. 1. Computed reactions of a simple model neuron stimulated from the inside (upper traces) and from the outside (lower traces). The neuron consists of different subunits (comp. Fig. 2). Stimulation with negative and positive 0.1ms current impulses at the inside of the cell body (A, B) and by an extracellular microelectrode 0.5mm away from the center of the cell body (C, D) as indicated by the tips of the arrows.
Every line shows the membrane voltage of a single compartment as function of time. A: local hyperpolarization, B: an action potential propagates towards the branching terminal region. Extracellular stimulation generates stimulated and hyperpolarized zones within the neuron in both cases C and D. Strongest reaction is within the axon, at a position which is rather far away from the electrode, especially in D.

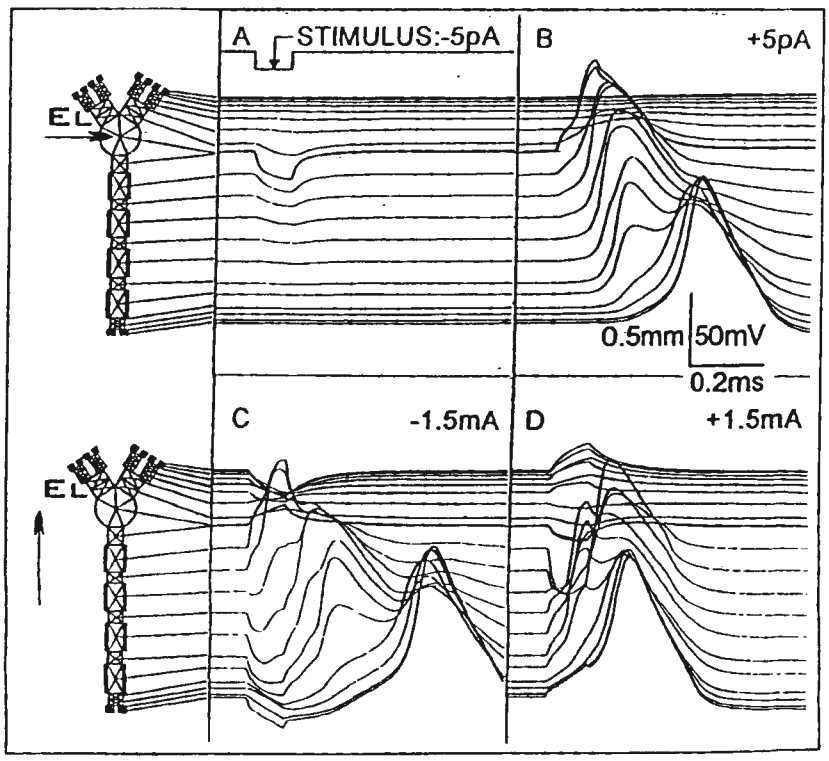

Compartment models

Current injection at the soma causes a situation rather similar to that of the 'space clamp' experiment of Hodgkin and Huxley: When the impulse is applied the strongest reaction is at the soma, but some of the injected current flows along the neuron and thereby the membrane voltages in the neighborhood of the soma is changed. (Fig.1 A, B).

Even a simple model of a neuron should consist of different subunits as shown in Fig. 2. A subunit is sometimes divided into several compartments small enough that the voltages at the inside ($V_{i,n}$) and at the outside ($V_{e,n}$) of the n-th compartment can be represented by a mean value. Every compartment has its individual shape and geometric and electric parameters.

According to Fig. 2 the current to the center point of the n-th compartment consists of a capacitive component, ion currents across the membrane and ohmic currents to the left and right neighbors, i.e. applying Kirchhoff's low results in

$$\frac{d(V_{i,n}-V_{e,n})}{dt}\cdot C_{m,n}+I_{ion,n}+\frac{V_{i,n}-V_{i,n-1}}{R_n/2+R_{n-1}/2}+ +\frac{V_{i,n}-V_{i,n+1}}{R_n/2+R_{n+1}/2}=I_{stimulus,n}$$

The stimulating influence to the neuron may be a synaptic input at the n-th compartment, or a current injection corresponding to $I_{stimulus}$ (not shown in Fig. 2), but for most compartments $I_{stimulus}$=0. With $V=V_i-V_e-V_{rest}$ we obtain the following system of differential equations for calculating the time courses of the reduced membrane voltages V_n: as a reaction of the compartments to the stimulating influence of the extracellular potential V_e:

$$\frac{dV_n}{dt}=\left[-I_{ion,n}+I_{stimulus,n}+\frac{V_{n-1}-V_n}{R_{n-1}/2+R_n/2}+\frac{V_{n+1}-V_n}{R_{n+1}/2+R_n/2}+\ldots +\frac{V_{e,n-1}-V_{e,n}}{R_{n-1}/2+R_n/2}+\frac{V_{e,n+1}-V_{e,n}}{R_{n+1}/2+R_n/2}+\ldots\right]/C_{m,n} \quad (2)$$

The dots in eqn. (2) are written for terms similar to the last one that have to be added in cases with more than two neighbor elements, e.g. at the cell body (soma) or in other branching regions.

Comparing eqn. (2) with (1) it is seen that the task of the stimulating current in every compartment can be performed by three components now: 1) the currents along the inside of the neuron, which are responsible for propagation of neural signals in natural situation (where V_e = 0 is usually assumed), 2) the currents resulting from the extracellular potentials ($V_{e,n-1}$, $V_{e,n}$, $V_{e,n+1}$) and 3) by current injection via synapses or inserted electrodes. According to point 1) - 3) the same compartment model can be used for the following applications, i.e. to simulate

- natural excitation (case 3a)
- excitation by current injection (case 3b)
- propagation of neural signals (case 1)
- artificial excitation or blockade of neural activites by applying electrical fields to the neural tissues (case 2).

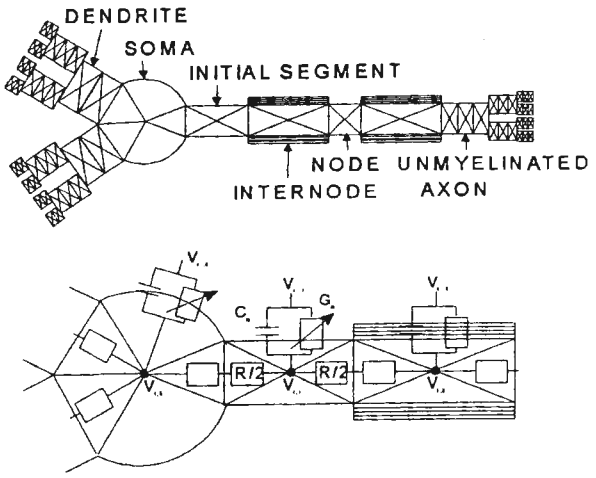

Fig. 2. Diagram of a neuron with subunits and part of an equivalent electrical network. Every subunit has its own membrane composition according to its physiological task. The electric parameters are shown for compartment 1: axoplasmic resistance to the neighbors (R/2 for cylinders), membrane capacity C_m and the membrane conductance G_m, which is only constant in compartments with passive membranes. In general, the ohmic membrane current consists of different types of ion currents that are governed by the rather complicated gating mechanisms of specific voltage sensitive ion channels.

Many published results on neural activities are based on compartment models, but most of them are concerned with axonal reactions only, where adequate membrane models are available. There exists rather few models for the different compositions of membranes of the other functional neural subunits.

Excitation by electrodes or by synaptic inputs - compartment models show the information processing along a neuron

Artificial excitation of a neuron can be done with extracellular electrodes. This technique is used in functional electrical nerve stimulation in order to allow deaf, blind and paralyzed patients to hear, to see and to move their limbs. With electric currents neural signals are also blocked in order to treat movement disorders or to suppress pain.

According to Eqn. 2 the influence of the extracellular potential on compartment n is

$$f_n = \left[\frac{V_{e,n-1}-V_{e,n}}{R_{n-1}/2+R_n/2}+\frac{V_{e,n+1}-V_{e,n}}{R_{n+1}/2+R_n/2}+\ldots\right]/C_{m,n} \quad (3),$$

which is the formulation of the "activating function" for neurons of arbitrary shape. The physical dimension of f_n is [Volt/sec] or [mV/ms], i.e. this form of the generalized activating function represents the velocity of voltage change in every compartment that is activated by the extracellular field. Changes in extracellular voltages, in the geometry and membrane capacity as well as the occurrence of branching elements cause irregularities in the sequence of f_n. In the case of a long straight unmyelinated axon the activating function becomes proportional to the second derivative of the extracellular potential along the axon (Rattay 1990).

The activating function is a powerful tool to obtain a first impression of the influence of an applied electric or magnetic field on a target neuron. Note that the information about stimulated (depolarized) regions, where f>0, and regions with hyperpolarizing effects (f<0) are obtained without any knowledge about the behavior of the voltage sensitive ion channels in the neural membranes.

In the following example the compartment model technique will be applied to the electrically stimulated human auditory nerve (details will be presented in a forthcoming paper).

The bipolar afferent mammalian auditory neuron connects the auditory receptor cell (inner hair cell) with neurons of the cochlear nucleus. In the natural situation a fluctuation (increase) of the receptor cell potential can cause a neurotransmitter release and thereby an action potential in the synaptic end of a fiber of the auditory nerve. This spike is generated in node0, passes the soma and travels along the central part of the axon. The geometry is shown in Fig. 3.

For simplicity we assume quasi-stationary potential distribution (neglecting tissue capacities) in an homogeneous extracellular medium. With this assumption the extracellular potential V_e can be calculated by

$$V_e = \frac{\rho_e I_{electrode}}{4\pi r} \quad (4)$$

where ρ_e is the extracellular resistivity and r the distance to the electrode, With Eqn. (3) the stimulating influence for every compartment can be calculated. The sign of the activating function f changes several times along the neuron (insert of Fig. 3) which means that the neuron consists of several activated and nonactivated (hyperpolarized) regions. Evaluation of the compartment model shows what is already predicted by the activating function: rather small changes in stimulus amplitude can change the points of artificial spike generation (Fig. 4). Fig. 5A shows the 'natural' spike generation by current entering the postsynaptic membrane of the first compartment which is simulated by current injection in node0.

node	Ve[mV]	f[V/s]
N0	445	607
N1	452	-3890
N2	339	2860
N3	300	61
N4	305	-421
N5	275	-2160
SOMA	175	9
N6	129	674

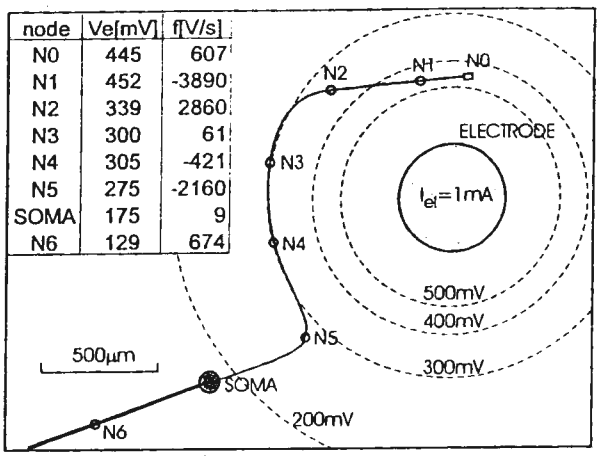

Fig. 3. Position of the human primary auditory nerve relative to a stimulating ring electrode which is inserted into a human cochlea. The mass electrode is assumed to be some mm away, the inhomogeneities in the conductive medium are neglected and therefore isopotential lines become circles. The inserted table shows the 'jumping' values of the activating function f when computed with one compartment per internode. Note the low value of f at node 3 caused by the nerve being close to an isopotential and that f_{soma} is still essentially lower, although V_e changes extensively. This low excitability is predicted by Eqn. 3 as a consequence of the high capacity of the soma membrane.

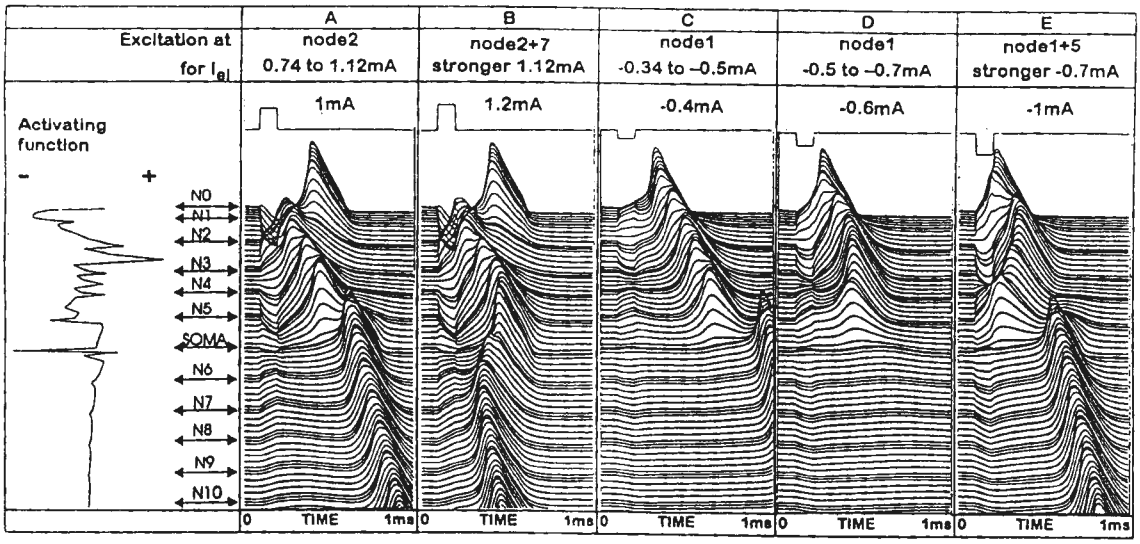

Fig. 4. Spike generation in a primary human auditory neuron by 100μs pulses. According to the activating function (left) the neuron is most excitable at node2 for positive stimuli; the maximum of f is within the passive membrane of the third internode. For negative electrode currents f predicts stimulating influence at node1, at node5 and at the unmyelinated part in front of the soma. Firing behavior changes when signal strength is varied. Every line in (A-E) shows membrane voltage for every compartment as function of time. Soma voltage appears as a single dark line in the center because of similar signal shape of soma and the two neighbored compartments with a center distance of 12.5μm to soma; reaction at nodes are center of triple lines. Note the delay in the axonal part when a 'dendritic' action potential passes the soma region (A,C,E). The rather small hyperpolarizing influence in the last dendritic internode hinders spike propagation into the axonal process (D).

Another application in functional electrical nerve stimulation is the blockade of neural activities by one side (antidromic) firing (Fig. 5C,D)

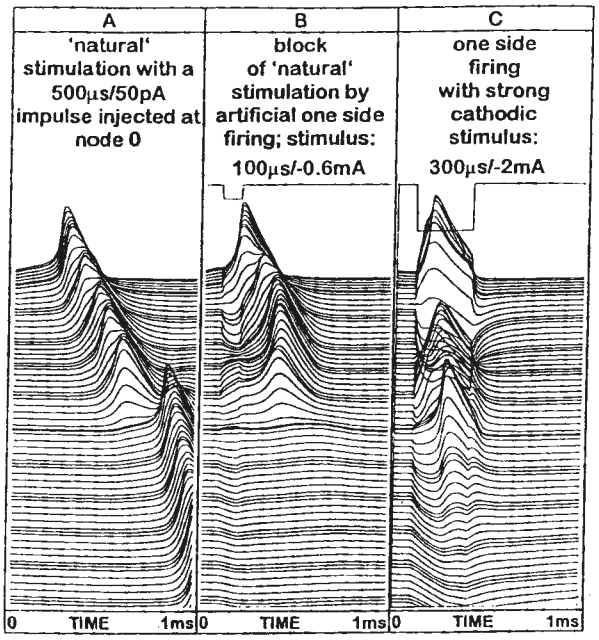

Fig. 5. Blockade of neural impulses by cathodic currents. (A) Simulation of synaptic excitation of neuron3. (B) Applying synaptic current and the block current as shown in Fig. 4D hinder excitation of the soma region. (C) A long strong cathodic pulse produces hyperpolarization of the axon, the soma becomes excited but not node6.

References

Belluzzi O. and O. Sacchi. 1991. A five conductance model of the action potential in the rat sympathetic neurone. Progr. Biophys. molec. Biol. **55**, 1-30

DeSchutter E. and J.M. Bower. 1994. An active membrane model of the cerebellar Purkinje cell: I. Simulation of current clamps in slice. J. Neurophysiol. **71**, 375-400

Hodgkin A.L. and A.F. Huxley. 1952. A quantitative description of membrane current and its application to conduction and excitation in nerve. J. Physiol. **117**, 500-544

Neher E. and B. Sakmann. 1976. Single-channel currents recorded from denervated frog muscle fibres. Nature **269**, 799-802

Rattay F. 1990. *Electrical Nerve Stimulation: Theory, Experiments and Applications.* Springer. Wien - New York

Rattay F. 1993. Simulation of artificial neural reactions produced with electric fields. Simulation Practice and Theory **1**,137-152

Staenke A., F. Rattay, H. Markum, M. Zartl and J. Hoyer 1998. Spike Propagation in Aplysia Neurons (this volume)

The contribution of a single neuron to the EEG signal - and an attempt to explain the cochleogram

Frank Rattay
TU-BioMed Vienna University of Technology
Email: frattay@email.tuwien.ac.at

Introduction

Although the electroencephalogram (EEG) was discovered more than a century ago and in spite of the fact that it is an important diagnostic tool, much remains to be clarified about the nature and the origin of the EEG. In order to understand the EEG signal as a result of collective effects within a neural network it seems important to investigate the contributions of the subunits of a single active neuron.

This article presents a method for estimating the potential distribution around a neuron, generated by its membrane currents. A two step routine is proposed to study the contribution of a single neuron to the EEG under quasi-stationary assumptions: At first the target neuron is represented by a chain of compartments, and in every compartment the total current across the neural membrane is calculated as a function of time. In the second step these currents are assumed to be sinks or sources at the center points of the corresponding compartments and the resulting potential distribution around the active neuron is calculated by superposition.

Current influx and outflux along a neuron

The membrane voltages changes essentially along an active neuron: region 1 may be excited while region 2 is at this moment not influenced by the propagating action potential and it is in the resting state. Therefore every compartment has a size that is small enough to be represented by a single electric circuit*).

The currents across the neural membrane have an essential influence on the electric field in the surrounding of the neuron. High current densities occur at the nodes of Ranvier, they are smaller in unmyelinated axons or at the soma membrane, rather negligible are the currents across the internodes. The current flow at the n-th compartment of the neuron can be calculated from*)

$$\frac{dV_n}{dt}=\left[-I_{ion,n}+I_{stimulus,n}+\frac{V_{n-1}-V_n}{R_{n-1}/2+R_n/2}+\frac{V_{n+1}-V_n}{R_{n+1}/2+R_n/2}+\ldots+\frac{V_{e,n-1}-V_{e,n}}{R_{n-1}/2+R_n/2}+\frac{V_{e,n+1}-V_{e,n}}{R_{n+1}/2+R_n/2}+\ldots\right]/C_{m,n} \quad (1)$$

where V_n denotes membrane voltage, $R/2$ is the resistance from the center to the border of the n-th compartment and $C_{m,n}$ is the membrane capacity (comp. Fig. 2 of Rattay 1998). Note that ion channel compositions changes essentially between neural subunits and it is of high importance to use in every compartment an adequate membrane model.

In the following example an action potential of a mammalian axon is travelling from the myelinated part into a non-myelinated (distal) region. The simulated axon consists of 12 nodes of Ranvier compartments calculated according to the CRSS model (Table 1) and 18 nonmyelinated segments with the same 6µm diameter (a 'warmed' HH model, with $k=12$ and doubled channel density, i.e. g_{Na}, g_K and g_L of the values in Table 1 are doubled). In the first segment a 0.1ms injected current impulse generates a propagating spike that is - with some difficulties - able to propagate into the unmyelinated terminal (Fig. 1).

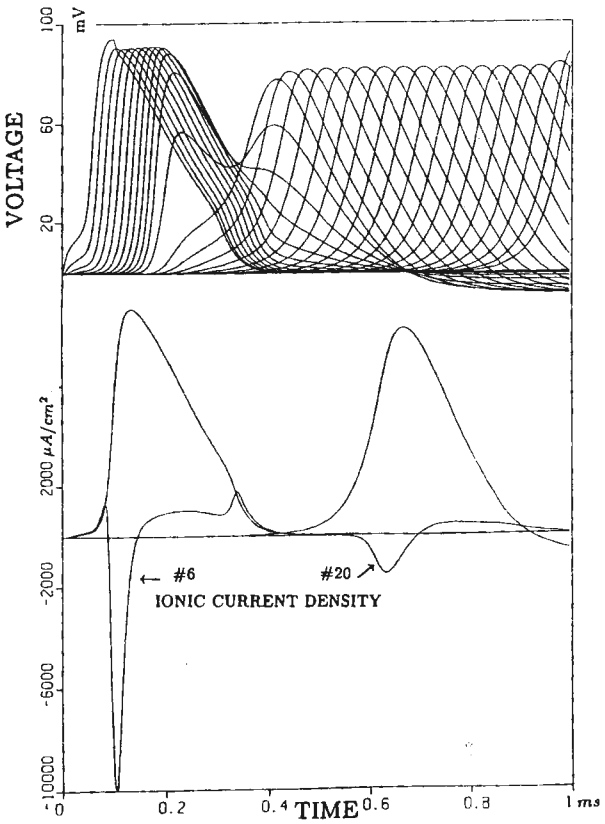

Fig. 1. Membrane voltages in a 30 compartment axon (top). The bottom traces show a copy of the action potentials of compartment #6 (node) and at #20 (unmyelianted axon) as well as the ion current densities. After 0.45ms membrane voltage and current are close to the resting values whereas compartment 20 starts to react at this time.

*) An introduction to the compartment model technique is found in the companion paper of this volume (Rattay 1998).

Note that the current densities at the nodes are about 10 times higher compared to that of the unmyelinated terminal (Fig. 1, bottom); but the current per unit length of the terminal is essentially higher because the nodal membrane segments are very short compared to the internodes (comp. e.g. Rattay 1995).

Significant contributions of current flow can be expected by collective effects in axons with a high degree of branching when a single neural impulse from the initial segment generates up to thousands of action potentials which arrive within a short time at the synaptic endings of the axonal tree. This effect is demonstrated in principle by the next 108 compartment model neuron which consists of a single dendrite (10 compartments), soma, initial segment, myelinated axon with 6 nodes and 7 internodes. The neuron is stimulated by a 0.05mA/10µs current pulse injected at the soma. On its way to one of the 16 end-compartments of the terminal region the generated action potential passes 30 compartments and four points of bifurcation. Propagation is delayed at the transition from the myelinated to the unmyelinated part of the axon (the same effect is seen in Fig. 1) and at every bifurcation (Fig. 2).

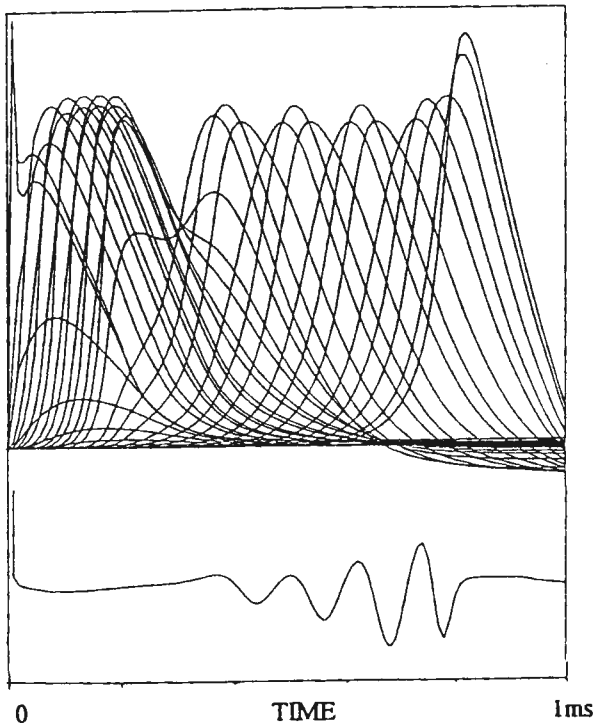

Fig. 2. Membrane voltages as functions of time. Because of symmetry in the branches there are only 40 different curves. The two high spikes (in the soma and in the initial segment) at the beginning result from the injected current, leading to a propagating action potential in the axon and an increase of voltage in the dendrite. The changes in propagation velocity are caused by the bifurcations of the axon and lead to oscillations in the extracellular potential.
The lower curve shows the extracellular potential calculated at 1mm above the soma.

Now we assume an infinite homogeneous extracellular medium with a current I from a single point source. The potential V_e at a distance r becomes

$$V_e = \frac{\rho_e I}{4\pi r} \quad (2)$$

where ρ_e is the extracellular resistivity. With Eqn. 1 we calculate in a first step the time evolution of the membrane currents for every compartment

$$I_n = I_{ion,n} + C_{m,n} \cdot \frac{dV_n}{dt} \quad (3)$$

The membrane currents are shown along the neuron in Fig. 3. After calculating these membrane currents every center point of a compartment is considered as a current source and the sum of their contributions describes the influence of the single neuron activity at a point of interest:

$$V_e(t) = \sum_n \frac{\rho_e I_n(t)}{4\pi r_n} \quad (4)$$

The resulting EEG contribution of the 108 compartment model neuron for an electrode positioned 1 mm above the soma is shown at the bottom of Fig. 2. An analysis of the computer simulation of this simple model neuron demonstrates that

1. the EEG contribution from the myelinated axon is rather small, compared to that of the soma,
2. the branching parts of the terminal can cause velocity reduction
3. the influence of some positive membrane currents can be annulled by negative currents from other regions of the same neuron.
4. collective effects (in the branching terminal) can be essentially stronger than from compartments close to the electrode.

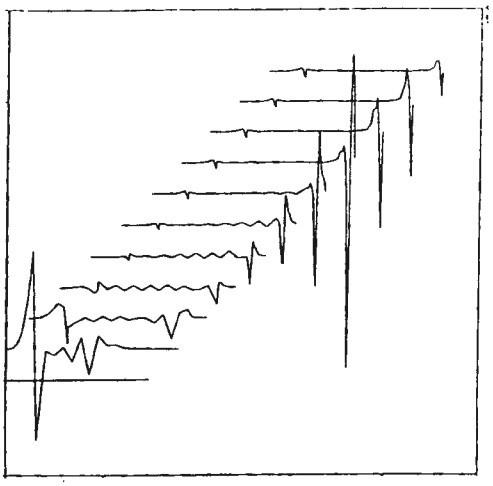

Fig. 3. Snapshots of membrane currents along a neuron in ten time steps. Note the strong signal at the beginning (line2, t=0.1ms) caused by the soma and initial segment and the even stronger currents at the terminal end (line 8, t=0.7ms) caused by the neural impulses when they reach the 16 terminal segments. The zigzag in lines 2-7 results from the different behavior of node and internode in the myelinated axon.

The cochleogram

The electrically evoked activities in the human auditory nerve can be measured with some of the electrodes of a modern cochlea implant. In the same way as for stimulation the measurement electrodes are positioned rather close to the neurons The neurons of the auditory nerve are bipolar and both processes are myelinated (comp. Fig. 3 of Rattay 1998 for the shape of the nerve relative to the electrode).

When stimulated naturally there is a time delay of about 300µs when the action potential crosses the soma region. This effect is similar to that observed in Fig. 1 when the low energy consuming myelinated fiber has to drive the spike into the energy vasting unmyelinated part (delay of spike). In case of human auditory nerves the energy of the spike of the periphery axon has to increase the membrane voltage of the relative large soma region which again causes a delay (comp. Fig. 5A of Rattay 1998 and Stüger et al. 1998). Such disturbances in propagation will also occur when the neurons are stimulated electrically (comp. Fig. 4 of Rattay 1998 and Stüger et al. 1998) and this may be the reason for the double peak in the cochleogram (Fig. 4). However such double peaks occur only in part of the measurements, an effect that may be related with the point of stimulus generation and perhaps in a greater number of degenered peripheral axons in patients that show no double peak responses.

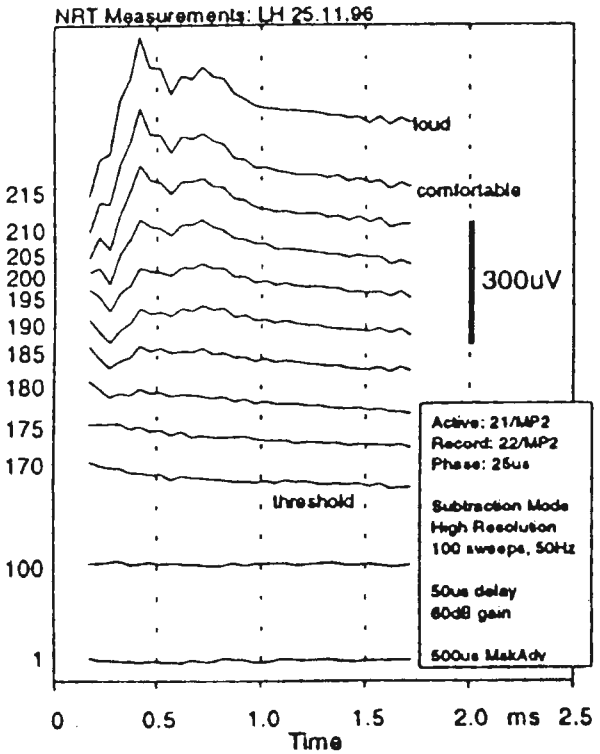

Fig. 4. Neural response telemetry from an human cochlear nerve that is electrically stimulated with increasing intensities. Note the double peaked signal. Reproduced from Dillier et al. 1997.

With the technique as described above we have calculated the voltage fluctuations resulting from the spiking of a single neuron under the simplified assumption of an infinite homogeneous extracellular medium (Fig. 5).

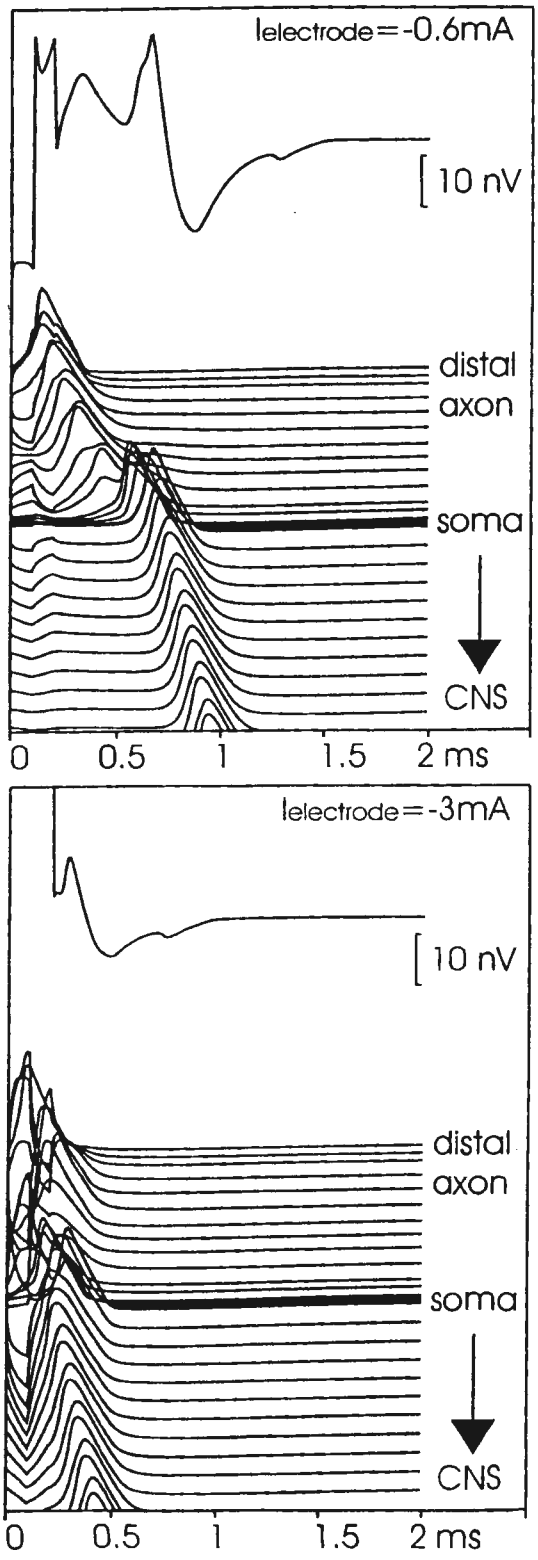

Fig. 5 Simulated nerve reactions for weak and strong biphasic stimuli. Upper traces: extracellular voltages at the electrode, lower traces membrane voltages along the neuron as functions of time. Note the double peak in one case only.

References

N. Dillier, W.K. Lai, M. Wyttenbach, H. Jakits, T. Spillman, T. Linder and U. Frisch 1997. First experiences with neural response telemetry (NRT) Report ENT Department University Hospital Zürich

F. Rattay 1990. Electrical Nerve Stimulation. Springer. Wien - New York

F. Rattay 1995. Propagation and distribution of neural signals: a modeling study of axonal transport. Physics of the Alive. 3, 60-67

F. Rattay 1998. Simulation of neural excitation with compartment models (this volume)

V. Stüger, F. Rattay and P. Lutter 1998. Modeling the electrical excitation of the mammalian auditory nerve (this volume)

HODGKIN-HUXLEY MODEL

$$\dot{V} = [-g_{Na}m^3h(V - V_{Na}) - g_K n^4(V - V_K) - g_L(V - V_L) + i_{st}]/c \quad \text{(HH-1)}$$

$$\dot{m} = [-(\alpha_m + \beta_m) \cdot m + \alpha_m] \cdot k \quad \text{(HH-2)}$$

$$\dot{n} = [-(\alpha_n + \beta_n) \cdot n + \alpha_n] \cdot k \quad \text{(HH-3)}$$

$$\dot{h} = [-(\alpha_h + \beta_h) \cdot h + \alpha_h] \cdot k \quad \text{(HH-4)}$$

with the coefficient k for temperature T (in ^oC)

$$k = 3^{0.1T-0.63} \quad \text{(HH-5)}$$

and

$$\alpha_m = (2.5 - 0.1V)/(exp(2.5 - 0.1V) - 1)$$

$$\beta_m = 4 \cdot exp(-V/18)$$

$$\alpha_n = (1 - 0.1V)/(10.(exp(1 - 0.1V) - 1)$$

$$\beta_n = 0.125 \cdot exp(-V/80)$$

$$\alpha_h = 0.07 \cdot exp(-V/20)$$

$$\beta_h = 1/(exp(3 - 0.1V) + 1)$$

$$V_{rest} = -70[mV]$$

$$V_{Na} = 115[mV], V_K = -12[mV], V_L = 10.6[mV]$$

$$g_{Na} = 120[k\Omega^{-1}cm^{-2}], g_K = 36[k\Omega^{-1}cm^{-2}]$$

$$g_L = 0.3[k\Omega^{-1}cm^{-2}], c = 1[\mu F/cm^2]$$

$$m(0) = 0.05, n(0) = 0.32, h(0) = 0.6$$

CRRSS MODEL

SWEENEY *et al.* (1987) transformed the original data of CHIU, RITCHIE, ROGERT & STAGG (1979) from experimental temperature $T = 14^oC$ to $T = 37^oC$. The following equations are called after the investigators the CRRSS model.

$$\dot{V} = [-g_{Na}m^2h(V - V_{Na}) - g_L(V - V_L) + i_{st}]/c \quad \text{(CRRSS-1)}$$

$$\dot{m} = -(\alpha_m + \beta_m) \cdot m + \alpha_m \quad \text{(CRRSS-2)}$$

$$\dot{h} = -(\alpha_h + \beta_h) \cdot h + \alpha_h \quad \text{(CRRSS-3)}$$

with

$$\alpha_m = (97 + 0.363V)/(exp((31 - V)/5.3) + 1)$$

$$\beta_m = \alpha_m/(exp((V - 23.8)/4.17))$$

$$\alpha_h = \beta_h/(exp((V - 5.5)/5))$$

$$\beta_h = 15.6/(1 + exp((24 - V)/10))$$

$$V_{rest} = -80[mV]$$

$$V_{Na} = 115[mV], V_L = 0.01[mV]$$

$$g_{Na} = 1445[k\Omega^{-1}cm^{-2}], g_L = 128[k\Omega^{-1}cm^{-2}]$$

$$c = 2.5[\mu F/cm^2]$$

$$m(0) = 0.003, h(0) = 0.75$$

Table 1. *Comparison of equations for membrane dynamics of unmyelinated and myelinated axons. V denotes the reduced membrane voltage in mV ($V = V_{membrane} - V_{rest}$); V_{Na}, V_K, V_L voltages across the membrane, caused by different (sodium, potassium, unspecific) ionic concentrations inside and outside the axon; g_{Na}, g_K, g_L maximum conductance of sodium, potassium and leakage per cm^2 of membrane; m, n, h probabilities for ionic membrane gating processes; α, β opening and closing rates for ion channels; c the capacity of membrane per cm^2; $m(0)$, $n(0)$, $h(0)$ values at the resting condtion where $V(0)=0$; i_{st} stimulus current.*
Note the high conductances and the missed potassium currents in the myelinated mammalian node as described by the CRRSS model.

Properties of Interhemispheric EEG Coherence during Sleep

O. Filz[1], P. Rappelsberger[2], J. Zeitlhofer[3], P. Anderer[4]

[1] Institute of Information Processing, Austrian Academy of Sciences
[2] Institute of Neurophysiology, University of Vienna
[3] Department of Neurology, University Hospital of Vienna
[4] Department of Psychiatry, University Hospital of Vienna

Summary

In this study, coherence analysis was applied to all-night EEG sleep recordings of 10 healthy volunteers in order to find criteria for an automatic classification of sleep stages. Spectral estimates were computed for 30 sec sleep stages obtained by visual scoring. Interhemispheric coherence between parasagittal leads (F3-F4, C3-C4, P3-P4, O1-O2) showed high dependence on sleep stages. The comparison of stages S1-W and REM-W showed similar results: in frequency bands Delta2 and Theta1 higher coherence was found during REM and during S1 compared with W in frontal, central and parietal regions. In Alpha and Sigma bands coherence was higher during W, most pronounced frontally and occipitally. S1-REM comparison showed higher coherence during REM, most dominantly in the central region. S2-S1 comparison revealed higher coherence during S2 in Delta1 with decreasing difference from frontal to occipital. In Alpha and Sigma bands coherence was higher during S1 frontally but it was higher during S2 parietally and occipitally.

Key words: sleep EEG, coherence, sleep stages

Introduction

This study deals with the contribution of coherence parameters for distinguishing sleep stages defined by the Rechtschaffen and Kales criteria (1968). Coherence is a spectral parameter that measures the correlation of frequency components of EEG signals derived from different locations on the scalp and may be interpreted as a measure for functional coupling or synchronisation of brain areas.

The criteria by Rechtschaffen and Kales were established to describe the sleep architecture of healthy subjects by visual inspection of 20 or 30 sec epochs. They define 7 discrete stages: Wake, REM, sleep stages 1, 2, 3, 4 and movement time. Rechtschaffen and Kales didn't introduce any topographic information of the EEG. The minimal configuration of a polygraphic recording is one EEG channel (either C3 or C4 referenced to the contralateral ear-lobe), two channels for vertical and horizontal eye movements and one channel for mental or submental EMG.

Nowadays we find a large number of studies dealing with multi-channel sleep EEG. For going beyond Rechtschaffen & Kales criteria, the examination of the micro-structure of sleep is of most interest. There are numerous results about spatial and temporal distribution of EEG parameters during sleep but only a few studies examin the cooperation of cortical areas using coherence or correlation analyses (e.g. Dumermuth et al. 1983; Nielsen et al. 1993; Corsi-Cabrera et al., 1996). Many of them can be hardly compared due to different recording and evaluation criteria but still they demonstrate that different brain states during sleep differ in EEG spectral parameters if coherence is considered. Therefor automatic sleep staging based exclusively on EEG spectral parameters appears promising. The visual scoring of polygraphic sleep recordings inheres the problem of subjective interpretation of rules. Coherence estimates may improve automatic classification and thus lead to a more objective assessment of sleep stages. At the same time they may provide additional information about the functional state of the brain.

Material and Methods

The study is based on whole-night sleep recordings of 10 healthy volunteers (7 females, 3 males, aged 20 to 35 years). EEG was recorded with 18 EEG electrodes according to the international 10/20 system, Fp2 was omitted, referenced to the average of both mastoid electrode signals. Band-pass settings were 0.5 to 30 Hz. EEG, 2 EOG channels and submental EMG were continuously written on paper. The whole-night sleep recording was divided into 10 minute periods: 7 minutes EEG and EOG were digitised continuously (sampling rate 102.4/s) and 3 minutes were needed for data storage on optical disc. The paper-records were visually scored according to Rechtschaffen and Kales (1968) criteria by 2 experienced electroencephalo-graphers. Time window was 30 sec.

Power spectra and cross-power spectra for the interhemispheric pairs F3-F4, C3-C4, P3-P4 and O1-O2 were computed using FFT and non-overlapping 2.5 sec epochs (256 samples) thus obtaining a frequency resolution of 0.4 Hz. Averaging in the time and the frequency domain yielded spectral parameters for the 30 sec epochs of the visual scoring in the frequency bands: Delta1 (0.4-2.0 Hz), Delta2 (2.4-3.6 Hz), Delta (0.4-3.6 Hz), Theta1 (4.0-5.6 Hz), Theta2 (6.0-7.6 Hz), Theta (4.0-7.6 Hz), Alpha (8.0-12.8 Hz) and Sigma (11.6-15.2 Hz). The final step was computation of coherence, the normalised cross-power spectrum.

Distribution of coherence was presented graphically for each sleep stage and each frequency band. In order to get quantitative measures of the distributions mean, median and lower and upper quartiles were estimated.

For a pairwise comparison of sleep stages, differences between the means and between the medians of corresponding frequency distributions were computed. In group studies this has the advantage that the results are independent of absolute coherence values which may vary considerably between subjects.

Only those results were considered significant when in at least 9 of the 10 subjects the same trend was observed, i.e. increase or decrease of coherence between stages. This corresponds to an error probability of $2\alpha \leq 0.05$ (sign test). The increase or decrease was considered weakly significant when it appeared in 8 of the ten subjects which corresponds to $2\alpha \leq 0.10$.

Results

The comparison of stage 1 (**S1**) and wake (**W**) shows significantly higher coherence during S1 frontally and centrally in the Delta2 band. There is also a trend of higher coherence during S1 in the Theta1 band frontally, centrally and parietally. In contrast, significant lower coherence occurred during S1 than during wake in the Alpha band frontally. Weakly significant lower coherence was also observed frontally and centrally in the Sigma band and occipitally in the Alpha-and Sigma band.

Coherence differences between **S2** and **S1** demonstrate a clear trend to higher coherence during S2. The only exception is S1 coherence in F3-F4 which is increasingly higher from the Theta1 to Sigma band. In the Delta1 band the difference between S2 and S1 is as high as 0.22 frontally and 0.15 centrally. Clearly higher coherence is also observed in the Sigma band parietally and occipitally. These results demonstrate that for differentiating sleep stages S2 and S1 interhemispheric coherences of Delta1 and Sigma bands seem to be most important.

Comparing stages **S3/4** and **S2** rather low differences not exceeding 0.05 were found. Most significant differences occurred in the Delta2, Theta1 and Theta2 bands frontally and the Delta1, Delta2 and Theta1 bands centrally, with higher S2 coherence. Contrary, weakly higher Alpha coherence during S3/4 was observed centrally and parietally. Summarising, the most significant differences between interhemispheric coherence during S3/4 and S2 were found in the frontal and the central regions, almost no differences appeared parietally and occipitally.

S1-REM comparison shows generally higher coherence during REM. Frequency bands mainly concerned are Delta2 to Alpha centrally with Theta2 and Alpha more pronounced and Delta2 parietally and occipitally.

The comparison between **REM** and **W** shows higher coherence during REM in the lower frequency bands Delta1 to Theta2, whereas coherence during wake was higher in the upper frequency bands Alpha and Sigma. Concerning location, the most essential results relate to frequency bands Delta2 and Theta1 from frontal to parietal and Alpha and Sigma frontally and occipitally.

Table I summarises the results of group analysis. We want to emphasize the differences between W, S1 and REM since these stages are usually difficult to distinguish.

Discussion

Scalp recorded EEG coherence turned out to be an essential large scale measure of functional relationships between pairs of neocortical regions. These measures are often closely related to cognitive or behavioural processes (e.g. Weiss and Rappelsberger, 1996; Rescher and Rappelsberger, 1996), but also to states of vigilance and sleep (e.g. Guevara et al., 1995).
Mathematically, coherence is defined as the squared normalised cross-power spectrum and may be interpre-ted as correlation coefficient in the frequency domain, i.e. correlation coefficient per frequency or frequency band. Coherence values can run from 0 to 1. Coherence 1 means that the corresponding frequency compo-nents of two EEG signals are identical and only amplitude differences and a constant time relation (phase delay) may exist. In case of coherence 0 the corresponding frequency components of both signals are not correlated.
The examination of the results of all ten subjects of the study showed considerable consistence concerning the global trends and correlation but also considerable differences concerning the absolute height of coherence values.
The problem inherent in almost all sleep analyses is the under-representation of some stages in the data, usually W and S1. This means that the results obtained for those stages are less reliable since they are based on a much lower number of epochs than e.g. the results for stages S2, S3/4 and REM. Nevertheless, the findings of group analysis are distinct and plausible.
In the EEG, stage S1 compared with W is characterised by an increase of the appearance of slow waves and a decrease of Alpha activity. In the interhemispheric coherence results this seems to be reflected by an increase in Delta2 and Theta1, however, predominantly only frontally and centrally. In the Alpha band coherence decreased most pronounced frontally and to a lesser degree occipitally. Coherence decrease in the Sigma band is closely related to the results in the Alpha band. This may be caused by our band definitions since there is a great overlap between both bands.
In stage S2 the characteristic EEG features are K-complexes and Sigma spindles. K-complexes have high portions of slow frequency components. This may result in the increase of Delta1 interhemispheric coherence when comparing S2 with S1. This increase is extremely pronounced frontally (0.22) and centrally (0.15). Regarding Sigma band and Alpha band the opposite interhemispheric coherence behaviour frontally on the one hand and centrally till occipitally on the other hand is striking. This may be caused by different properties of frontal and parietal frequency components represented by spindles (Trenker and Rappelsberger, 1996; Zeitlhofer et al. 1996; Broughton and Hasan, 1995). Coherence increase between both hemispheres (0.15 between P3-P4) may probably be due to highly coherent parieto-occipital spindle activities, i.e. closely linked cortical generators in both hemispheres. In contrast, frontal spindles seem to be generated by a different mechanism with dissociating frontal cortical areas caused by subcortical-cortical pathways leading to coherence decrease (-0.16 between F3-F4).
Only little coherence differences were found comparing S3/4 and S2. Most coherence decreases appeared frontally and centrally in the low frequency bands. This is rather surprising since enhanced slow wave activity during S3/4 was expected to lead also to higher coherence.
Coherence differences between stages REM and W were similar to those between S1 and W but more pronounced: higher coherence during REM in Delta2 and Theta1 frontally and centrally, lower coherence in Alpha and Sigma frontally and occipitally. The results give the impression that both Delta2 and Theta1 on the one hand and the very low Delta1 band on the other hand relate to different functional properties. Delta1 seems to be a good indicator for stage 2 and deeper stages whereas Delta2 and lower Theta seem to have selective power to distinguish between W and S1 and W and REM.
Distinction between S1 and REM by means of interhemispheric coherence turned out to be not very powerful. There is a trend of lower coherence centrally from Delta2 to Alpha but the differences do not exceed 0.07. For the determination of REM stage eye movements and muscle activity cannot be replaced.
Concerning frequency bands we found that for interhemispheric coherences there were almost no differences between Delta1 and the entire Delta band. On the other hand, high similarities between Delta2 and Theta1 coherences were found. In most of our comparisons of sleep stages those two bands showed about the same trends, except S1-REM comparison.
The presented study demonstrates relations between interhemispheric coherence and sleep stages which may support automatic sleep staging in combination with other parameters, like spindles, K-complexes, Delta power, rapid eye movements and slow eye movements.

		δ_1	δ_2	ϑ_1	ϑ_2	α	σ
S1-W	F3-F4		++	+		---	-
	C3-C4		+++	+			-
	P3-P4			+			
	O1-O2					-	-
S2-S1	F3-F4	+++		-	--	--	---
	C3-C4	+++					+
	P3-P4	++				++	++
	O1-O2	+	++		+		+++
S3/4-S2	F3-F4		--	---	--		
	C3-C4	--	--	--	-	+	
	P3-P4					+	+
	O1-O2	+					
S1-REM	F3-F4						
	C3-C4		-	-	---	--	
	P3-P4		--		-		
	O1-O2		--				
REM-W	F3-F4		++			--	--
	C3-C4		+++	++	+		
	P3-P4	+	+	++			
	O1-O2	+				--	--

Table I: Significant interhemispheric coherence differences between sleep stages as indicated in the left column. Positive difference: +++ (in 10 of 10 subjects); ++ (in 9 of 10); + (in 8 of 10); negative difference correspondingly.

Acknowledgement

This study was started in the framework of the BIOMED-1 concerted action ANNDEE (BMH1-CT94-1129) and it is continued within the BIOMED-2 project SIESTA (BMH4-CT97-2040), both sponsored by the European Commission, DG XII, and the Austrian Federal Ministry of Science and Research. For more information on SIESTA see: http://www.ai.univie.ac.at/oefai/nn/siesta/

References

Broughton R., Hasan J. (1995) Quantitative topographic electroencephalographic mapping during drowsiness and sleep onset. Journal of Clinical Neurophysiology 12(4): 372-386.

Corsi-Cabrera M, Guevara MA, Arce C, and Ramos J. (1996) Inter and intrahemispheric EEG correlation as a function of sleep cycles. Prog. Neuro-psychopharmacol. & Biol. Psychiat. Vol 20: 387-405.

Dumermuth G., Lange B., Lehmann D., Meier C.A., Dinkelmann R., Molinari L. (1983): Spectral analysis of all-night sleep EEG in healthy adults. Eur. Neurol. 22: 322-339.

Guevara MA, Lorenzo I, Arce C, Ramos J and Corsi-Cabrera M. (1995) Inter and Intrahemispheric EEG Correlation during Sleep and wakefulness. Sleep, 18: 257-265.

Nielsen, T., Montplaisir J., Lassonde M. (1993): Decreased Interhemispheric Coherence during Sleep in Agenesis of the Corpus Callosum. Eur. Neurol. 33: 173-176.

Rappelsberger P. and Petsche H. (1988): Probability Mapping: Power and Coherence analysis of cognitive processes, Brain Topography, 1, pp.46-54

Rechtschaffen A and Kales A, (Eds). (1968) A Manual of Stadardized Terminology, Techniques and Scoring System for Sleep Stages of Human Subjects. Los Angeles: Brain Information Service, Research Institute.

Rescher B. and Rappelsberger P. (1996): EEG-changes in Amplitude and coherence during a tactile task in females and in males, Journal of Psychophysiology, 10, pp.161-172

Trenker E., Rappelsberger P.: Requirements for automatic sleep spindle detection using artificial neural networks, Medical & Biological Engineering & Computing, 34, Part 2: 225-226, 1996

Weiss S. and Rappelsberger P. (1996): EEG coherence within the 13-18 Hz band as correlates of a distinct lexical organisation of concrete and abstract nouns in humans, Neuroscience Letters, 209, pp.17-20

Zeitlhofer J., Gruber G., Anderer P., Asenbaum S., Schimicek P., Saletu B. (1997): Topographic distribution of sleep spindles in young healthy subjects. J. Sleep Res. 6: 149-155.

Simulation of EEG signals with autoregressive models

M. Essl

Institute of Neurophysiology, Waehringerstrasse 17, A-1090 Vienna

Marike.Essl@univie.ac.at

1 Introduction

EEG coherence is an essential tool for the description of functional relationships between brain regions. This measure is defined as the squared normalised cross-power-spectrum of two signals (Jenkins and Watts, 1968).

However, EEG coherence is highly dependent on the recording technique, since the signal at the reference input of the differential amplifiers has a great influence on the shape of the EEG signals. In praxis, definite information about the properties of the reference signal is not available and can only be estimated based on pre-knowledge and experience. Unambiguous results can only be obtained by simulation studies using a data model with known spectral properties. A study concerning the reference problem when computing EEG coherence was presented by Essl and Rappelsberger (in press).

2 Method

EEG signals can be simulated according to assumed and pre-given properties. This can be realised by autoregressive processes (Rappelsberger, 1989). In the same way different reference signals can be simulated to study their influence on coherence.

2.1 Autoregressive models

Coherent EEG signals may be simulated by a two-dimensional autoregressive process of the first order:

(1)
$$x_t = a_{11} \cdot x_{t-1} + a_{12} \cdot y_{t-1} + z_{1t}$$
$$y_t = a_{21} \cdot x_{t-1} + a_{22} \cdot y_{t-1} + z_{2t} .$$

The signal x_t is dependent on its own past x_{t-1} and y_{t-1}, the past of the signal y_t. Signal y_t depends on its own past y_{t-1} and the past x_{t-1} of signal x_t. z_{1t} and z_{2t} are noise processes. The AR-coefficients a_{11}, a_{12}, a_{21}, a_{22} determine the spectral properties.

For the simulation of a reference signal which is incoherent to signals x_t and y_t, a one-dimensional AR-process of the third order can be used:

(2) $$r_t = a_1 \cdot r_{t-1} + a_2 \cdot r_{t-2} + a_3 \cdot r_{t-3} + z_{rt}.$$

The reference signal r_t is dependent on its own past r_{t-i} and the autoregressive parameters a_i for i=1,2,3, respectively. z_{rt} is a random process. This linear system (2) can be described as an linear filter with a random process z_{rt} at the input and the signal r_t at the output (Jenkins and Watts, 1968).

2.2 Stability criteria

Every linear system such as (1) and (2) can be characterised by its transfer function $H(f)$ in the frequency domain. Autoregressive processes can be seen as recursive linear filters. Since under certain circumstances these types of filters can start oscillating, stability criteria have to be considered. Therefore autoregressive-parameters must be selected with restrictions: The poles of the system need to lie inside the unit circle. Poles are given by the zeros of denominator of the transfer function.

2.3 Simulation

Modelling consists of: Spectral properties like e.g. a certain coherence value in a given frequency band are assumed. That means coherence between both signals x_t and y_t and spectral properties of the reference signal r_t are pre-given. The next step is computation of the corresponding autoregressive parameters using one- and two-dimensional processes. Then signals according to the computed autoregressive parameters are generated. EEG signals are simulated according to the differential amplifier condition. This is followed by the computation of coherence between the distorted signals. And finally, values of pre given coherence and coherence of simulated signals are compared and give a measure for the influence of the distortion, which depends on the properties of the reference signal.

3 Results

Figure 1 shows simulated signals: K1 and K2 are signals with the given spectral properties, R1=K1-Rf and R2=K2-Rf are EEG like signals with the reference Rf. In this example synchronised activity with coherence 1 and a peak in the alpha range was assumed. The reference signal has also a peak around 12 Hz. Reference with incoherent activity is modelled. This reflects in praxis the cases of reference recording using single or averaged non-cephalic electrodes. Reference signals without coherent signal portion lead to an increase of coherence between both signals examined.

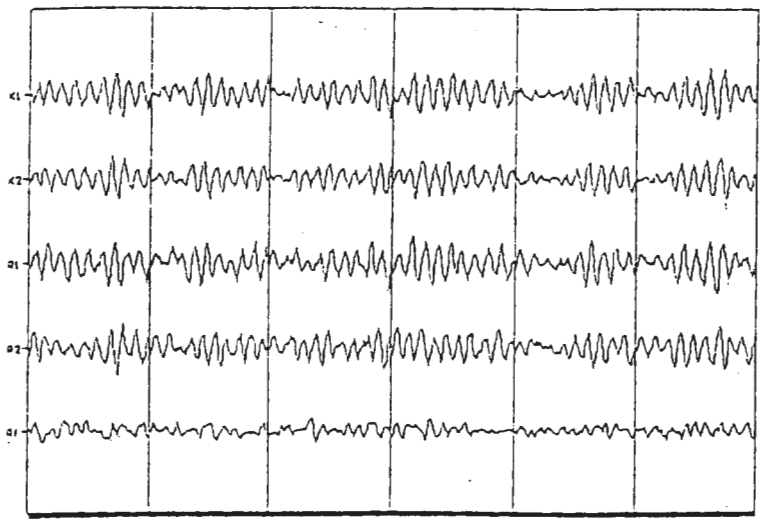

Fig. 1: Simulated EEG signals by means of two-dimensional autoregressive process of the first order. K1 and K2 are simulated signals, R1 and R2 which are K1-Rf and K2-Rf, respectively are referenced signals and Rf is the used reference signal.

Data was modelled according to Rappelsberger (1989) with a peak in the alpha range and coherence value of 1. This yielded coherence increase due to the reference signal for low coherence values and a decrease of high coherence value with the same reference signal.

A coherent signal portion in the reference signal may decrease computed coherence compared with the pre given value. This was demonstrated by a linear coherence model (Essl and Rappelsberger, in press). Comparing both coherence values, pre given and simulated, respectively, yields a measure of the influence of the spectral properties of the reference signal.

4 Discussion

This study models EEG signals to investigate the influence of reference signals on EEG coherence. Ideally, the reference signal should approach zero amplitudes (Rappelsberger, 1989). The main aim was to study the influence of different derivation techniques on coherence using autoregressive models with known properties. Experimental findings show different EEG coherence values due to different reference signals (Essl and Rappelsberger, in press).

The given example with a reference activity incoherent to both signals simulates the case of reference recording using single or averaged non-cephalic electrode signals. In the example ahead low pre given coherence is increase due to the reference signal, but high coherence values are slightly decreased with the same reference signal.

Reference effected coherence tend to be higher than the pre given coherence. Low pre given coherence is increased by the reference signal quite tremendously, whereas high pre given coherence value is effected only moderately. These findings are the results of a linear coherence model (Essl and Rappelsberger, in press).

The model described here will be used for systematic studies in future. Both types of reference signals will be considered, with and without a coherent signal portion.

References

ESSL, M. and RAPPELSBERGER, P. (in press): 'EEG coherence and reference signals: experimental results and mathematical explanations', Med.&Biol. Eng.&Comput.

JENKINS, G. M. and WATTS, D.G. (1968): 'Spectral analysis and its application', (Holden Day, San Francisco)

RAPPELSBERGER, P. (1989): 'The reference problem and mapping of coherence: A simulation study', Brain Topography, 2(1/2), pp.63-72

Acknowledgment

This study was supported by the Austrian *Fonds zur Förderung der Wissenschaftlichen Forschung,* Project P11572 and by the *Austrian National Bank,* Project NB5665.

Slow Potential Topography and Cognitive Anatomy

Herbert Bauer, Claus Lamm und Oliver Vitouch

Slow potential topography (SPT) has already proven applicable and useful in cognitive neuroscience. It gives a fairly direct measure of activity levels of different cortical areas. The brain signals on which SPT is based are very slow amplitude changes in the scalp recorded EEG. The EEG does not just consist of the commonly known delta, theta, alpha, beta and gamma frequency components, it also has a DC-potential component. The amplitude of this component varies with the activity level of the generating structure. Scalp locations usually show negative potential values relative to frequently used reference sites, e. g. the mastoids or ear lobes. Roughly spoken this negativity becomes more intense if the generating structures become more active and vice versa. When we record this signal from many locations distributed evenly over the scalp in parallel, we are able to monitor regional changes of activity levels. Having a subject doing a particular cognitive task several times this kind of recording enables identification of cortical structures involved in processing the task via averaging. In this way we are modeling the cognitive architecture of the cerebral cortex.

Figure 1 shows topographies that evolved during reading aloud. These topographies are grand averages of 15 female (left) and 15 male (right) subjects who read 8 one-line sentences six times. DC-potentials were recorded from 22 locations and zeroed at the start of reading a line. The topographies therefore represent the DC-potential changes that have appeared at a latency of 5 seconds.

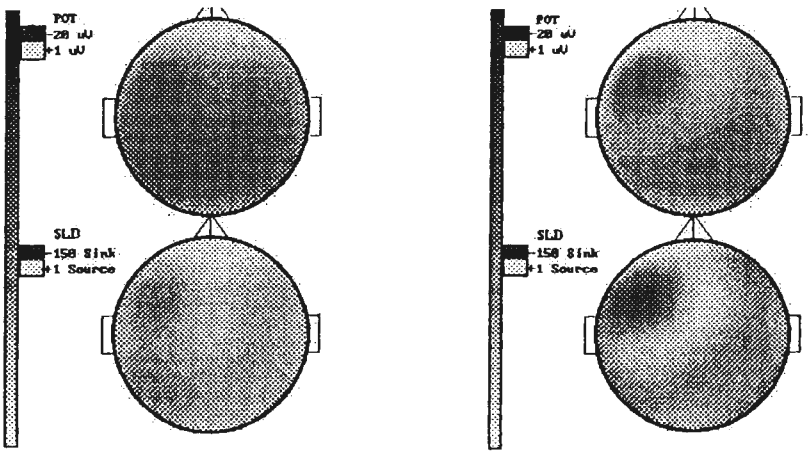

Figure 1. Mean slow potential and CSD topographies of female (left) and male (right) subjects during reading aloud. Dark areas indicate increased activity.

There is a clear lateralization of activity in males whereas females show an even left/right distribution of activity. Generally only language relevant areas became activated. The CSD-maps further illustrate these observations.

This result resembled nicely a fMRI observation reported by Shawitz et al. (1995). In their study, male and female subjects had to check pairs of syllables for rhyming; this task involves phonological coding, which is also an essential component of reading aloud.

Such observations demonstrate that the application of SPT or other modern imaging techniques enables more than just corroborating traditional knowledge in functional neuroanatomy. Additionally, brain functional models based on very indirect experimental evidence may be validated.

Another example contributes more of this. In this study (Vitouch et al., 1997), subjects had to check in two separate experimental runs pairs of cubes or pairs of semantic relations on identity.

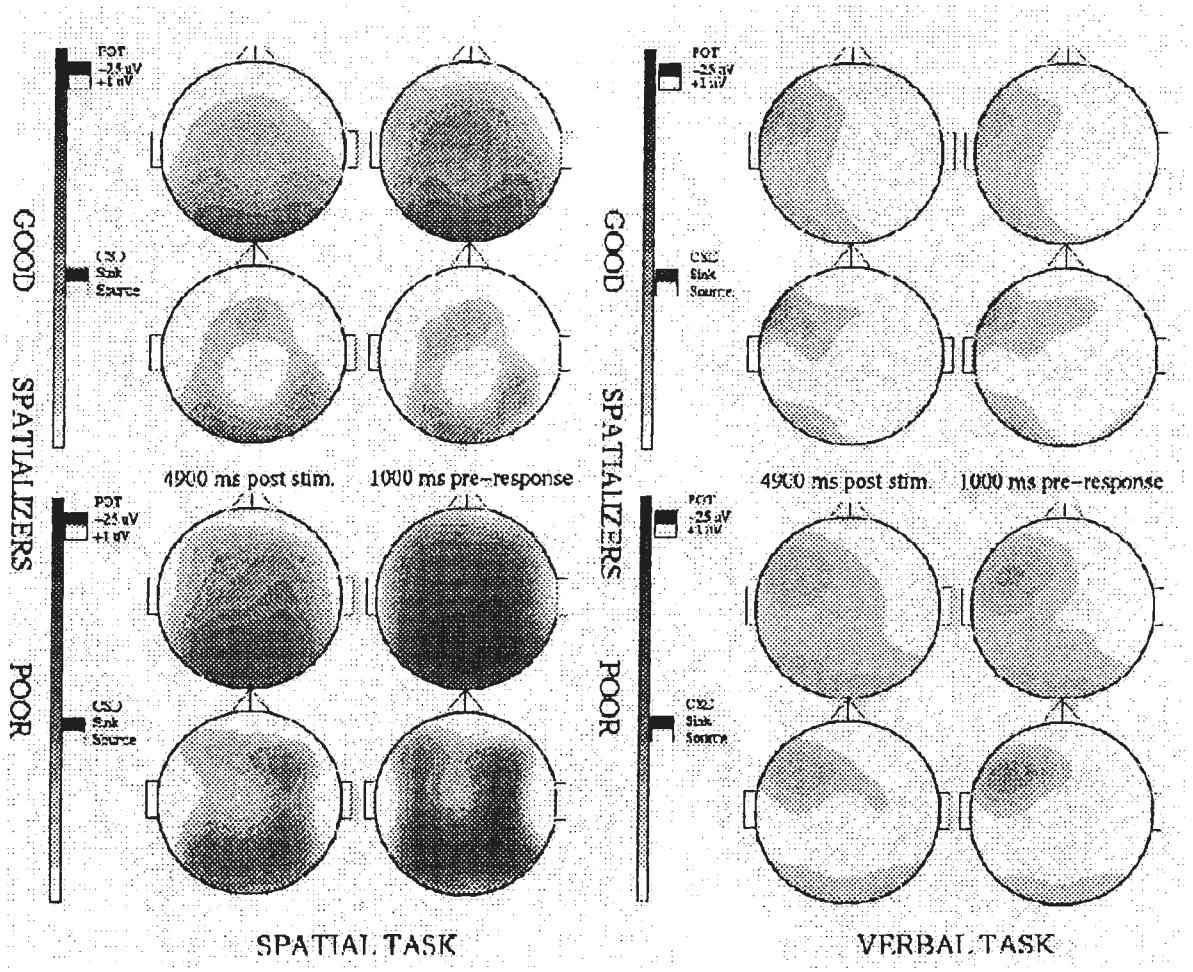

Figure 2. Mean slow potential topographies and CSD-maps of good (upper half) and poor (lower half) spatializers processing spatial (left) or verbal (right) tasks.

Cubes had different patterns on the 3 visible sides and subjects had to find out if there is a possible match of the 3 patterns when mentally rotating one of the cubes. Item presentation was subject-paced and there was ad libitum time to process each item. These spatial tasks have been derived from test-theoretically analyzed spatial test items (3DW, Gittler, 1990) which have proven to challenge essentially one and the same dimension of ability in all subjects. This feature is usually called Rasch-homogeneity or unidimensionality of a test.

Figure 2 shows task-specific group results. Verbal tasks evoked left hemisphere activity (all Ss were right handed) in posterior frontal and parietal areas. Spatial tasks evoked occipital and parieto-temporal activity. Both observations are in keeping with traditional functional neuro-anatomy so far, but again a differential aspect yielded interesting additional information.

All subjects were pre-selected in order to form two extreme groups: very good and pretty poor spatial test performers. As can be seen with the spatial task results in the figure, good spatializers clearly show less activity (amplitude- and area-wise) than poor ones (at the same latency). This is especially remarkable because good spatializers also had shorter processing times - they accomplished decisions faster with less neuronal effort. Good spatializers showed less 'Investment of Cortical Effort' (ICE, Vitouch et al., 1997). This experiment has been replicated with a comparable sample of female subjects (Bauer et al., in prep.) and revealed an identical pattern of results.

These observations, not accomplishable by means of traditional neuro-psychological or test-psychological methods, again reveal that particular cognitive functions may be implemented and configured differently in different brains.

According to the origin of slow potential changes, it can be said that good performers had less cortical neurons active when processing the spatial tasks. But the data do not tell about reasons for higher effectiveness with smaller cell populations. Some speculations come to mind: good performers had better algorithms implemented and configured - a more effective 'wiring', so that more basic processing steps could be done in parallel and/or that redundant operations could be avoided. With poor performers, additional parieto-temporal structures were co-active to support their less efficiently working processors.

Test-analytical studies revealed that the spatial items used in these experiments loose this property of unidimensionality when processed under speed conditions, i.e. within a given period of time per item. Therefore we conducted another follow-up with comparable male and female samples and presented items computer paced and with a constant presentation time

adjusted for good and poor spatializers (according to the mean processing times observed in the first study).

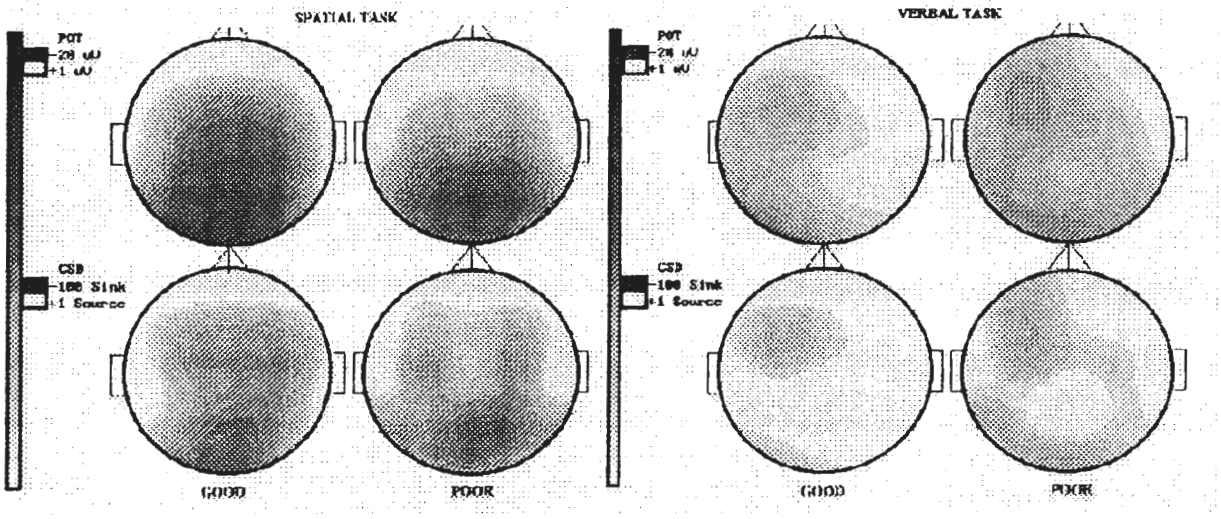

Figure 3. Mean slow potential and CSD maps (5sec latency) of good and poor spatializers processing spatial (left) and verbal (right) tasks under speed conditions.

Preliminary results from the male sample study show that the differences in the topographies of good and poor performers are not visible anymore and topographies look more alike those observed with poor performers of the first study (see Figure 3). Poor performers completed significantly less tasks than good ones. As a preliminary interpretation one could say that poor performers did not have additional processing capacity in spare and therefore showed unchanged topographies. With the good ones, similar happened as with poor performers under power conditions: parieto-temporal structures became integrated supporting the spatial processor.

In sum such observations demonstrate that cognitive functions are variably implemented and configured in the brain. Differential aspects can be investigated more directly now by means of modern imaging techniques and differences in particular abilities can be recorded at a physiological level. As it seems, even particular conditions in a given situation may codetermine the configuration of a particular cognitive processor.

Apparently the processing machinery, within certain anatomical and physiological constraints though, becomes tailored according to the actual challenge.

References

Bauer et al., in preparation.
Gittler (1990) Weinheim, Germany: Beltz Test.
Shawitz et al. (1995) Nature, 373, 607-609.
Vitouch et al. (1997) International Journal of Psychophysiology, 27, 183-199.

Artificial and Biological Neural Nets: A Comparison

Alice Mladenka [1,2], Frank Rattay [1]

[1] TU BioMed, Technical University of Vienna
[2] Siemens AG Austria

Abstract

Although artificial neural networks (ANNs) are supposed to have a biological background, they are far from reaching the computational abilities of real neurons and networks. This paper shows some of the similarities as well as the differences between artificial and biological network structures. A closer look to the structural and functional properties of biological neurons and networks may help to improve the efficiency of ANNs.

Artificial Neural Networks

An artificial neural network (ANN) is a modern highly parallel computational tool that is based on some fundamental properties of biological neurons in a rather simplified way. There exist several different types of ANN, and not all are related to a biological background.

ANNs are built up of simple processing units, called neurons (Figure 1). The units are interconnected by weights or synaptic strengths, which are a primitive model of biological synapses (positive synaptic strengths are called excitatory, negative ones are called inhibitory).

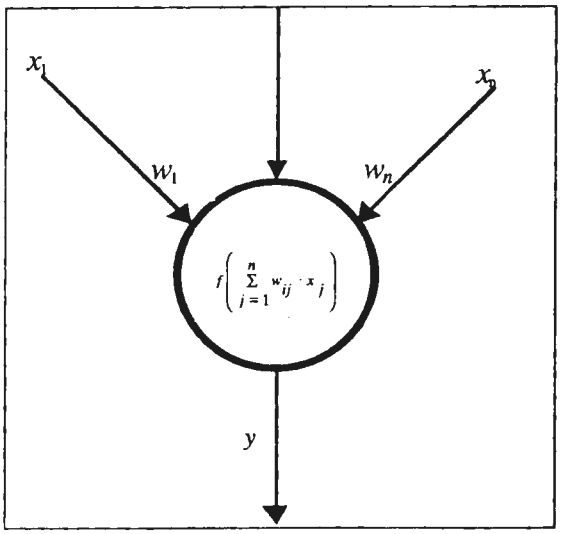

Figure 1 Schematic representation of an artificial neuron. The inputs $x_1, \ldots, x_n$ are collected from the connecting units, multiplied with the connection strengths $w_1, \ldots, w_n$ and then summed up in the processing unit. A linear or nonlinear activation function f is applied to the result.

Most ANNs use threshold units that simply sum up the weighted inputs that are collected via the synaptic connections from the other neurons. Therefore, the artificial unit outlines rather the cell body of a neuron than the whole cell itself, and the function of the synaptic weights is restricted to strengthening (excitatory) or weakening (inhibitory) of the input values, whereas the biological neuron has a more complex structure and much more possibilities to act and react.

To increase the computational power of the network, sigmoidal activation functions like $\tanh x$ are used to transform the inputs in a nonlinear way.

Some networks use only one-directional links (feedforward-networks), others allow also backward connections (recurrent networks).

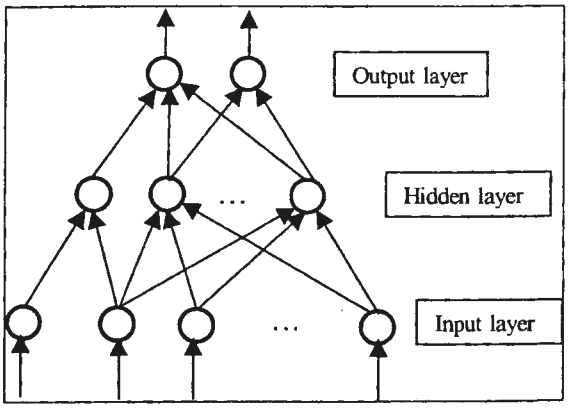

Figure 2 Schematic representation of an artificial neural network with forward connections between the layers. This is the most commonly used neural network type. It has no backward connections and does not even allow connections between neurons of one layer.

The neurons can be arranged in different layers with connections only between the layers (e.g. multi-layer perceptrons, Figure 2), or in a kind

of lattice (map) with fully connected neurons (e.g. Hopfield or Kohonen networks).
The computational power of ANNs is due to their ability to learn, i.e. they adaptively change their weights according to a learning rule to compute a transformation of the inputs into the output values. After the network has been trained, it can be used on new unknown data to test the network's ability to generalize. If the network has got enough information about the input data, it is able to generalize the main features also to unknown or defective inputs (e.g. with some missing values). Therefore, ANNs can be used for tasks like function approximation and pattern recognition, e.g. in speech or image processing.
Nevertheless, ANNs cannot obtain a similar performance than the human brain, and often their success is restricted to very specific problems and conditions. A closer look to the structural and functional properties of biological neurons and networks may help to improve the efficiency of ANNs ([13]).
Two important features of biological neurons and ensembles of nerve cells are not yet taken into account in the theory of artificial neural networks: the individuality of nerve cells and the time structure of neural patterns.

Individuality of Biological Neurons

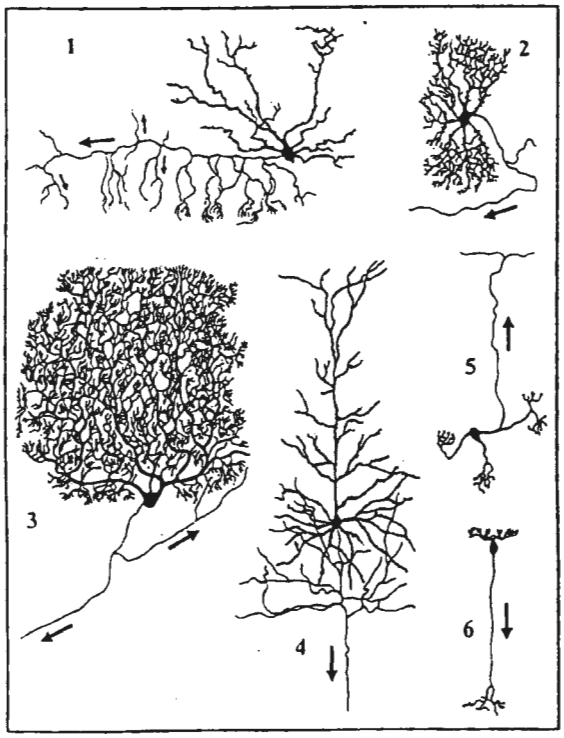

Figure 3 Different types of neurons in the brain [6]: 1. basket cell (cerebellum), 2. Neuron from the brain stem, 3. Purkinje-cell (cerebellum), 4. Pyramidal cell (neocortex), 5. Körner cell (cerebellum), 6. Bipolar neuron (retina). Note the different shapes of the dendrites and the axon terminals.

The brain utilizes many different types of neurons (they differ in shape as well as in function and their operational area in the brain, see Figure 3), and no two neurons have exactly the same structure. Examples are Purkinje cells in the cerebellum with the typical dendritic tree that lies almost within a plane [14], or pyramidal cells and stellate cells in the cortex that are part of microstructures in the neocortex [16].
There exist neurons that act as pacemaker cells (e.g. in deeper brain structures) as well as neurons that simply fire at the on-set or off-set of an impulse (e.g. in the auditory cortex), others fire with the same frequency than the stimulating signal. Each neuron is an extremely complex entity due to the microstructure of the cell.

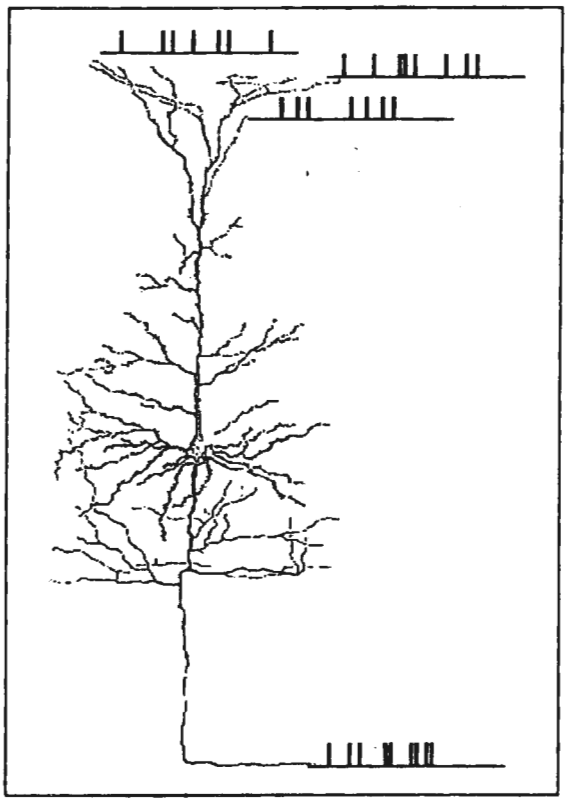

Figure 4 Schematic representation of a biological neuron (pyramidal cell in the neocortex). The neuron collects inputs in form of spike trains (electric impulses) that are propagated through the dendrites to the cell body. At the initial segment of the soma, the axon hillock, one or more action potentials are produced when the membrane voltage crosses a certain threshold.

The electrical properties of the cell are determined by ion channels in the cell membrane that regulate the exchange of various types of ions (Na^+, K^+, Ca^{++}, and many more). The ionic concentration inside and outside the cell influences the short-term as well as the long-term behavior of the neuron (e.g. long-term potentiation or depression that are involved in memorization processes). This leads to an individual behavior of the nerve cell that may also cause different reactions to similar stimuli.

The electric pulses of a neuron are called action potentials. The neuron fires as soon as the membrane voltage has reached a certain threshold (and the neuron is not in its refractory period, where it has to recover from previous spiking; no action potentials can be produced within this time).
The action potentials are then propagated by the axon to the end terminals of the neurons and via synapses they form the input to connected neurons (Figure 4). The "all-or-nothing" law says that once an action potential is produced, it is able to propagate to the end terminals of the cell without any losses. But this law does not hold true for all situations – in reactions to high frequency stimuli some of the spikes may be lost (see also Figure 5).
Not only the membrane of the soma is actively influenced by ionic channels, also the dendrites have a more awkward task than simply convey the synaptic inputs to the cell body for linear summation (the action potentials may propagate back into the dendritic tree which will lead to changes of the ionic concentrations in the dendrites and therefore indirectly influence the propagation of following electric impulses) [11]. As the cell membrane is not passive, the neuron effectively performs a multiplication, i.e. the firing rate is proportional to the product rather than the sum of its inputs [9].

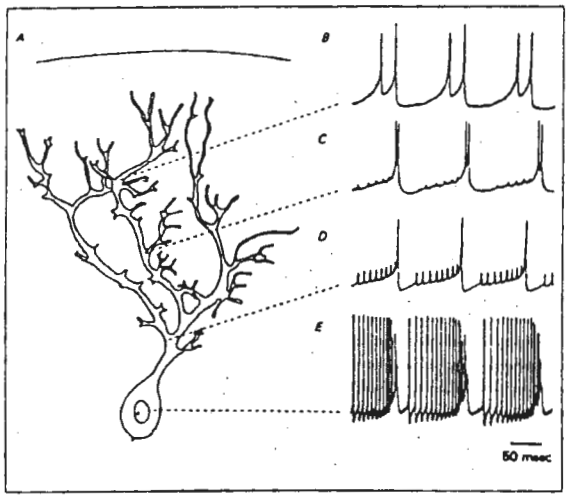

Figure 5 Relationship between somatic and dendritic action potentials after current injection through the recording electrode. Note that at increasing distances from the soma the fast spikes are reduced in amplitude and are barely noticeable in the dendritic recordings [12].

Action potentials may show different shapes in different parts of the neuron (Figure 5): in the dendritic part away from the soma, high frequency spikes may be reduced in amplitude which leads to different forms of spiking patterns.
Some neurons act rather local (e.g. stellate cells), in the cortex they are mostly inhibitory [16], others have widespread connections to neurons in different areas of the brain (e.g. pyramidal cells, which are almost always excitatory). One single neuron can have as many as 10 000 synaptic contacts to other neurons and receive the same number of inputs. Biological synapses are highly complex units that utilize electrical as well as chemical mechanisms and may work on different time scales (short- and long-term potentiation of postsynaptic neurons). Synapses work with many different chemical substances, the neurotransmitter, which can cause different reactions in the postsynaptic membrane and even influence the presynaptic membrane of the synaptic connection. Therefore, synapses do not simply inhibit or excite the postsynaptic neuron and use this "weight factor" like ANNs to strengthen or weaken the input signal, but they have a wide range of possibilities how to influence the reaction to a signal, dependent on both the pre- and the postsynaptic membrane.

Time structure in neural networks

Electric activity of neurons in the brain leads to complex spatio-temporal firing patterns. The information can be encoded using a rate code (a time-averaged firing rate) or an interval code (single spikes and intervals between them) [7].
Most ANN models are restricted to a rate code, i.e. their outputs can be interpreted as mean firing rates. In biological neurons, the mean firing rate is directly related to the stimulus intensity. Time-averaged firing rates need a time interval of at least 100 ms, where the specific structure of the spiking pattern is not taken into account. However, this is not sufficient to describe neuronal activity, because even single spikes of a single neuron may contain important information about the stimulus [2].
Additionally, some brain functions have to discern firing patterns containing a time difference of 10 µs (e.g. directional hearing) or react to a stimulus within a few ms [15]. Therefore, biological neurons use both a rate and an interval code [4]. Nevertheless, there may exist a great variability in the timing of the spikes, although neurons are capable of processing with high temporal precision (less than 1 ms) [15]. Additionally, coherence in firing or synchronization between the firing of a group of neurons may be used as a code to link features that belong to the same pattern and to separate them from other patterns [1], [8].
Temporal codes are more efficient than rate codes, because even if the mean firing rate is the same, temporal patterns may differ in their spike trains [5]. A main feature of information

processing in the brain is the redundancy – sometimes much more neurons than necessary perform a task. This leads to a high tolerance for noisy or imprecise spiking patterns, and low intrinsic noise can rather help than hinder neurons to react on external stimuli (e.g. Brownian motion in the inner ear) [10].

Biological neurons may be arranged in layers (e.g. cortex), with connections within one layer or between different layers, and throughout these layers there often exists a microstructure, e.g. neurons that have to fulfill a similar task build up small microcolumns (Figure 6). But the brain does not confine to these local circuits. There exist long-distance connections between different areas of the cortex and also between the two hemispheres and between the cortex and deeper brain structures. In this way, the brain uses serial and parallel pathways as well as local feedback loops.

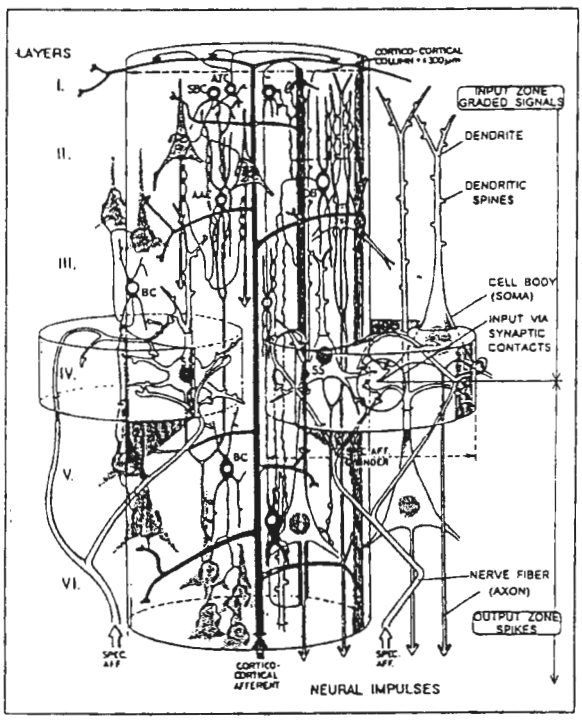

Figure 6 Microcolumns in the neocortex [14]. Through the six layers of the neocortex, neurons with similar tasks are organized in small microcolumns. The small stellate cells form effective local inhibitory circuits, the pyramidal cells are responsible for the long-range excitatory exchange of information with other cortical areas and with deeper brain structures.

This high connectivity of different types of neurons using serial as well as parallel pathways, together with a temporal and spatial information coding, leads to the enormous efficiency and adaptivity of biological neural networks.

References

[1] Abeles M. 1991. *Corticonics.: Neural Circuits of the Cerebral Cortex.* Cambridge University Press, Cambridge.

[2] Bialek W., Rieke F. VanSteveninck R.R., Warland D. 1991. Reading a Neural Code. Science **252** pp. 1854-57.

[3] Crick F.H.C. 1979. Thinking about the Brain. Scientific American 9/79 pp. 181-88.

[4] Domany E., VanHemmen J.L., Schulten K. (eds.) 1997. *Models of Neural Networks II: Temporal Aspects of Coding and Information Processing in Biological Systems.* Springer New York.

[5] Ferster D., Spruston N. 1995. Cracking the Neural Code. Science **270** pp. 756-57.

[6] Firbas W., Gruber M., Mayr R. 1988. *Neuroanatomie.* Verlag Wilhelm Maudrich.

[7] Gerstner W., VanHemmen L.J. 1997. Coding and Information Processing in Neural Networks. In [4] pp. 1.94.

[8] Hopfield J.J. 1995. Pattern recognition computation using action potential timing for stimulus representation. Nature **376** pp. 33-36.

[9] Koch Ch. 1997. Computation and the single neuron. Nature **385** pp. 207-210.

[10] Mainen Z.F., Sejnowski T.J. 1995. Reliability of Spike Timing in Neocortical Neurons. Science **268** pp. 1503-6.

[11] Markram H., Lübke J., Frotscher M., Sakmann B. 1997. Regulation of Synaptic Eficacy by Coincidence of postsynaptic Aps and EPSPs. Science **275** pp. 213-15.

[12] Mel B.W. 1994. Information Processing in Dendritic Trees. Neural Computation **6** pp. 1031-85.

[13] Pfützner H., Nussbaum C. Booth T., Rattay F. 1995. Physiological Analoga of Artificial Networks. Studies in Applied Electrodynamics ISEM, Cardiff, GB.

[14] Rattay F., Pfützner H. 1995. Neural Nets: The Brain and the Computer. Proceedings Eurosim'95 pp. 99-104.

[15] Sejnowski T. 1995. Time for a new neural code? Nature **376** pp. 21-22.

[16] White E.L. 1989. *Cortical Circuits: Synaptic Organization of the Cerebral Cortex.* Birkhäuser, Boston.

A novel neurosimulator to predict propagation of information in neuronal systems.

Peter Slowik and Lars Mehnen
Vienna University of Technology

In modern computer science every program or algorithm is being build out of fix program statements which are fetched from the program code one after another. There are several attempts to make a programs run parallel, but the fix and linear way a program code is being worked survives because of its simplicity. Fuzzy logic and other theories are trying to overcome the problem of fixed data structures, but it has never been tried to make the program statement itself flexible. This model shows how a simulation of a neuron complex can be used for dynamic programming in data and code using the basic capabilities of a natural neuron.

Neuronal systems are a network of neurons interconnected by synapses. Information is processed and forwarded in the neuron system with the help of neural impulses. The knowledge about the anatomical characteristics of a neuron helps to get an overview about the natural behavior of whole neuron complexes, which have been optimized by evolution since millions of years. Mathematical models are very helpful for the understanding of the physiological processes in neurons. By interpreting the mathematical solutions of these models, one can achieve some information about the system itself, which cannot be reached by present laboratory methods. Creating mathematical models is often much cheaper and more productive than empirical measurements.

However, models which describe the temporal system behavior with the help of big and complex differential equations systems need a lot of computational time. In addition, another negative effect of these coupled differential equation is the impossibility of running them in parallel. To get rid of these effects we made some abstractions and optimizations on the model in order to obtain a neuron simulator for general use.[1]

To define a neuron system complex, a special language is actually being developed. This language describes not only the spatial structure, but also the time structure of each potential spike in a neuron. This definition language has been realized system independently in an ASCII format file. By this mean it is possible to store, rearrange and transfer the whole simulation to another machine at any given time of the simulation run. For example: a situation can be copied with the same initial conditions on to different computer systems and treated with different simulation conditions. While reading the definition file the simulator will optimize the neuron system structure, transforming the spatial structure of the neuron system to a temporal and spatial structure of the neuron to its interconnections. The time that a spike needs to reach a synapse will be predicted. By the help of this transformation, the complex spatial tree

[1] The simulator is written in the C++ programming language. Reason for this decision was: the advantage of the object oriented programming style is combined with a high level language compiler generating highly optimized fast machine code. Object oriented design and the usage of operator overloading offers the possibility to use abstract data types and to add higher level data types (for example linear lists) to the basic capabilities of the C++ programming language. One of C++'s major innovations is the idea of combining data and instructions together in a construct called class or object. Object oriented programming allows to group data with the operations that can be performed on that data. This concept is taken one step further in C++ by allowing to derive new classes from existing ones to add more capabilities on more specific data. These characteristics are very useful especially for connecting actuators, sensors and some "special" objects used for the evaluation of signals within the existing system.

structure of the neurons can be simplified to linear lists. The neural impulses can jump from synchronization point to synchronization point by awaiting the predicted run time, and therefore it's not necessary to work off the whole natural tree recursively. The time behavior is controlled by a global time control algorithm. The global time is used for temporal synchronization between neurons.

The simulator is designed to be very flexible and therefore can easily be extended and used as base for other simulations concerning neuron systems. The simulation data may be analyzed at run time with specially developed statistical variables or at any time after the simulation has ended. Spike times and localization are saved for post simulation analyses and can be used as initial conditions for further simulations.

The simulator provides a new kind of programming. For the first time there exists the possibility of time dependent programming and data coding together and thereby new concepts for data processing can be realized. The flexibility of the definition of the spatial and temporal structure provides the simulation of nearly natural processes, but also clearly experimental or abstract programs simulating fictive processes.

The components of the simulation model in detail:

The concept of synchronization points (synapses) allows formation of some sort of procedure or program blocks. This feature supports finding functional and cohering parts and thereby helps to find independent "code", necessary for the parallelisation of these blocks.

The neural impulses are passed over to the next neuron as soon as the global system time has reached the local predicted spike time. This effect builds up a time buffer that can be used for synchronization within parallel systems, minimizing communication overhead between several computers.

The global timebase enables to overcome the problem of an exponential growing overhead for synchronizing all the dependent subsystems. All further effects concerning time dependent behavior can be neglected.

The base unit of the global time (tic) can be freely selected. Note that this influences the accuracy of the calculation (simulation). If the time base (tic) is too large, the neural impulses will begin to overlap resulting in inaccuracy and some spikes can be lost. A natural nerve fiber is able to transfer spikes with a maximum rate of 1 kHz leading to the basic time unit of 100 µsec for an adequate simulation. The global time counter can simulate an interval of about 119 hours, restricted by the maximum numerical value a 32 bit variable can accept before overflow.

The time engine produces a continuos flow of similar time intervals. If the time unit (tic) expires, the status of every synaptic connection and the trigger zone of the neuron will be recalculated resulting in a new neuronal state, initiating the next simulation interval, while the synapses and the trigger zone serves as synchronization points.

Information flow in a neuronal system:
Example: A neuron that gets an input that is too weak to propagate into the axon area.

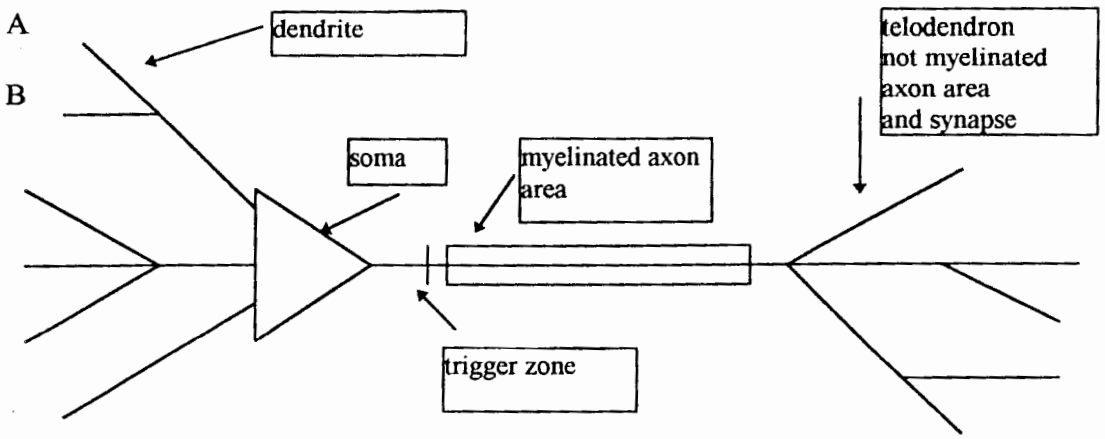

Data is represented by spikes. The following three graphs show how the spike is propagating through the dendritic area, damped down all the way in the tree. One spike is inducted into dendrite A, part of the current leaves through dendrite B, the rest is too weak to cause an action potential in the trigger zone.

Branch A:

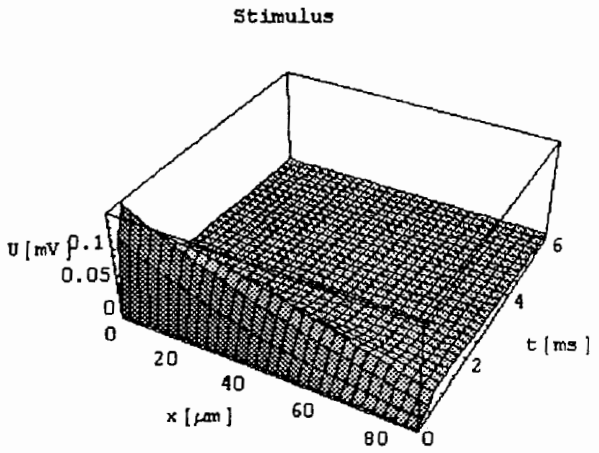

Branch B:

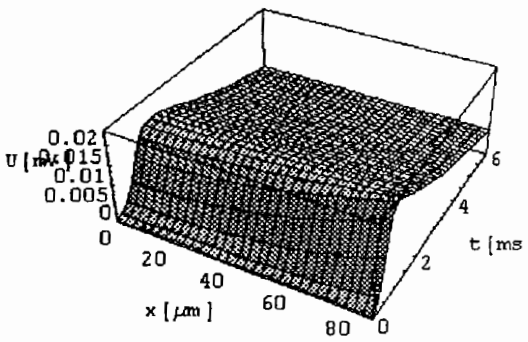

Connected branches leading to the soma

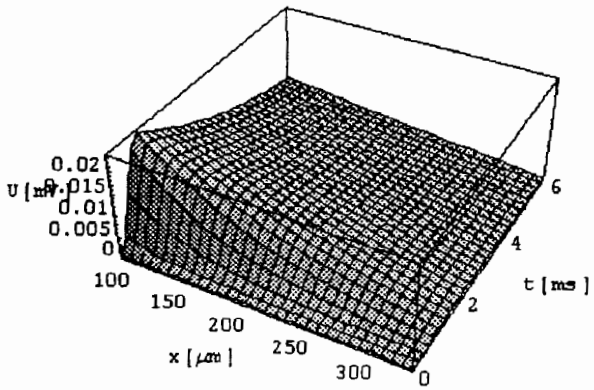

To bring some basic logical functions into the system, evolution has developed to the method of exciting and inhibiting a potential spike while propagating in a neuron. If the inhibition hits the spike exactly (time and location) or is being activated a little bit before, the spike is nearly eliminated. This leads to the time logical function: if inhibition spike hits another spike, the spike will be erased or damped down.
A constant spike frequency of a neuron can therefore be controlled dynamically by inhibition frequency. This leads to a basic dividing functionality, witch can be simply inverted to multiplication using the same inhibition method. The next two graphs show a spike running down to the soma normally and if it is inhibited.

without inhibition:

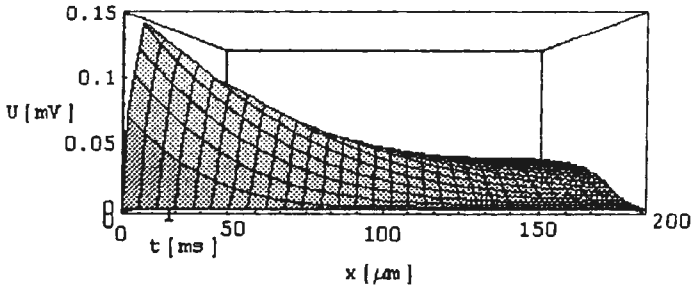

with inhibition at x=87,5 μm

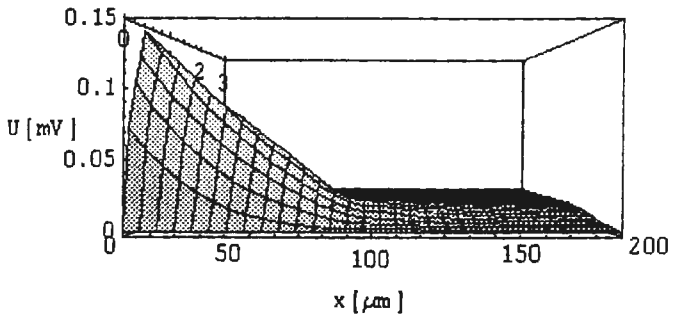

It is possible with the help of these inhibitory synapses to realize time dependent programs.
The basic behavior of inhibitory synapses is speed and efficiency. This makes them an excellent choice for time synchronized structures. For the first time this simulator enables a time dependent and dynamic programming.

Quantum-Neurodynamics – and its relation to cognition and consciousness

Gustav Bernroider
Institute of Zoology, University of Salzburg
A-5020 Salzburg

Introduction

Whereas adaptive brain processes involving synaptic plasticities such as learning and memory have seen a convincing amount of clarification during the recent years of brain science, the conceptually most challenging phenomena such as perception, cognition and emotions remain enigmatic. The last decades of sensory neurobiology have been based on the neuron doctrine stating that i) all sensory information stems from real-time observations of the activity of the organisms own neurons (e.g. Bialek, et al., 1991), ii) the state of neural firing at a given instant of time is a necessary and sufficient condition to explain sensory processes (Barlow, 1972) and iii) neural transformation involves the early segregation or separation of single features belonging to one percept among millions of widely distributed cortical neurons -population coding- (e.g. Knudsen, et al., 1987). What is completely missing however, are explanations how the spatio-temporal variation in the firing rate of a large collection of place-specific neurons is composed into a coherent and unique experience or percept. Although candidate processes such as synchronization of firing rates on fine temporal scales have been proposed (Gray, & Singer, 1989; Singer, 1995), the neural equivalent of a sensory 'experience' is still a complete mystery.

Because of this deficit some consens has evolved that it needs an extension of the neuron doctrine into a more broad brain-theory that renders the relation of the neurophysical to the neuro-phenomenal, providing predictions on first-person experiences that are possibly based on physical concepts. More recent approaches have used the notion of quantum physics, involving action orders of 10^{-34} [kg m^2 s^{-1}] (Hameroff & Penrose, 1996; Stapp, 1996; Bernroider et al., 1996; Bernroider, 1997). These views are accompanied by an enduring dispute whether these very small action orders at the atomic scale can be of any significance to the concepts of electrophysiology (Scott, 1996). After all, it is hard to see, how quantum phenomena could effect the propagation of nerve impulses described by the Hodgkin-Huxley model. However, this problem has many shades and there is an increasing list of empirical evidence for the decisive role of local gating charges and electrodynamics at the Planck-scale that puts neural quantum concepts into a new and very promissing frame.

The view of the present work is that a theory dealing with the phenomenon of 'experience' which is intrinsic to the notion of perception, cognition and emotion, is principly incompatible with the traditonal neuron doctrine. Instead these doctrine have to become expanded to account for i) the construction of higher level brain issues from the lowest level above physical significance, ii) non-local interactions of neural systems or states according to quantum properties in physics and iii) a transition from purely physical information states into their underlaying phenomenal properties.

Diagrammatics

Here we look at the universal objective and the observing brain as a continuous connected whole – where both entities become only partly and transiently separated by phase transitions. From an ontological perspective this is in accord with the 'holistic' or 'conceptually monistic' view of brain function (e.g. Pribram, 1991; Winkler, 1997) or 'Mach's principle in perception' (Mogi, 1997). To describe some ideas for short, it needs a 'diagrammatic aid' to visualize the principles. Processes of the present type could be seen from the traditional Cartesian view outlining point events in space-time and available from diagrammatic perturbation theory based on Feynman's diagrams (Figure 1) as discussed previously (Bernroider, et al., 1996).

From Huygen's construction of Feynman graphics (FG) one is led to the opposite view of an enfolded geometric structure proposed by Bohm (1993). Bohm interpretes time in Feynman's graphics as related to an 'implication parameter' that reflects the degree of enfoldment of universal structures. Differences in time are presented by differences of radii of contacting spheres. The laws of temporal evolution of a system or state are implicit in this representation. Points in FGs become centers of spheres, either converging or diverging, with incoming waves decreasing to spheres of zero radius (points) and outgoing waves increasing. The implication parameter is represented by the radius of spheres – converging spheres therefor 'unfold' to a specific space-time point in the FG notion. BGs show the entire space-time trajectory of particles or signals at once – as an unbroken wholeness provided by a succession of contacting spheres.

The view available from Bohm's diagrams very closely reflects the way how a neural dynamic state space in the sense of the present work could be arranged. The dynamic configuration behind it discerns continuous 'brain lines' rather reflecting on discrete state shifts.

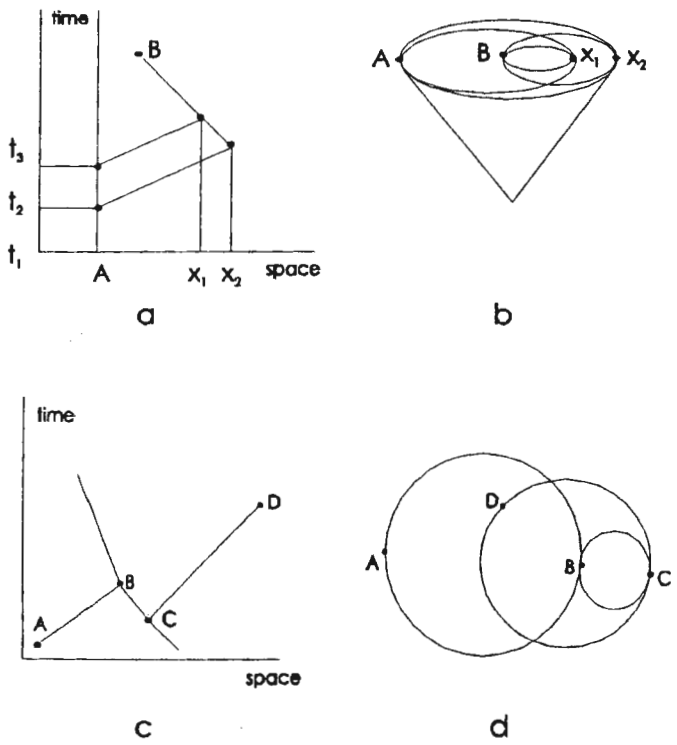

Figure 1:

Neural state space presentations using Feynman diagrams (a) and (c) and their Huygen counterparts as Bohm graphics (BG) (b) and (d).

In (a) signals are emitted from source A at times t_2 and t_3 and reflected back onto location B from an intermediate layer X_1 and X_2.
In © the paths involve a backward turn in time from B to C

The BG equivalents in (b) and (d) are based on Huygen's principle of a spherical evolution of light signals – here the radii of contacting spheres reflect differences in time as the signal propagates.

Unfolding the neurophysical – or Bohm's principle in experience

To implement the ideas expressed above and put them into practice for brain modelling one needs to address now at least two points: 1) what are the signals and 2) what are the constraints impossed by the brain to exchange these signals. To cut it short, both questions cannot be answered yet with confidence. The signals must be provided by passive and active membrane properties of neurons, but cannot be reduced to the macroscopic exchange of action potentials without violating the drammatic role of dendritic potentials as temporal coincidence detectors and temporal filters (e.g. Pribram, 1991). Organizational constraints on signal exchange may obviously be provided by the brains specific anatomy. However, to identify the decisive aspects of organization is far beyond reach at the very state of art. The view adopted here is in favour of Mogi's idea that the firing of neurons should be seen rather as an *interaction-connected activity* than a selective response activity (Mogi, 1997). In other words, spiking of neurons does not signal a particular (e.g. sensory) information but it signals the particular 'role' a neuron plays in relation to all other neurons at a given instant of time with respect to a particular situation.

One obvious way to message this role would be to eliminate the 'predisposed' or 'stimulus conditioned' situation of a neural unity – e.g. a single cell. As mentioned above the 'segregation' of information along wide spread neurons is what can be clearly identified from sensory processes. Quite logically the elimination of segregated information implies to focus these signals onto one point in space-time – one point on Feynman's diagram or converging spheres in Bohm's diagram. In the sense of Bohm that is to 'unfold' the brains activity into an 'explicate' order, reducing the implication parameter provided by the radius of Huygen's spheres to a circle with zero extension.

The present theory has led to the implementation of interaction-modulated neural activities unfolding a set of brain states onto a single space-point according to the FG in Figure 1a or the BG equivalent in Figure 1b. The details of this implementation have been reported previously (Bernroider, et al., 1996). The basic modul of this concept is a pair of neurons in close and reciprocal contact (Figure 2a) – signals can go anywhere . It is the emerging arrangement of neurons (the anatomy of a larger set of neurons) that gradually guides the signals propagation into particular paths, an initially diffuse 'network' that self-organizes the exchange of information. The only and basic constraint is provided by the explication onto a single space-point at a given instant of time.

a

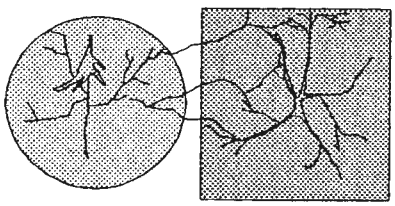

b

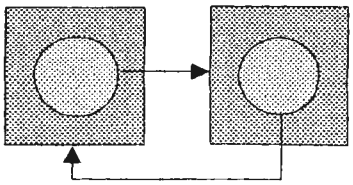

Figure 2:

a) the basic modul of a focusing signal concept – the axonal source domain is given spherical – the dendritic target domain is shown square

b) a schematic outline of an reciprocally connected modul with feedforward and recurrent connections

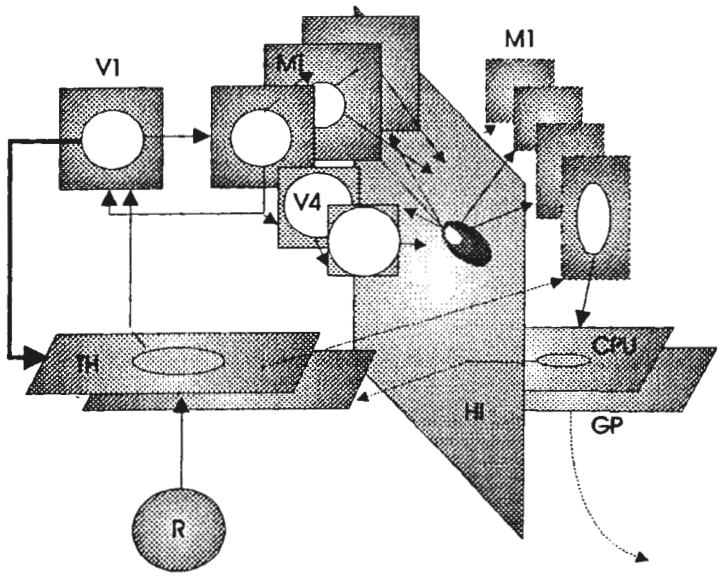

Figure 3: modellistic reconstruction of major parts of a mammalian forebrain based on the above moduls and using explicating (space-time focussing) arrangements as described in the text.

Conclusion

The classical neuron doctrine of a stimulus coding exchange of action potentials among place coded nerve cells is not compatible with the 'binding problem' of segregated features into a single and conscious percept. Instead I adopt a notion that is based on the self-organizing spread of passive and active membrane properties under the constraint of an 'explicating', i.e. space-time focusing principle of signal propagation. Neural codes are less response-selective but more 'interaction-selective' – focusing of stimulus-caused segregated signals onto single points carries the message behind a neurons role within a large population of engaged cells.

References:

Bernroider, G., F. Ritt, E.W.N. Bernroider, Forma, 11, 141-159, 1996
Bernroider, G. Conscious. Res. Abstracts, Elsinore, Denmark, 44, 1997
Bialek, W., F. Rieke, DeRuyter, R. Van Stevenick, D. Warland, Science, 252,1854-1857, 1991
Bohm, D. & B. Hiley, The Undivided Universe, London, Routledge, 1993
Gray, C.M. & W. Singer, Proc. Natl. Acad.Sci., USA, 86, 1698-1702
Hameroff, St. & R. Penrose, J. Consciousness Studies, 3,1, 36-53, 1996
Knudsen, E. I. , S. DuLac & S.D. Esterly, Annu. Rev. Neurosci., 10, 41, 1987
Mogi, K. Conscious. Res. Abstracts, Elsinore, Denmark, 42, 1997
Pribram, K.H. Brain and Perception, Lawrence Erlbaum Assoc. Hillsdale, New Jersey, 1991
Winkler, F.G. Conscious Res. Abstracts, Elsinore, Denmark, 35, 1997
Scott, A., J.Consciousness Studies, 3, 5-6, 484-491, 1996
Singer, W. Science, 270, 758-764, 1995
Stapp, H.P., J. Consciousness Studies, 3,3,194-210, 1996

Neural encoding: what SR cannot do and what possibly it could do

Donatella Petracchi
Istituto di Biofisica del CNR, Via San Lorenzo 26, 56127 Pisa (Italy)

Stochastic resonance (SR) is a very simple phenomenon that arises in bistable systems under the action of an external periodic perturbation and of their internal noise. The typical example is that of a point mass moving in a double-well potential profile. In the presence of thermal noise, the point moves mainly inside a single well and only occasionally jump from one well to the other, crossing over the energy barrier separating the two states. Let us now apply an external force, periodically tilting the potential profile, but so weak that when applied alone it is unable to cause transitions; nevertheless, its presence modulates the probability of thermal transitions and partially synchronises the jumps on the periodic signal. This system can be thought of and realised as an electric circuit in which the periodic perturbation is the input signal (the stimulus, in physiological terms) and the position on the x axis of the point mass is the output signal. If we consider $x(t)$ as the output signal, we see that the excursion of $x(t)$ is greater in the presence of noise (without noise the motion is confined to the small oscillations inside a single well). Moreover, it is possible to outline in $x(t)$ the periodic perturbation, because the probability of jumping is modulated by the applied force. By spectral analysis it is possible to measure the amplitude of the Fourier component at the stimulus frequency and its ratio to neighbouring components (signal-to-noise ratio, SNR). It is intuitive that when the noise is very small the transitions are very rare and the component at the stimulus frequency is small and very noisy. As internal noise increases (or external noise is added), the signal transmitted to the output (and also the output SNR) increases, because synchronised jumps often occur. Further increasing the input noise eventually results in a damage to the transmission, because transitions occur now so often that they are no more synchronised by the stimulus.

This is what has been called stochastic resonance - the existence of an optimum for the transmission at a given level of the input noise. The name SR in unhappy, since it evokes the features of a real resonant system and leads to a mixing of concepts. It is possible that the name itself (stabat rosa in nomine....) has contributed to some unrealistic expectations. Unmotivated expectations towards SR and more in general towards non linear system can be retraced in some of the hundreds of papers that have been published on SR, mainly in the last four years, particularly in editorial comments [1,2]. The specific expectation on SR has been that this was a method to overcome the traditional methods of linear analysis, allowing to detect signals which are considered undetectable. The

maximum which appears in the curve SNR vs. noise has been "read" as a real improvement of SNR_{out} compared to SNR_{input} and this has kindled the attention on SR. In the early days of SR, an improvement of SNR_{output} over SNR_{input} was measured due to a technical flaw in performing spectral analysis by a computer (computers cannot or do not automatically apply the sampling theorem). The error was quickly identified, but the hope that SR can be the key to solve puzzling problems persists.

For instance SR has often been associated with the issue of the effects on living organisms of weak electromagnetic fields of extremely low frequencies (ELF, 50 Hz) produced by power lines. This is a very controversial issue [3, 4, 5]. The electric field inside a living organism, mainly made of water, due to environment electric or magnetic fields appears so small compared to the thermal noise on the potential across a cell membrane, that it seems impossible to detect it or to be damaged/helped by its effect. Adair [3] claims that in the absence of a very sharp resonance any effect is impossible. Nevertheless, in a very recent debate [5, 6] (on the Nature issue of August '97), the idea that stochastic resonance can be a tool that makes ELF effects possible is discussed.

Another issue often associated with stochastic resonance is the extreme sensitive of sharks and other elasmobranchs to the electric fields due to the respiratory activity of the prey. The minimum field that the fish can perceive is evaluated to 10 nV/cm in the water [7]. and the usually accepted value for SNR is 10^{-7} [8]. Actually this evaluation does not resist to an analysis which takes into account the real anatomical situation [9]. The organ which senses the electric field - the Lorenzini ampulla - has specialised structures: long canals electrically insulated from the surrounding, which report the gradient along the body directly onto the electroreceptors [10]. Thus elasmobranchs use a simple trick to sense the stimulus - they take advantage of the fact that they have an extended body. In the actual anatomic situation, the SNR evaluation increases to 10^{-2} (10^{-3}, if one considers not only the thermal noise but also the additional noise due to the stochastic switching of ion channels). It is still not easy to detect such a signal, but it is not far from possible. Direct evaluation of the rms noise and of the noise bandwidth in the electroreceptors is required for a deeper analysis. It is singular that the astounding evaluation of SNR as 10^{-7} has been accepted and considered as a basis for speculations in the SR community.

It is clear from a very general point of view that it is not possible for any non linear system to overcome the performance of linear analysis. Let us consider an input signal due to the combination of a periodic forcing term and of gaussian noise. A possible definition of gaussian noise is that its power spectrum gives a complete information on it (under the resolution used). A sinusoidal perturbation is also characterised by its amplitude and frequency and the two things combined together allow to say that the power spectrum gives a complete information on the input. Therefore a non-linear

method cannot exist to treat this signal in order to obtain something more - the information obtained by its Fourier analysis is complete. Moreover, analytical calculations of SNR_{output}/SNR_{input} for systems with SR have been reported [11, 12] (Kiss, Bialek) which clearly show how much this ratio is lesser than 1. The recent letter of McClintock and Dykman published in Nature [13] (January 1998) seems to be clear on the fact that there is no hope in this direction.

How strong is the tendency to look for tools overcoming the linear ones in the analysis of signals is however shown by two papers due to L. B. Kiss and coworkers [11, 14]. In these paper the issue of SNR_{output}/SNR_{input} is correctly discussed for signals small compared to the noise. In a second section threshold devices are used to reconstruct a pulse train on which a low noise was superimposed. It is possible to do this by using an extra information on the signal, and it can be done better without using stochastic processes. However, the important point is that a price is to be paid for the resulting improvement of SNR - namely, the absence of information on the input amplitude in the output signal. For instance, if the original pulse sequence was an amplitude-modulated carrier, all the information would be lost in the output signal. This kind of applications actually do not deal with the detection of small signals embedded in noise, but with the use of non linear tools (threshold crossing is an example) to extract features from a pattern - a typical issue for the nervous system.

Once the fact is accepted that SR is not a magic tool for the detection of small signals, the fact persists that SR or more precisely stochastic transmission of information is present in biological systems. Since the first paper revisiting old electrophysiological results on the auditive nerve fibres [15], stochastic encoding or transmission has been found in several systems and at several levels [16-19]. Therefore the problem of the SR role(s) in biology has to be considered.

I just suggest here several possible answers to this problem. Let us consider first the case of ion channel switching. Ion channels are known bistable systems, or possibly multistable systems. The continuous switching from the open to closed configuration and its control by different factors (membrane potential, calcium concentration, chemical transmitters) is the key for the communication of a cell with external world. Let us consider the voltage-gated channels. What happens can be described in the following way: the channels open and close randomly, but the probability of opening/closing is modulated by the membrane potential. If the dependence of the rate constants on the potential is steep (as it can be), openings and closings synchronise on the potential and the number N(t) of channels which are open at time t can vary a lot in a stimulus cycle. Now when a channel is closed there is no current, when it opens the current is V/R, R being the resistance of the channel, considered as an ohmic element. The jump between 0

and V/R can be much higher than the peak-to-peak amplitude of the time-varying component of V/R. Therefore, when the rate constants for the closed-open transitions depend very steeply on the potential, the current flowing through the membrane can be much more modulated than in the case where the channels are constantly open. Indeed, the current is given by N(t)*V(t)/R, while in the second case it is only N*V(t)/R. Obviously this current, even for the optimal value of the internal noise (i.e. of the rate constants), is more noisy than the input signal or of the corresponding current flowing trough an ohmic conductor; however, the peak-to-peak amplitude is greater. Therefore the stochastic mechanism acts as an amplifier enhancing the amplitude of the current flowing through the membrane. Could the same peak-to-peak current be obtained in a different way? The answer is yes - it can be done increasing the channel number. However the channel proteins can be expensive for the metabolism and there are constraints on the number of proteins that can be inserted into the membranes. So there are several possible reasons to prefer the stochastic switching, completely independent of the relative improvement of SNR_{out}. Moreover the proteins have a lot of energetically nearly equivalent states and they switch thermally among these states, so stochastic transmission is ready at hand for cell communication.

A different role that is possible to conceive for stochastic encoding in neural activity is the possibility to transmit information about high frequencies using nerve fibres that cannot go so speedy, as it occurs in auditory system. Moreover stochastic encoding could be simpler to read than the patterns transmitted when deterministic phase-locking occurs.

A last role that it is possible to envisage for stochastic encoding is that it can be the basis of a very elementary mechanism of "attention". If different neural signals are transmitted together through so-called multimodal neurons [20-21], the signals coming from one line can modulate the noise level or equivalently the threshold for firing of a second line. A simple mechanism like this could account in some instances for animal behaviour [20]; as in the case of ion channel switching it could be realised at low cost (without involving specific neural interactions). If however this is actually the case should be checked by specific experiments.

References

1. Glanz, J. 1996. Physicists advance into biology. *Science* 272: 646-648.
2. Tsong, T.Y. 1994. Exquisite sensitivity of electroreceptor in skates. *Biophys. J.* 67: 1367.
3. Adair, R.K. 1991. Constraints on biological effects of weak extremely-low-frequency electromagnetic fields. *Physical Review A*, 43:
4. Weaver, J.C., and R. D. Astumian. 1990. The response of living cells to very weak electric fields: the thermal noise limit. *Science* 247: 459-462.
5. Astumian R.D., R. K. Adair, J.C. Weaver. 1997. Stochastic resonance at the single-cell level. *Nature*, 388: 632-633.
6. Bezrukov S.M., I. Vodyanoy. 1997. Stochastic resonance at the single-cell level (reply), *Nature*, 38: 633.
7. Kalmijn, A.J. 1982. Electric and magnetic field detection in elasmobranch fish. *Science* 218:916-818.
8. Block, S.M. 1992. Biophysical principles of sensory transduction. In *Sensory Transduction*. D. P. Coirey and S. D. Roper, editors. Rockefeller Univ. Press, New York, 1-17.
9. Cercignani G. and D. Petracchi. 1998. A comment on the sensitivity of fish to low electric fields. Submitted to *Biophys. J.*
10. Waltman, B. 1966. Electrical properties and fine structure of the ampullary canals of Lorenzini. *Acta Physiol. Scand.* 66, Suppl. 264:1-60.
11. De Weese M. and W. Bialek. 1995. Information Flow in Sensory Neurons, *Il Nuovo Cimento*, 17D, 733-741.
12. Kiss L.B. 1995. Possible Breakthrough: Significant Improvement of Signal to Noise Ratio by Stochastic Resonance, Proc. of 3th Conf. on Nonlinear Dynamics (AIP press), 1-15.
13. Loerincz K., Gingl Z., Kiss L.B. 1996. A stochastic resonator is able to greatly improve signal-to-noise ratio. *Physics Letters A*, 224: 63-67.
14. Dykman M.I. and P.V.E. McClintock. 1997. What can stochastic resonance do? *Nature*, 344.
15. Longtin A., A. Bulsara, D. Pierson & F. Moss. 1993. Bistability and the dynamics of periodically forced sensory neurons. Biol. Cybern. 70: 569-578.
16. Pei X., L.A. Wilkens and F. Moss. 1996. Light enhances hydrodynamic signaling in the multimodal caudal photoreceptor interneurons of the crayfish. *Neurosphysiol. J.*, 76, 3002-3011.
17. Ditzinger T. and H. Haken. 1990. The Impact of Fluctuations on the Recongnition of Ambiguos Patterns,Biol. Cybern.,63,453-456.
18. Cordo P., J.T. Inglis, S. Verschueren, J.J. Collins, D.M. Merfeld, S. Rosenblum, S. Buckley and F. Moss. 1996. Noise in human muscle spindles, *Nature*, 383: 769-770.
19. Collins J.J., T.T. Imhoff and P. Grigg. 1996. Noise-enhanced tactile sensation, *Nature*, 383: 770.
20. Douglass J. K., L. Wilkens, E. Pantazelou and F. Moss. 1993. Noise enhancement of information transfer in crayfish mechanoreceptor by stochastic resonance, *Nature*, 365: 337-340.
21. Braun, H.A., H. Wissing, K. Schaefer, and M. Hirsch 1994. Oscillation and noise determine signal transduction in shark multimodal sensory cells. *Nature* 367:270-273.

STOCHASTIC RESONANCE IN THE INNER EAR: THE EFFECTS OF ENDOGENIOUS TRANSDUCTION CHANNEL NOISE AND STEREOCILIARY THERMAL MOTIONS ON THE HUMAN HEARING THRESHOLD IN VARIOUS FREQUENCY BANDS

Ilse Christine Gebeshuber*, Juliana Pontes Pinto°, Richardson Naves Leao°, Alice Mladenka* and Frank Rattay*

** TU-BioMed, University of Technology, Wiedner Hauptstr. 8-10/1145, 1040 Wien, Austria*
° Medical School, Federal University of Uberlandia, Brazil

ABSTRACT

A compound model for inner hair cells, focusing on the Brownian motion of the stereocilia, the mechano-electric transduction and the spiking patterns in the primary auditory afferents at several positions along the tonotopical axis is used to reproduce important features of the human hearing threshold for pure tones.

Introduction

In this study we examine the effects of stochasticity in the mechano-electric transduction process (i.e. the transduction of the mechanic sound wave into action potentials) on the ability of the brain to detect low level signals of several frequencies. Without any acoustic input, the spontaneous firing rate in auditory nerve fibers is up to 160 spikes/s (Relkin and Doucet, 1991). The first neural responses at barely threshold intensities appear to be a decrease in spontaneous activity, and phase locking of spike discharges to the stimulus cycle. This is not to say that the fiber will fire in response to every cycle of a near-threshold stimulus. Rather, even though the overall discharge rate may not be significantly greater than the spontaneous level, those spikes that do occur will tend to be locked in phase with the stimulus cycle (Hind, 1972).

The human hearing threshold curve for pure tones is a nonlinear function of frequency. The minimum intensity of a sound wave leading to a perception in the frequency band from 20 Hz to 15 kHz covers about eight orders of magnitude. In the highly sensitive region between 2 kHz and 5 kHz, intensities as small as 10^{-12} W/m^2 are sufficient to evoke sensation (Fig. 1).

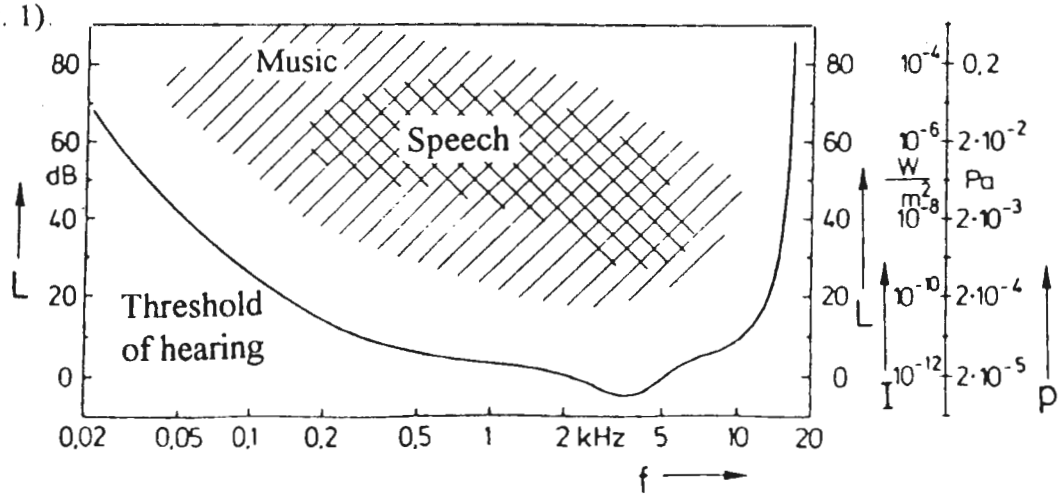

Figure 1: The human hearing threshold curve for pure tones. The intensity is scaled in dB and in W/m², the pressure is scaled in Pa. Note that the pressure coats 7 orders of magnitude, the intensity 14 orders. In the region between 2 and 5 kHz, the hearing threshold is lowest. Adapted from Zwicker, 1982.

Materials and Methods

Some of the sources of stochasticity in the mechano-electric transduction process are (1) the thermal motions of the inner hair cell (IHC) stereocilia, which cause displacements sufficient to open transduction channels and evoke action potentials in the fibers of the cochlear nerve, (2) endogenious transduction channel noise, (3) Ca^{2+} induced neurotransmitter release, which causes jitter in the spiking times (i.e. the fiber does not spike exactly at the same time when the same signal is presented several times, but with a certain normally distributed delay) and (4) the refractory period of the cochlear nerve fibers.

Thermal motions of the IHC stereocilia

The Brownian motion of the tips of the IHC hair bundle is calculated using a reduced version of the model described in Svrcek-Seiler *et al.* The overall displacement x of the hair bundle for stimulation with weak signals is the sum of the bundle movements due to Brownian motion x_{Brown} and the deterministic signal induced displacements x_{det}:

$$x = x_{Brown} + x_{det}, \qquad x_{det} = amp \cdot \sin(\omega \cdot t), \qquad x_{Brown} = \int v_x \, dt$$

$$v_x = \int (-\omega_0^2 \cdot x_{Brown} - \beta \cdot v_x + \frac{rnd}{cint}) \, dt, \qquad rnd = ou(10^{-15}, 0, \sqrt{\frac{2kT}{m} \cdot \beta \cdot cint})$$

where *amp* and ω denote the amplitude and the angular frequency of the stimulating signal, v_x is the velocity of the stereocilary bundle in the physiologically relevant x direction (displacements toward $+x$ result in an increased open probability of the transduction channel, displacements toward $-x$ result in an decreased open probability, in the resting state, about 15 % of the 60 transduction channels are open), $\omega_0 = \sqrt{3C/m}$ (where C, the stiffness of a stereocilium, is measured as the ratio between an external horizontal force applied to its tip and the resulting horizontal tip-displacement) is the undamped angular eigenfrequency, β is the damping constant, *rnd* is a random number (Ohrnstein-Uhlenbeck noise) with zero mean and a standard deviation depending on temperature T, mass m and damping constant β (numerical parameters for the hair bundle taken from Denk *et al.*, 1989), *cint* is the integration step size, set to 10^{-6} s.

The r.m.s. (root-mean-square) value of the intrinsic bundle noise, x_{Brown}, is about 2 nm, the cut-off frequency about 100 Hz. In our simulations, the effects of signal-to-noise ratios from 0.25 to 1 were investigated, this equals stimulation of the hair bundle with pure tones with peak amplitudes between 0.7 and 2.8 nm (i.e. r.m.s amplitudes between 0.5 and 2 nm). The frequencies of the stimulating deterministic signals ranged between 200 Hz and 10 kHz.

Transduction and endogenious transduction channel noise

A model for the mechano-electrical transduction in inner hair cells (Rattay *et al.*, in press) is used to calculate the potential fluctuations in the IHC. The model uses equivalent electric circuits for cell membrane and cytoplasm (RC-components and batteries). The transduction channel kinetics are modeled as a two state Markov processes with no memory (i.e. the probability of the channel being open is only determined by the displacement dependent open probability, and not by the time the channel has already been open or closed). In the resting state, the transduction channel open probability is about 15%, for displacements in range of a few nanometers the relation to the open probability obeys to p_{open}=0.155+0.006x (with x in nm). The channels flickers between the open and closed states and the open and closed time histograms can be fitted by a single exponential. The inner hair cell membrane time constant is τ=0.255ms, therefore the IHC potential is a low-pass filtered picture of the stereociliary displacements with additional noise because of the stochastic components in channel gating.

Spike generating process

A threshold function computes the spiking times in the nerve fibers: A receptor potential change of 0.1 mV, a value which is sufficient for neurotransmitter release in hair cells (Hudspeth, 1989), is assumed to induce the first spike and a jump of the threshold voltage to a high value, followed by exponential decrease to its resting state at 0.1 mV above the resting potential. When the threshold voltage function again crosses the IHC voltage, the next spike arises (Fig. 2). The time constant of the threshold curve is adjusted to reproduce the absolute refractory period of the afferents of 0.8 ms, according to the value reported by Javel, 1990. The spiking rate caused by a very weak signal does not exceed the spontaneous rate but the nerve impulses become with increasing signal strength more and more phase-locked to the maxima of the acoustic input, i.e. with increasing signal-to-noise ratio the spiking pattern becomes more regular (see Gebeshuber *et al.*, in press).

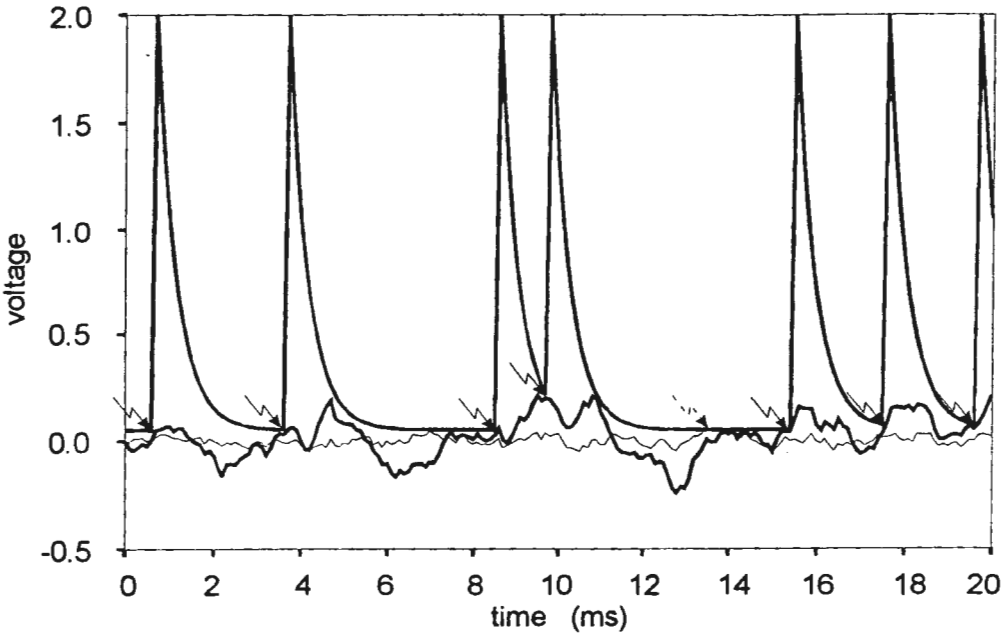

Figure 2: Simulated receptor potential changes and resulting firing behavior. The noise in the voltage fluctuations evoked by a weak 500 Hz signal alone (thin line, hypothetical case without Brownian motion) is because of the endogenious transduction channel noise. Only in one case (marked by dashed arrow at 13.5 ms) those fluctuations are large enough to reach the threshold of spiking at 0.1mV. The compound fluctuations caused by sinusoidal tone + thermal fluctuations with a signal-to-noise ratio of 0.2 show the enhancing effect of the noise: 7 spikes occur within 20ms, they are distributed to connecting auditory nerve fibers. The recovery behavior after spiking is modeled by an exponential decay of the threshold curve: As soon as the voltage fluctuations cross the threshold curve again, a new spike can occur.

Results

The distances between the peaks in the interspike interval histograms (ISIHs) are closely related to the period duration of their stimuli: with increasing signal-to-noise ratio (SNR), the ISIH becomes gradually more regular, i.e. finally the time between the peaks of the histogram is equivalent to the period duration. Figure 3 shows the ISIHs for one nerve fiber connecting to an IHC in the 2 kHz region of the cochlea for a signal presentation time of 1 s (100 spikes) and signal-to-noise ratios of 0, 0.25, 0.5 and 1. Because for pure tones, frequency information in auditory nerve fibers is coded via phase-locking, we took the number of spikes occurring in the first halves of multiples of the period duration as a measure of information contained in the ISIH (informative spikes).

The percentage of informative spikes for the 2 kHz signal is calculated as follows: the half of the period duration is 0.25 ms, therefore the spikes occurring at times between 1 and 1.25 ms, between 1.5 and 1.75 ms, between 2 and 2.25 ms, etc. are added and their percentage (in this case, 70% of informative spikes) of the total number of spikes in the ISIH is calculated. This gives the data point for signal-to-noise ratio 1 at 2 kHz in Figure 4, which shows the percentage of informative spikes for signal frequencies of 200 Hz, 500 Hz, 1, 2, 5 and 10 kHz and signal-to-noise ratios of 0.25, 0.5 and 1 for a single nerve fiber and a signal presentation time of 1 s (100 spikes). Even for noisy signals, the number of informative spikes is highest in the 2 kHz regime. Compare to Figure 1, but note that Figure 4 is in semi-logarithmic scale.

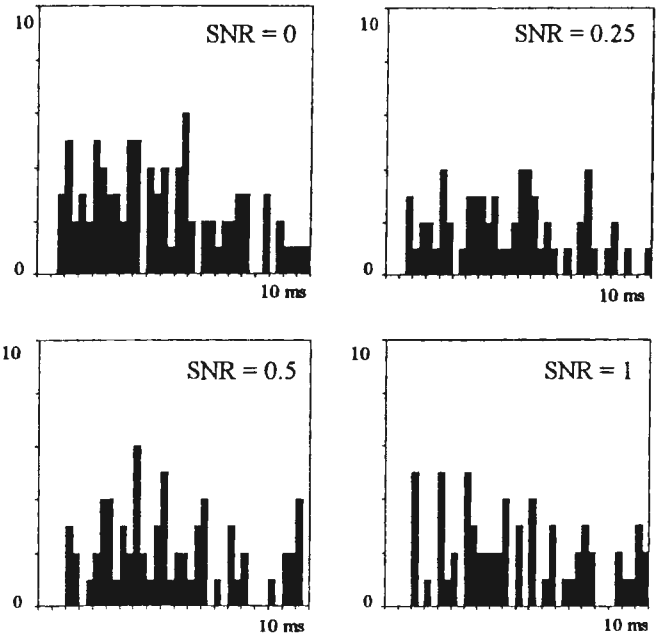

Figure 3: Interspike interval histo grams for a stimulus frequency of 2 kHz and signal-to-noise ratios of 0 (no signal present), 0.25, 0.5 and 1 of a highly sensitive nerve fiber in the 2 kHz region of the cochlea. Multiples of period duration (0.5 ms) are marked with tics at the horizontal axis. The bin width is half the period duration (0.25 ms). With increasing SNR, the pattern of the histogram becomes more and more regular, i.e. the high bins tend to coincide with the first halves of multiples of the period duration.

Discussion

Figure 4 roughly reproduces the human hearing threshold curve for pure tones (see Fig. 1). Note that the 2 kHz signal contains even for weak signal-to-noise ratios a high number of informative spikes. The stochastic displacements because of the Brownian motion of the stereocilia enhance especially in this frequency range the information contained in the spiking pattern.

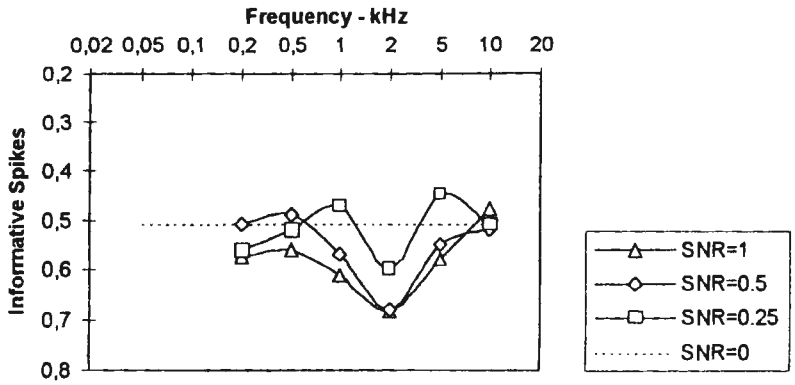

Figure 4: Percentage of informative spikes for different signal-to-noise ratios and frequencies.

Ongoing investigations take into account the IHC innervation density of a normal human cochlea, which is a nonlinear function of frequency (i.e. of the position of the IHC in the tonotopically arranged cochlea). In the frequency region between 0.7 kHz and 1.7 kHz, the innervation density reaches its maximum of about 15 nerve fibers per IHC (Spoendlin et al., 1989), therefore for the same signal presentation time the number of informative spikes will be multiplied. Taking into account the in this study neglected jitter in the firing times (i.e. the fact that spikes occur not immediately after crossing the threshold curve, but with a certain normally distributed time shift with variance of about 50 μs) reproduces the steep slope in the high frequency regime of Fig. 1, since for frequencies above 5 kHz the jitter destroys the phase-locking effects, and therefore the information about the high frequency signal can only be detected by an increased spiking rate in the afferent nerve fibers coming from a certain region in the cochlea.

Further studies should take into consideration the varying patterns of the Brownian motion of the stereocilia which change along the tonotopical axis and which might be tuned to the enhancement of frequencies according to the tonotopical position of the IHC, the adaptation process of the transduction channel kinetics and the stochastic resonance phenomena recently demonstrated (Jaramillo, personal communication) in the transduction channels and in the Ca^{2+} channels in the basolateral IHC membrane.

References

Denk W., W.W. Webb and A.J. Hudspeth (1989) „Mechanical properties of sensory hair bundles are reflected in their Brownian motion measured with a laser differential interferometer." Proc. Natl. Acad. Sci. USA 16, 5371-5375

Gebeshuber I.C., A. Mladenka, F. Rattay and W.A. Svrcek-Seiler (in press) „Brownian motion and the ability to detect weak auditory signals." in Chaos and Noise in Biology and Medicine (Ed: C. Taddei-Ferretti) World Scientific, Singapore

Hind J.E. (1972) „Physiological correlates of auditory stimulus periodicity." Audiology 11, 42-57

Hudspeth A.J. (1989) „How the ear's works work." Nature 341, 397-404

Javel E. (1990) „Acoustic and electrical encoding of temporal information." in Cochear implants - Models of the electrically stimulated ear (Eds. J.M. Miller and F.A. Spelman) Springer Verlag New York, 247

Rattay F., I.C. Gebeshuber and A.H. Gitter (in press) „The mammalian auditory hair cell: a simple electric circuit model." J. Acoust. Soc. Am.

Relkin E.M. and J.R. Doucet (1991) „Recovery from prior stimulation. I: Relationship to spontaneous firing rates of primary auditory neurons." Hear. Res. 55, 215-222

Spoendlin H. and A. Schrott (1989) „Analysis of the human auditory nerve." Hear. Res. 43, 25-38

Svrcek-Seiler W.A., T. Biró, I.C. Gebeshuber, F. Rattay and H. Markum (accepted) „Micromechanical Models for the Brownian Motion of Hair Cell Stereocilia." J. Theor. Biol.

Zwicker E. (1982) Psychoakustik (in German). Springer-Verlag, Berlin · Heidelberg · New York (Hochschultext), 34

Non-linear dynamics and biological neuronal ensembles: application of Chaos Theorie to analysis and modelling.

Claudia Mongini und Helmut Pockberger
Institut für Neurophysiologie, Universität Wien; Währingerstr. 17 A-1090 Wien - Tel: 43 1 40480 616(624)
email: Helmut.Pockberger@univie.ac.at

Introduction:

With the continuous development in the theory of non-linear dynamcis and it's application to new algorithms it became feasible to investigate the nature of data-sets as e.g. intracellular recordings of nerve cells or EEG. In the past several attempts have shown that such approaches can be fruitful. In this paper we present an example of how activities of single neurons can be described within the frame of non-linear dynamics, and how such an analysis can be used for model prediction. The overall aim of such an approach is, of course, a better understanding of neuronal activity under certain conditions. This asks for a feasible model which simple enough allows simulation of neuronal activity on the one hand and controlling of activity on the other hand.

Epileptic activity represent an extreme case of neuronal activity. It is brought about by an imbalance of excitation and inhibition. Under physiological conditions the dynamics of excitatory and inhibitory phenomena holds the system - i.e. the neuronal network - in a metastable state with many degrees of freedom. Such high dimensional systems can hardly be treated by with current methods of non-linear analysis. Under epileptic conditions however the dimensionality is drastically reduced. This makes an approach as the one chosen by us more feasible from a mathematical point of view.

Experimental data collection and analysis:

The data sets presented herein stem from various experiments done in so-called hippocampal slice preparations. This methods allows long-term intracellular recordings on the one hand and manipulation of the environment on the other hand. Epileptic activity was induced by adding 100 µMol bicuculline to the perfusion medium. Bicuculline inhibits GABAergic inhibitory synaptic transmission thereby inducing hyperexcitability. Under proper experimental conditions this leads to nervous activity well comparable to the one observed in temporal lobe epilepsy. In general one distinguishes preseizure (interictal) and seizure activity. Pre-seizure activity is characterized by more or less regular burst discharges of single neurons. Seizure activity consists of rhythmic membrane potential oscillations with superimposed action potentials.

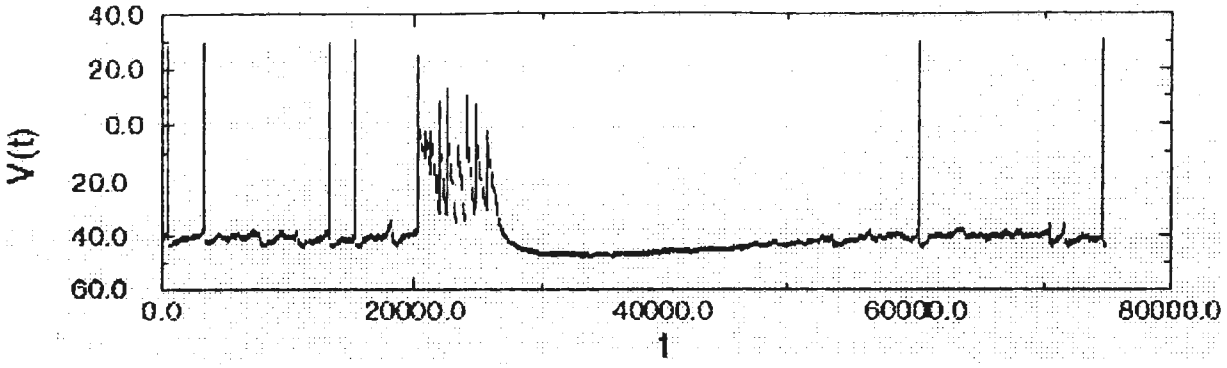

Fig. 1: Membrane potential of a CA1 hippocampal pyramidal neuron under epileptic conditions - from point 20000 onwards a short seizure is seen.

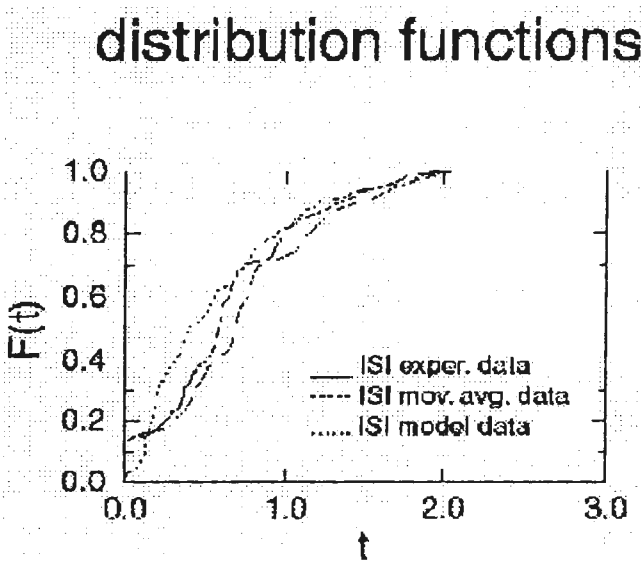

Fig. 2: Comparison of interspike interval (ISI) analysis or experimental data and model data.

Non-linear analysis of both types of activity was commenced using standardized methods - e.g. reconstruction of the attractor from the time series, calculation of the correlation integral by the Grassberger-Proccacia algorithmus. This, however, turned out to be less useful than other methods, which inspect the dynamics within the attractor space and thus allowed prediction about future behavior of the system. For that we applied the Farmer-Sidorowitch algorithm, which is more suitable for our data than the calculation of Lyapunov exponents. Thus we were able to demonstrate non-linear recurrent activity, which served as a starting point for our modeling approach.

Modeling:

For modeling pre-seizure activity we considered the Fitzhugh-Nagumo model as a starting point.

$$\varepsilon\, dv / dt = v(v - 0.5)(1 - v) + w - a - \eta$$
$$dw / dt = v - w - b$$
$$d\eta / dt = \lambda\eta + \lambda\xi$$

where z(t) is Gaussian white noise (this last equation was added following the method of Longtin). It consists of two coupled differential equations related to the Hodgkin-Huxley equations. This model is not intended to be an accurate model of spike activity, in the sense of reproducing the shape and amplitude accurately. It intends rather to exhibit as clearly as possible those basic dynamic relationships between the variables of state which are responsible for the properties of threshold, refractoriness, and finite and infinite trains of impulses. For our purpose we modified these equations, so we could reproduce the distribution if interspike intervals (ISI) of experimental data.

$$dv / dt = 200 * (v(v - 0.5)(1 - v) + w - 1/6\sqrt{12} - \eta)$$
$$dw / dt = b$$

b is the distribution function of ISI under experimental conditions.

The ISI function can be varied either by using a fixed spiking threshold and varying the function that regulated the velocity by which the threshold is reached, or by varying the spike threshold itself. We implemented both methods: In the first case we obtained strong oscillations of the resting membrane potential (this was not observed n our experimental data). In the second case a high proportion of background noise due to the variation of spike threshold dominated.

We assume that a combination of both types exist, so that the variation from e.g. pre-seizure to seizure activity can be reduced to a variation of either membrane noise level or characteristic membrane oscillations.

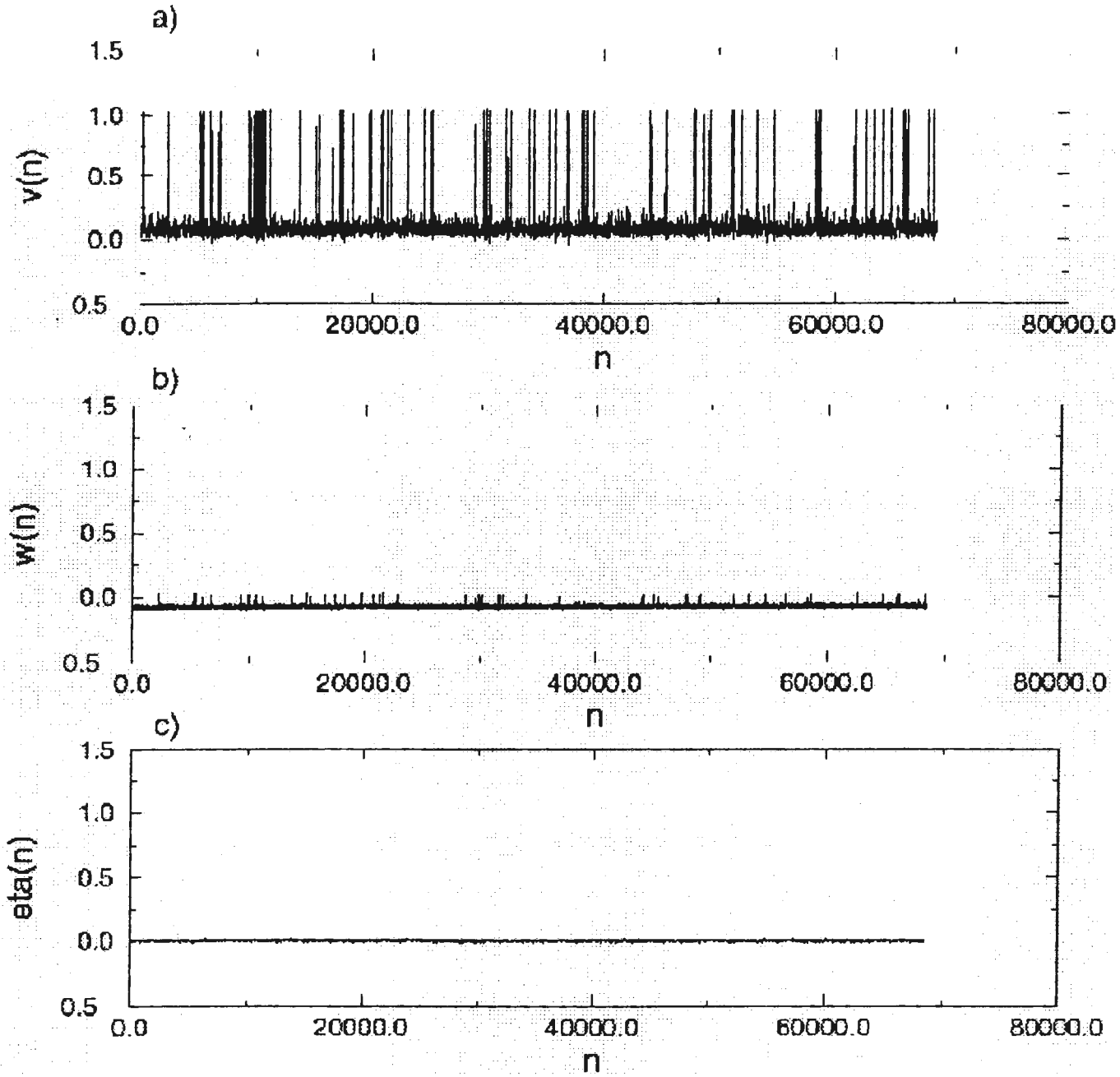

Fig. 3: Simulation of pre-seizure activity by the method of spike threshold variation: a) time series of membrane potential, b) threshold function and c) colored noise.

References:

Farmer J.D. and Sidorowitch J.J. (1987) Predicting chaotic time series Phys.Rev.Lett. 95, 845-848

Fitzhugh R (1961) Impulses and Physiological States in Models of Nerve Membrane. Biophys.J. 1, 445-466

Hodgkin A.L. and Huxley A.F. (1952) A quantitative description of membrane current and ist application to conduction and excitation in nerve. J. Physiol. 117, 500-544

Longtin A. (1993) Stochastic Resonance in Neuron Models. J.Statist.Phys. 70, 309-327

Theiler J., Eubank S., Longtin A. Galdrikian B. and Farmer J.D. (1992) Testing for nonlinearity in time series: The method of surrogate data. Physica D 58, 77-94

Spike Propagation in Aplysia Neurons

Alexander Staenke, Frank Rattay, Harald Markum,
Max Zartl and Jörg Hoyer
Email: e9025656@fbma.tuwien.ac.at

Introduction

In neurons action potentials (APs) are responsible for the transport of information along the axon. The frequency of the APs, respectively the interval between APs encodes this information. Therefore changes of the interval between axonal spikes alter the information contained in a train of APs. A prerequisite for a constant interval between subsequent APs, when propagating along an axon, is an identical conduction velocity (CV).

Different CVs of APs change the interval during propagation, and change herewith the encoded information. Waxman and Swadlow (1976) reported, that a single AP is followed by a sequence of events, influencing excitability and CV of neurons: 1) relative refractory period - 2) supernormal period with accelerated CV - 3) subnormal period which causes a decrease of conduction velocity.

In various experimental settings an alteration of CV could be shown for subsequent APs during repetitive firing. For the central nervous system an activity dependent change of CV has been demonstrated in visual callosal axons of the rabbit (Swadlow and Waxman, 1978), and in the parallel fibers of the rat cerebellum (Kocsis et al., 1983). Furthermore in human peripheral nerves the latencies of compound APs were also determined by the history of prior activity (Potts et al., 1994).

Experiment

For the experimental approach of our investigations we used the giant neurons of the marine snail Aplysia californica. In this preparation APs can be registered using intracellular recordings from single identified neurons, independent from the stimulation procedure.
CV was measured by simultaneous intracellular recordings from the somata and axons of cells R-2 and Pl-G (Frazier et al., 1967; Kehoe, 1972). A third electrode impaled into the cell soma provided intracellular electrical stimulation. Herewith it was ensured that stimulation took place at one end of the distance between the recording electrodes.

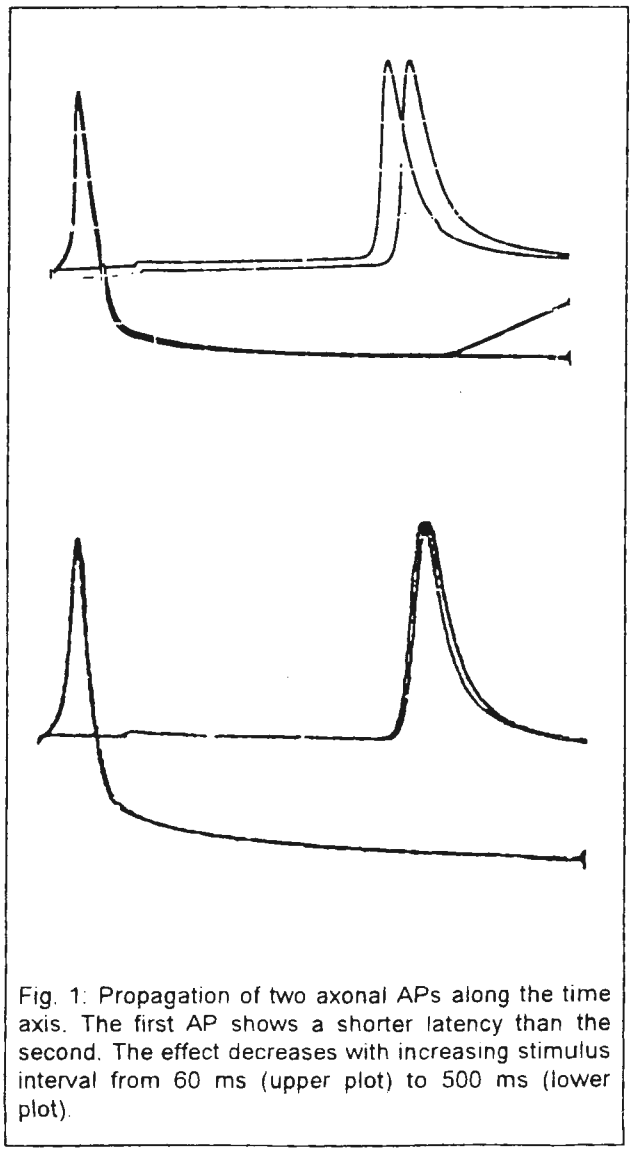

Fig. 1: Propagation of two axonal APs along the time axis. The first AP shows a shorter latency than the second. The effect decreases with increasing stimulus interval from 60 ms (upper plot) to 500 ms (lower plot).

In our experiments the distance between the two electrodes varied between 3 and 45 mm. CV was determined from the distance between the two electrodes and the time interval between the APs registered from the two electrodes. The measurement of CV was not influenced by time lacks between stimulus and AP-initiation. This advantage is only given for the giant snail neurons, but not for neurons of vertebrates, as used in the above cited investigations.

We were able to show that in neurons of Aplysia repetitive stimulation elicits an activity dependent depression of CV. In each single experiment CV was constant under control conditions. Depending on the experimental setup, it varied in different experiments from 0.75 to 1.1 m/s. Repetitive stimuli with an interval from 60 ms upwards were used to produce a train of APs. This range corresponds to the subnormal period in Waxman and Swadlow (1976). With an interval of the stimulus from 60 ms to 1000 ms we registered a reduction of CV of a succeeding AP, compared to the CV of an AP under control conditions. The reduction of the CV depends on the interval of stimuli, up to 6.7% for a 60 ms interval, decreasing to 0 % at 1000 ms (Fig. 1). Using trains of stimuli with constant intervals, the reduction of CV is identical for the second and all succeeding APs (Fig. 2). This indicates, that the process responsible for reorganisation of the disturbancies caused by a conducted AP is not interrupted by an additional AP and no summation takes place.

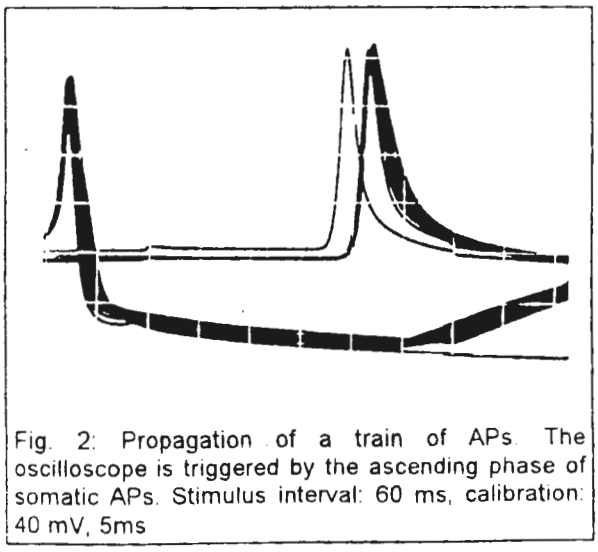

Fig. 2: Propagation of a train of APs. The oscilloscope is triggered by the ascending phase of somatic APs. Stimulus interval: 60 ms, calibration: 40 mV, 5ms

Modeling

To simulate the neuron we used a model which consists of two main parts. Part one being the soma and part two the axon. For the soma the model for R-15 has been used (Canavier et al., 1991). The soma was modeled as a sphere with a diameter of 250 µm. Included in the model are the ionic currents responsible for the fast dynamics of the APs as well as pump, exchanger and background currents, that contribute to the slow dynamics of the membrane voltage. Under space clamp conditions the differential equation describing the time-dependant changes in the membrane voltage V is:

$$C_m \frac{dV}{dt} = -(I_{Na} + I_{Ca} + I_{Sl} + I_{NS} + I_K + I_R + I_L + I_{NaCa} + I_{NaK} + I_{CaP} - I_{stim})$$

The fast sodium current I_{Na}, the fast calcium current I_{Ca} and the delayed rectifier are modeled as voltage gated ionic currents. The slow calcium current I_{Sl} and the non specific cation current I_{NS} are also voltage gated but include a calcium concentration dependent term as well. The remaining currents are either background currents (instantaneous) or pump currents. While R-15 is able to produce bursting activity, R-2 is not. Therefore we had to eliminate this feature in the model which was accomplished by setting the slow calcium current I_{Sl} to zero.

The second part of the model is the axon. To simulate an Aplysia axon of 0.9 cm length and diameter d = 35 µm we used a compartment model that consists of 90 elements each of which has a length of Δx = 0.01 cm. The resistivity ρ_a of the axoplasm was assumed as 0.1 kΩcm and membran resistivity ρ_m was set to 2 kΩcm^2. Ionic currents in each of the compartments were calculated with the Hodgkin-Huxley equations. For the Hodgkin-Huxley equations and for details on the compartment model see Rattay (1998) in this volume.

Simulation

In the simulation the soma was a stimulated with a 250 nA current that lasted for 10 ms. The first current pulse started after 300 ms and the stimulus interval was set to 80 ms so that the succeeding pulses started after 390 ms and 480 ms. APs were generated in the soma and propagated along the axon. Fig. 3 shows the APs corresponding to the three current pulses in compartment number 20 of the axon. It can be seen that the time interval between all three APs is constant and therefore they all have the same CV. Several simulation runs with different stimulus intervals had no influence on the CV. This result of the computer simulation is in contrast to the effect that was found experimentally.

Discussion

The time dependent change of membrane voltage in the n-th compartment is given by

$$C_m \frac{dV_n}{dt} = -I_{ionic,n} - I_{ohmic,n}$$

The voltage change in the n-th compartment depends on the ionic current that runs across the membrane and on the ohmic current that runs along the axon. In the model all ionic currents are described by the Hodgkin-Huxley equations and are relativley fast, typically in the range of several milliseconds (comp. Fig. 4). After an AP occurs the membrane voltage returns to its resting state in about 8 to 10 ms. In the Aplysia axon there seems to be a very slow potassium current which we think is responsible for the decrease of CV. Since this current is not modeled in the Hodgkin-Huxley equations a modification might be necessary to obtain a correct description of all processes in the neuron.

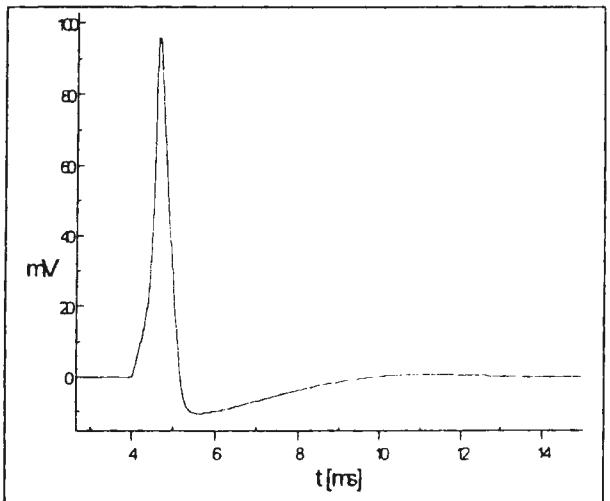

Fig. 4: Time structure of a typical AP from the Hodgkin-Huxley equations.

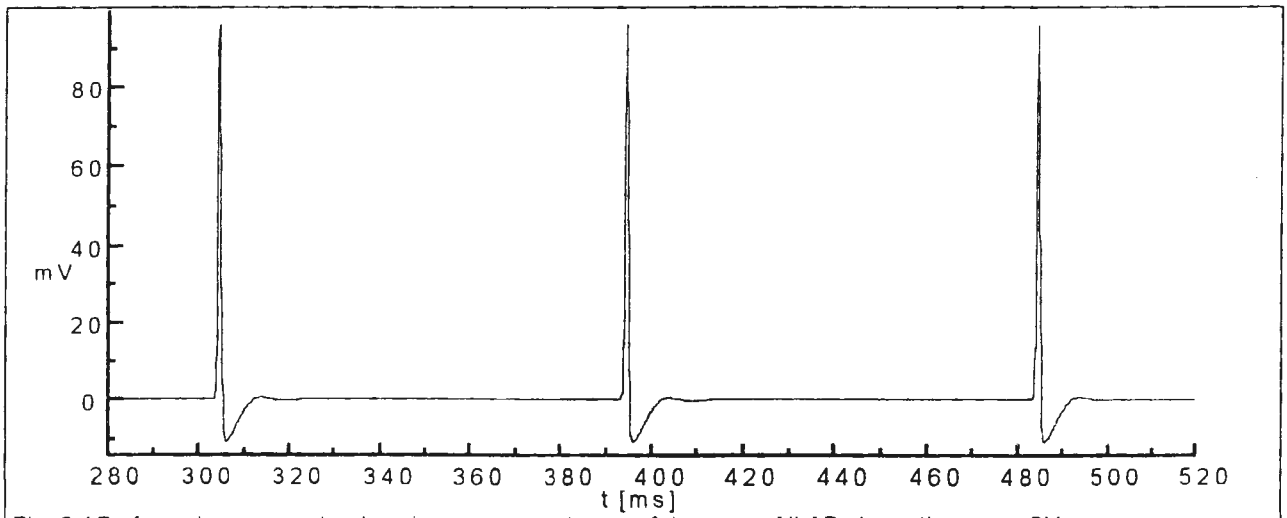

Fig. 3 APs from three current pulses in one compartment of the axon. All APs have the same CV.

Conclusion

Experiments with the neuron R-2 and P-IG of the Aplysia snail find a decrease in CV of subsequent APs during repetitive firing. The decrease disappears when the stimulus interval of the injected current becomes about 1000 ms. The aim of this investigation was to simulate this effect with a model neuron. The experimental situation could not be reproduced by the computer simulation. The description of the ionic currents given by the Hodgkin-Huxley equations is obviously not sufficient to produce the effects observed in the experiment. In further research one can try to add an additional gating mechanism with slow dynamics to account for the processes with the large time constant found in the Aplysia neuron.

References

Frazier, W. T., Kandel, E. R., Kupfermann, I., Waziri, R., Coggeshall, R. E., 1967. Morphological and functional properties of identified neurons in the abdominal ganglion of Aplysia californica. J. Neurophysiol., 30:1288-1351.

Kehoe, J. S., 1972. Three acetylcholine receptors in Aplysia neurons. J. Physiol., 225:115-146.

Kocsis, J. D., Malenka, R. C., Waxman, S. G., 1983. Effects of extracellular potassium concentration on the excitability of the parallel fibers of the rat cerebellum. J. Physiol. 334:225-244.

Potts, F., Young, R.,Shefner, J. M., 1994. Long lasting excitability changes in human peripheral nerve. Muscle & Nerve 17:74-79.

Swadlow, H. A., Waxman, S. G., 1978. Activity dependent variation in the conduction properties of central axons. Physiology and Pathophysiology of Axons. Raven Press, New York.

Waxman, S. G., Swadlow, H. A., 1976. Morphology and physiology of visual callosal axons: evidence for a supernormal period in central myelinated axons. Brain Research 113:179-187.

Canavier, C. C., Clark, J. W., Byrne J.H. 1991. Simulation of the Bursting Activity of Neuron R15 in Aplysia. J. Neurophysiol. 6: 2107-2124.

Rattay, F. 1990. Electrical Nerve Stimulation. Springer. Wien - New York

Modeling the Electrical Excitation of the Mammalian Auditory Nerve

Vincent Stüger, Frank Rattay and Petra Lutter
Vienna University of Technology
Email: e9025588@fbma.tuwien.ac.at

Introduction

The behavior of the electrically stimulated auditory nerve has been studied by many researchers in the last 30 years. The electrical stimulation of auditory nerve neurons is used to restore hearing sensations to patients with profound sensorineural hearing loss. Cochlear implants are effective in helping these profoundly deaf people regain some degree of hearing. While the potential efficacy of an implant is very high, it remains challenging to accurately predict its actual usefulness in any particular patient. In addition, the neural mechanisms by which an implant provides acoustic information to the central auditory system are not well known. Now that measurement techniques to record human nerve responses have been improved considerably, an attractive experimental counterpart opens up.

Not all the effects measured in the electrically stimulated primary auditory nerve by neural response telemetry are well understood today, as for example the double peak phenomenon seen in the cochleogram (Diller et al., 1997, Rattay, 1998). In order to get a better understanding of these phenomena, we focused on the development of a detailed nonlinear model of the mammalian auditory neuron, consisting of several coupled nonlinear compartments.

The Model

The auditory nerve fibers provide a direct synaptic connection between the hair cells of the inner ear and the cochlea nucleus. The large majority of the auditory neurons innervate the inner hair cells. These neurons are myelinated and bipolar and have their cell bodies located in the spiral ganglion. The mathematical model consists of compartments for dentrite, axon, soma, nodes, internodes and hillock.

The voltage sensitive membrane was modeled using the Hodgkin and Huxley equations (1952), adjusted for mammlian membrane characteristics. The Hodgkin and Huxley model reflects important experimental phenomena such as multiple spiking and a chronaxie value of about 340 μs (Colombo and Parkins, 1987).

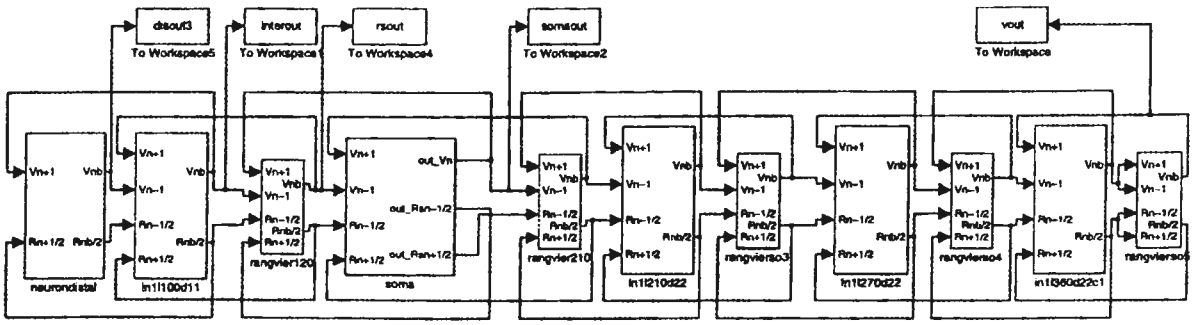

Fig 1: This figure illustrates the block structure of the human primary auditory nerve Matlab model. The connections between the blocks are defined by lines.

Every compartment has its individual geometrical and electrical parameters. The current of the n-th compartment consists of a capacitive component, ion currents aross the membrane and ohmic currents to the

left and right neighbors (Rattay, 1990, 1998).

A model of a primary auditory neuron was built using Matlab™ 5.0 and Simulink™ 2.0. The block oriented programming structure of Simulink™ is very helpful in building up a compartment model, because each compartment can be represented by a single block. These blocks can be combined in different ways. It is therefore rather simple to change the model structure or to exchange, for example, the type of ion channel equations used in a certain part of the neuron.

The model was also optimized for fast computation, which allows to compute the models response to signals up to 500 *ms* in a tolerable time period.

Modeling the soma makes the difference

The morphological data of the auditory neuron in human beings and animals differ considerably. (see Fig. 2) While the soma of the human auditory neuron is covered by two satellite cells only, the soma of almost all animals is isolated by several layers of satellite cell membrane. This causes different reactions in the somatic region. The spike propagation of a cat's neuron (Liberman et al., 1984) was compared to the one of a human neuron (Felix et al., 1997). The neuron was excited by a rectangular pulse injected into the initial region of both neurons. The spike propagation in the dentritic region was similar. In the somatic region of the human auditory neuron the transmission velocity was considerably reduced. Much of the spike's current is needed to load the capacity of the soma. Therefore, two phenomena can be seen. First, a spike can be canceled at the soma, if its current is too small or if two spikes follow one another in a short time interval. Secondly, the transmission velocity over the soma is reduced. There is a time difference of about 300 μs between the pre- and post- somatic spike (Fig. 3). In order to show the influence of the number of myelin layers on the propagation velocity, the number of myelin layers covering the cat's soma was changed (Fig. 4). By reducing the number of myelin layers, the time difference between the pre- and post somatic spike increases.

In the human auditory neuron another interesting phenomenon can be observed. A small portion of the time delayed somatic spike runs back to the dentrite region. So even in the dentride a double peak can be recognized, even the second current peak is much weaker than the original spike (Fig. 3).

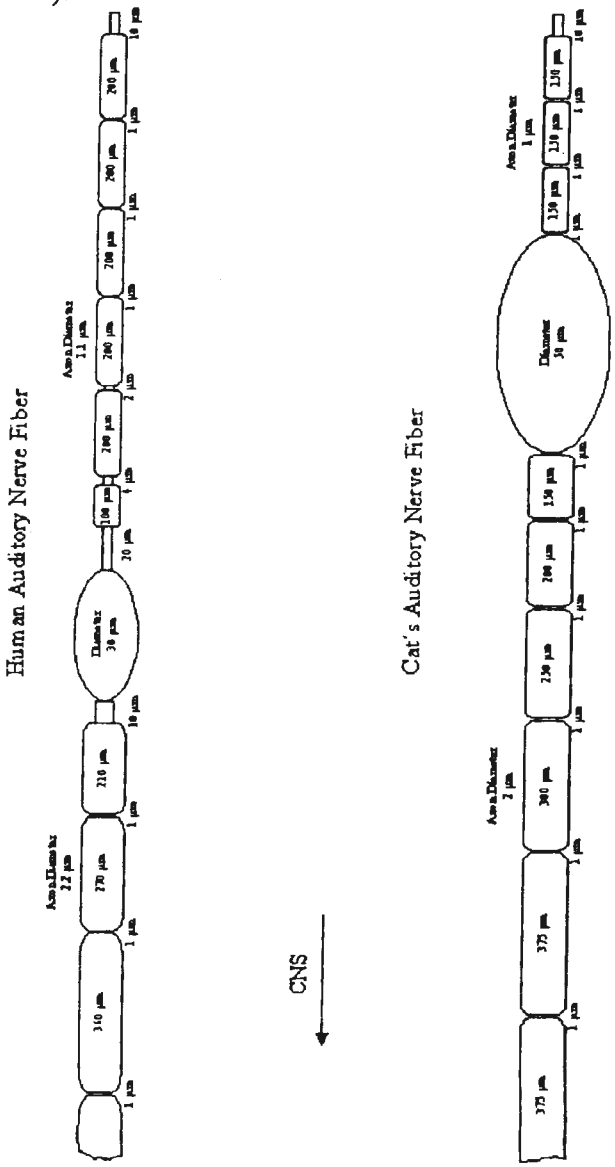

Fig. 2: Schematic picture of a primary human auditory neuron (Felix et al., 1997) and cat's auditory neuron (Liberman et al., 1984).

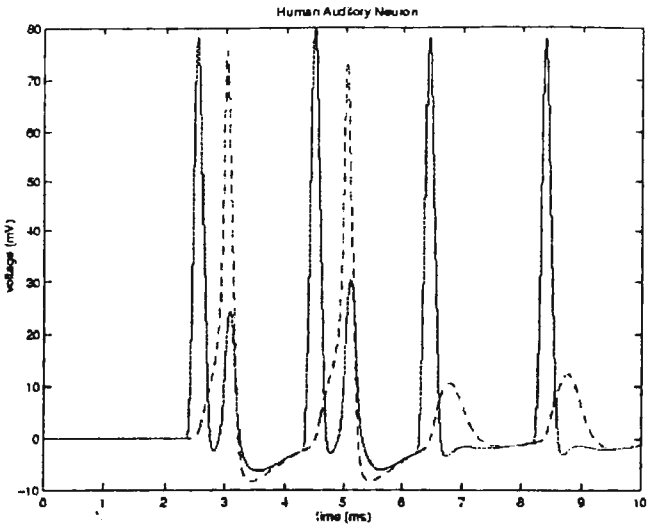

Fig. 3: Response of a human auditory neuron to injected rectangular stimulus of 530 Hz. The time delay between the pre- and post somatic spike is about 300 μs. The stimulus frequency is also slightly above the critical frequency of 500 Hz, at which all spikes pass the soma. Note that a small amount of the postsomatic current travels back along the dendrite.

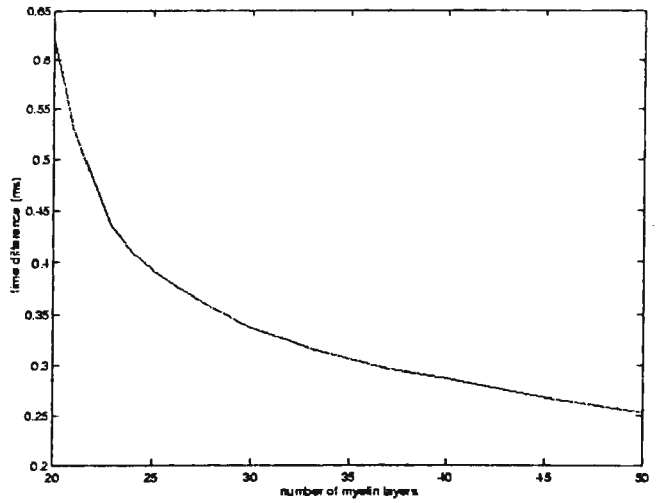

Fig. 4: Time delay at the soma as function of the number of myelin sheets. A better isolated soma makes the transmission faster and allows higher spiking frequencies to pass the soma.

The extracelluar stimulation of the human auditory neuron.

In a first approach, we assume quasi stationary potential distribution in a homogeneous extracellular medium. The influence of the extracellular potential on the n-th compartment is given by the so-called "activating function" (Rattay, 1990, 1998).

$$f_n = \left[\frac{V_{e,n-1} - V_{e,n}}{R_{n-1}/2 + R_n/2} + \frac{V_{e,n+1} - V_{e,n}}{R_{n+1}/2 + R_n/2} \right] \Big/ C_{m,n}$$

By the assumption of a homogeneous extracellular medium, the extracellular potential can be calculated by

$$V_e = \frac{\rho_e I_{electrode}}{4r\pi}$$

where r is the distance to the center of the electrode, and ρ_e is the extracellular resistivity.

The results of the computer simulation show, that even small changes in the electrode position can have a great influence to the point of spike generation. For more accurate results a computation of the inhomogeneous potential distribution will be done. The complex geometry of the cochlea, with several areas of different conductivity is expected to have some influence to the point of spike generation (Fig. 5).

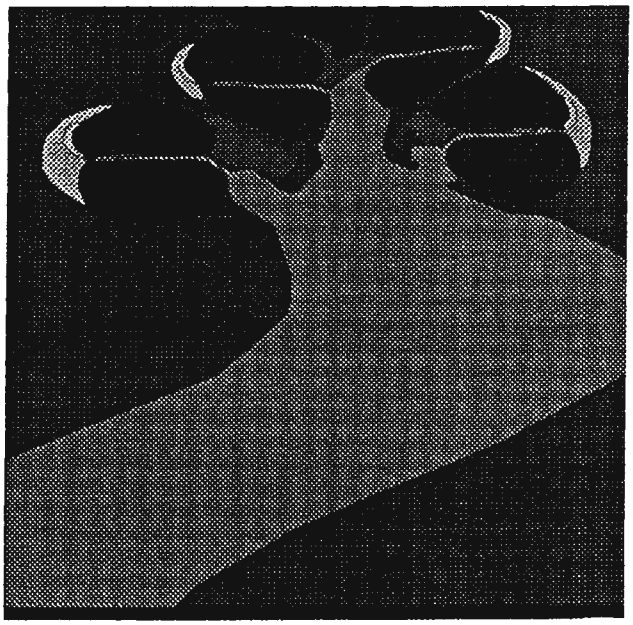

Fig. 5: Cross section of a human cochlea illustrating the complex geometrical properties.

References

Colombo J. and Parkins C.W., 1987: A model of the electrical excitation of the mammalian auditory nerve neuron. *Hearing Research* 31, p. 287-312.

Diller N., Lai W.K, Wyttenbach M., Jakits H., Spillman T., Linder T. and Frisch U., 1997: First experiences with neural response telemetry (NRT). Report ENT Department University Hospital Zürich.

Felix H., Gleeson M.J, Polak M., Johnson L.G: The Cochlear Neurons in Humans. Progress *in Human Auditory and Vestibular Histopathology.* Amsterdam/ New York, 1997, 73-79

Hodgkin A.L and Huxley A.F, 1952: A quantitative description of membrane current and its application to conduction and excitation to conduction and excitation in nerve. *J. Physiol.* 117, 500-544

Liberman C.M. and Oliver M.E., 1984: Morphometry of Intracellularly Labeled Neurons of the Auditory Nerve: Correlations With Functional Properties. *J. of comparative Neurology* 223, p. 163-176.

Parkins C.W. and Colombo J., 1987: Auditory-nerve single neuron Thresholds to electrical stimulation from scala tympani electrodes. *Hearing Research* 31, p. 267-286

Rattay F., 1990: *Electrical Nerve Stimulation.* Springer, Wien – New York.

Rattay F., 1998: Simulation of neural excitation with compartment models. (this volume)

Rattay F., 1998: The contribution of a single neuron to the EEG signal – an attempt to explain the cochleogramm. (this volume)

Stüger V., 1996: Hearing into the Auditory Nerve of Cochlea Implant Persons by Computer Simulation. Diploma Thesis, TU Wien.

Appendix

Human Auditory Nerve Fiber	Cat's Auditory Nerve Fiber
Distal Fiber: Diameter: 1 μm Internodes: passive membrane 40 layers of myelin Nodes: active membrane HH-equations adjusted k=12 10 times channel density	Distal Fiber: Diameter: 1 μm Internodes: passive membrane 40 layers of myelin Nodes: active membrane HH-equations adjusted k=12 10 times channel density
Soma: Diameter: 30 μm passive membrane 5 layers of satellite cells	Soma: Diameter: 50 μm passive membrane 50 layers of satellite cells
Central Fiber: Diameter: 2 μm Internodes: passive membrane 60 layers of myelin Nodes: active membrane HH-equations adjusted k=12 10 times channel density	Central Fiber: Diameter: 1 μm Internodes: passive membrane 60 layers of myelin Nodes: active membrane HH-equations adjusted k=12 10 times channel density

A Flexor and Crossed Extensor Reflexes Model using Neural Networks

Richardson Naves Leão[1], Juliana Pontes Pinto[1], Edilberto Pereira Teixeira[2] and Flávio Pereira Oliveira[2]
[1]Medical School , Federal University of Uberlândia - Brazil
[2]Electrical Engineering Department, Federal University of Uberlândia -Brazil
e-mail: edilbert@ufu.br

Keywords: Flexor Reflex, Crossed Extensor Reflex, Neural Networks

Abstract - We propose an Artificial Neural Network (ANN) model of flexor and crossed extensor spinal reflexes. The ANN architecture was designed regarding the descriptions of spinal circuits from previous articles. To evaluate this model, we used the learning rules of backpropagation. In a first approach, MATLAB was a suitable tool for simulation. The final model was able to interpret the muscle input and process it into an output with a suitable error ratio, approaching to the biological spinal flexor and crossed extensor reflex. The results may be used as a starting point for Functional Electrical Stimulation (FES) application.

Introduction

Unless from the muscles innervated by the cranial nerves, each somatic muscle receives its motor innervation from the spinal cord. The spinal cord plays an important role connecting muscles to the brain. Although, the spinal cord is more than just a connecting organ. It contains complete neural circuits that develop important neural tasks. Some reflexes are generated inside the spinal cord. These involuntary reflexes execute important tasks keeping the tissue integrity. As the neurocircuitry connections are placed inside the spinal cord, they can save time in a fast answer, because they do not depend on complex neural pathways.

The flexor and crossed extensor reflexes (FER) are examples of spinal cord reflexes. The FER are elicited while a painful stimulation is made in skin receptors e.g. burning, cutting or pressuring. If the noxious stimulus occurs in the flexor side, flexor muscles are contracted and they pull the limb. However, in the opposite side, the extensor muscles are activated and the limb movement pushes the subject away from the painful object [2, 7].

The noxious stimulus activates afferent sensitive fibers by skin receptors (thermal, touch etc.) that produce activation of the neuron pool at the posterior horn of the spinal cord. These neurons activate interneurons at the anterior horn, and these ones, produce action potentials in flexor muscles motor neurons - this phenomenon is named flexor reflex. Meanwhile, at the opposite side of the stimulus, other interneurons are activated, producing stimulation in extensor muscles motor neurons and inhibit flexor muscles motor neurons. This action is called crossed extensor reflex.

One of the skin receptors that elicits the FER is the Pacinian corpuscle. These corpuscles are special neural structures composed by a neuron with a sensitive non-myelinated ending surrounded by a capsule of closely packed membranes (lamellae). The Pacinian corpuscles transduce mechanical information into action potentials. The nerve ending is excited just at the onset and the offset of stimulation [1, 3]. In other words, if you apply a triangle stimulus to this corpuscle, only two action potentials will occur: one in the rising phase and another at the decaying phase of the stimulation (fig. 2).

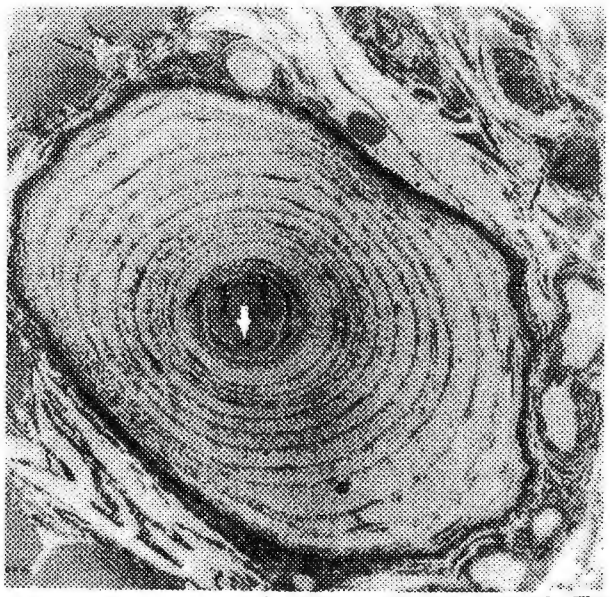

Figure 1. Electronmicrography [100x] of a Pacinian corpuscle. The arrow shows the nerve ending. The fibrous structure surrounding the nerve - the lamella. This structure is responsible for the mechanical interface of this corpuscle. It is found in deep parts of dermis (hypodermis).

The changes in the ionic flux inside the receptor can finally produce action potentials in spinal cord interneurons. According to the firing times the decision of what is noxious or not is made.

In the present paper, a model of the flexor and crossed extensor reflexes is proposed using artificial neural networks (ANN), specifically, the backpropagation algorithm. The input and output parameters are based on previous studies of mathematical models of the Pacinian corpuscle and muscle activity [4, 7].

In humans, several kinds of inputs elicit the reflexes, however, in this paper we will just consider the influence of the pressure in the Pacinian corpuscles. The reasons for this choice is obvious, the Pacinian corpuscles are extensively studied, and the data obtained by animal experiments can predict the behavior of this receptor in human [1].

Methods

The main point of this work is the simulation of the FER using computational methods. Due to the adaptive features of all neuron systems, the processing elements might classify different input patterns in output groups obtained by the behavior of real reflex circuitry found in literature.

ANN are often used to simulate biological neural circuits. To simulate a FER model we have used ANN to decide if an external stimulus was noxious or not. We have used a multilayer perceptron trained by backpropagation. The network classifies the stimulus as painful or not and produces a proportional output to the flexor muscle and the opposite extensor muscle.

The input system

The Pacinian corpuscle produces two spikes per cycle of stimulation after the threshold is reached, i. e. one at the beginning and one at the end of the stimulus (fig. 2) [1, 4]. This characteristic facilitates the simulation because the input that is given to the ANN is not a complex train of spikes.

A group of two Pacinian corpuscle with different thresholds can describe the intensity of the pressure stimulation by the delay of their action potentials (fig. 3). Summarizing, if a minimum pressure variation produces an action potential in a very sensitive Pacinian corpuscle at a time t=0, another Pacinian corpuscle with a higher threshold produces an action potential in a time t>0. The delay determines if the stimulus was noxious or not. Obviously, a sudden variation of pressure means a powerful noxious stimulus.

Eight different slopes of linear (ramp) stimulation were applied to the model. To adapt these curves to the Pacinian corpuscle response, the input data were processed in the transfer function as follow:

$$y(x) = \frac{a}{\pi}[\tan^{-1}(bx - c) + k\pi] \qquad (1)$$

where a = 11, b = 3.795, c = 3.4 and k = 0.41. This equation has been determined by the result of least-squares approximation of the final values of the receptor potential which were generated by decapsulated corpuscles after stimulation with ramps of different slopes [4, 5, 6]. According to Grandori and Pedotti, two others transfer functions should be applied to simulate the frequency characteristics of the corpuscle, however, as just one period of stimulation is applied to the corpuscle, frequency here is irrelevant.

We have used arbitrary units in stead of real units because these data were used just for training. All the data was set just at the simulation time to avoid the error caused by temperature variations and computer performance. The values from the equation 1 represents the ANN input.

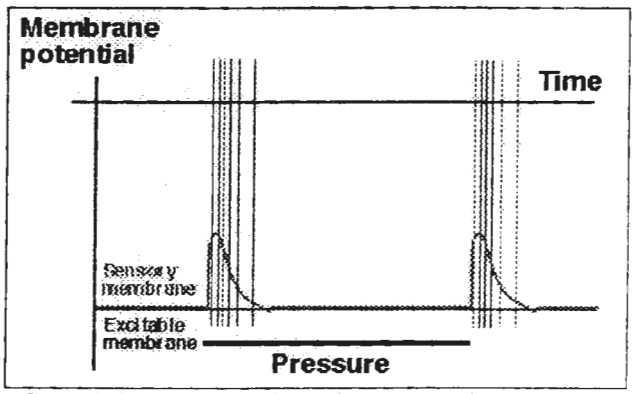

Figure 2. Pacinian corpuscle membrane potential due to a linear pressure stimulation. Observe that the membrane responds at the onset and at the offset of the stimulation.

The ANN

The neural network used in this simulation is a three layer perceptron composed by an input layer with 5 neurons, a hidden layer also with 5 neurons and an one-neuron output layer. The backpropagation learning rule was used in training section. It is a supervised learning network that adjusts its weights in order to produce an output pattern similar to a previous established target (desired output). The backpropagation stops the training when the error reaches a pre-established value [10].

To obtain the target for the training section, eight different ramp slopes were computed by eq. 1, adapting the linear stimuli to the Pacinian corpuscle lamella behavior. The output from eq. 1 was derived and the receptor potentials were obtained (fig. 3). Afterwards, an initial threshold was set, and, when the receptor potential reach this threshold, the neuron (Pacinian corpuscle) fires. After the time that each action potential occurs, a muscle contraction must be evoked (like in FER behavior). The muscle stimuli

intensities increase indirectly proportional to the time when the action potentials occurred. When the noxious stimulation ends, the limb must return slowly to the steady state. The network output was converted to a linear decay by software implementation. The final target pattern had 7 peaks at the time that the 7 strongest stimuli reached the threshold (because the last stimulation did not reach the threshold in time).

The input and the desired output were presented as 2 vectors, for each input pattern there was an output pattern placed at the same position in the X axis. The stimuli data was applied to Hodgkin-Huxley (HH) equations for the membrane external voltage, using the model of Grandori and Pedotti Pacinian Corpuscle [3, 4, 5, 6, 8]. Afterwards, from the membrane external voltage, peaks time were obtained; these peaks determined the time necessary for the network to recognize the input pattern.

The network initialization sets were randomly chosen by special function at the Neural Networks Matlab Toolbox (initff) and we used a maximum number of epochs equal to 10^6 and an error goal equal to 0.1 as training sets. The transfer functions used on the net were hyperbolic tangent sigmoid transfer functions.

Results

To adjust the weights and bias, the number of training epochs requested by the network was very large. The proper features of the backpropagation algorithm request a long time to be computed. The processor system needed much more time to process the sensory data (few seconds) than the biological FER (some milliseconds). However, once the network reached the error goal, the processing time of the data into the network is rather short.

ANN work in a different manner compared to biological networks due to a large amount of variables that exist in a biological neuron and the lack of backward connections in the artificial system. Nevertheless, in our model the neural net adapted to the conditions in which it was submitted and worked similar to the FER.

Discussion

The purpose of this model was to evaluate neural network models of motor systems to be used as processing systems for functional electrical stimulation (FES). One reason to implement the FER in neural

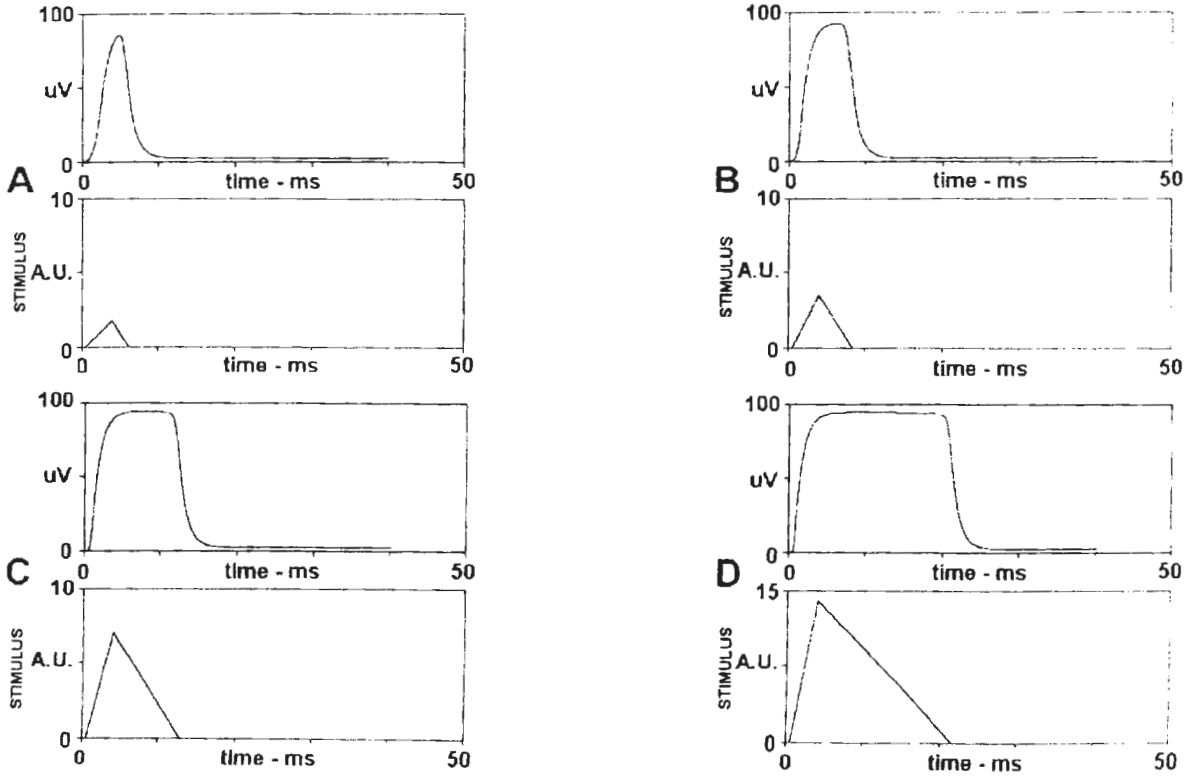

Figure 3. Voltage response of 4 different stimulation ramp slopes samples. We applied a linear stimulation in the corpuscle. Just the rising phase was consider; note the decaying phase to reach the steady state. The stimulus intensity were increased from the case A to D. As fast the rising phase reaches a predetermined threshold value (in the voltage curves) as fast the spike will occur. The delay between two spikes carry the information of the intensity stimulus. So, considering that a spike from a very sensitive corpuscle denominated γ occurs at the beginning of the stimulation, another corpuscle, with a bigger threshold, fired at a time t after the γ corpuscle fired. Then, a short value of delta t, is related with a strong stimulus.

networks is because if we would produce an accurate mathematical model of these reflexes, the final calculation time would make the model unavailable for FES usage.

In spite of the large time used by the network to adapt its bias and weights, trained feedforward networks do not spend long time in processing and, using a small amount of neurons, the delay depends more on the processor system than on the network method. Nevertheless, note that backpropagation architecture is not biologically plausible as it does not allow true forwards time, real time learning.

The output has the task to control a muscle system. Our model consider the muscle force response linear. This consideration can only be used for small length variation, however, a good muscle system should take into account the nonlinear behavior of the stimulated muscle fibers. This is a subject for further studies.

Conclusion

In the majority of total spinal cord traumas the FER is preserved after medullar shock phase and therefore, there is no meaning to implement this system alone in a patient. However, there are some evidences that walking pattern in humans are produced inside the spinal cord by medullar circuits, and the FER circuitry, as well as the stretch reflex circuitry are important pieces of this gait generator [9]. This is well known in inferior animals and, to produce a gait generator similar to the biological one, an available method would be mount one generator by simple medullar circuits interconnected.

References

[1] Bolanowski Jr., S. J., Zwislocki, J. J., 1984, Intensity and frequency characteristics of Pacinian corpuscles. I. Action potentials. *J. Neurophysiol.*, 51(4): 793-811.

[2] Eyzaguierre, C., Fidone, S. J., 1977, *Fisiologia del Sistema Nervioso.* Panamericana, Buenos Aires.

[3] Grandori, F., Pedotti, A., 1980, Theoretical analysis of mechano-to-neural transduction in Pacinian corpuscle. *IEEE Trans. Biomedical Eng.*, BME-27: 559-565.

[4] Grandori, F., Pedotti, A., 1982, A mathematical model of the Pacinian Corpuscle. *Biol. Cybern.*, 46: 7-16.

[5] Hodgkin, A. L., Huxley, A. F., 1952a, The components of membrane conductance in giant axon of Loligo. *J. Physiol.*, 116: 473-496.

[6] Hodgkin, A. L., Huxley, A. F., 1952b, A quantitative description of membrane current and its application to conduction and excitation in nerve. *J. Physiol.*, 117: 500-544.

[7] Massion, J. Fonctions Motrices. *Encycl. Méd. Chir., Neurologie*, 17.002 D10, 11-1994, 28p.

[8] Rattay, F., 1990, *Electrical Nerve Stimulation.* Springer-Verlag Wien, New York.

[9] Sepulveda, F., Cliquet, A., 1995, An artificial neural system for closed loop control of locomotion produced via neuromuscular electrical stimulation. *Artif. Organs*, 19(3): 231-237.

[10] Simpson, P. K., 1990, *Artificial Neural Systems - Foundations, Paradigms, Applications and Implementations.* Pergamon Press.

Computersimulation of stimulating denervated muscle fibers by skin electrodes

M. Reichel, F. Rattay, W. Mayr

Institut für Biomedizinische Technik und Physik, AKH-Wien u. TU-Wien

Abstract

In the last 25 years research in functional electrical stimulation (FES) of denervated skeletal muscle has mainly been dealing with experiments to empirically get the right stimulation parameters (amplitude, pulse width, frequency, impulse shapes, ...) and proper electrode design and configuration.

In the course of the study, two submodels has been developed and combined: 1) finite element modelling of the electrical potential distribution in 2-D human thigh and 2) a Hodgkin & Huxley type model to calculate fiber excitation and action potential propagation.

Persisting denervation leads to a decay of muscle cells and a partially substitution by fibroblasts occur. Therefore the electrically activation of the tissue growth more difficult and biphasic stimulation pulses up to 200ms in duration and 60-100V amplitude are needed to cause a contraction of the denervated muscle. An example shows the field distribution and the stimulated activity and propagation of the action potential in one representative muscle fiber of a well trained M. rectus femoris.

Clinical investigations by Kern (1995) showed that involution of atrophy and consequently reduction of required impulse duration can be achieved. Shorter stimulation impulses enable higher stimulation frequency and hence near normal tetanic muscle contractions.

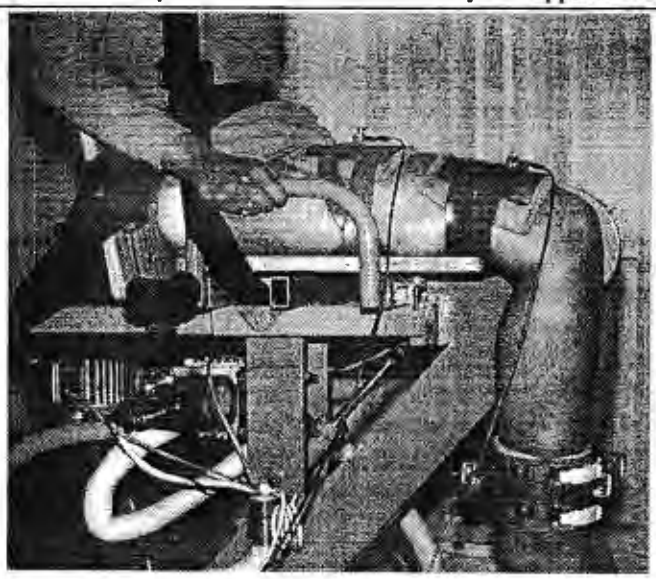

Fig. 1: Force measuring chair for isometric torque (force) measurement during FES of the denervated quadriceps femoris by large skin electrodes.

Introduction

The theory of the electric field is well known, but it is difficult to calculate the field in living tissue, since the conductors involved have different areas of conductivity, furthermore the field depends on direction of muscle fibers and intramuscularly fibroblasts. In order to determine the activation for each muscle fiber (with the help of the activation function), the direction of each muscle fiber has to be known and the electric field along the fiber has to be calculated as a function of the applied electric current and potential at the electrodes, respectively (Rattay 1990).

The excitement of the muscle fiber varies in a wide range, dependent on the active and passive membrane parameters and the intracellular and extracellular medium.

The whole simulation of the combined models is necessary to quantitatively observe all the processes which happen during FES and to optimize the effects caused by the applied voltage. This simulation can substitute the most animal experiments which are nowadays done to investigate FES for denervated muscle, with all known disadvantages like 24 hours special nursing of the animals, long-time experiments (which are necessary to get long-time denervated muscles), the nearly impossibility of FES by skin electrodes, infections caused by implanted electrodes contacted and supplied by transcutanic wires, animal size determination caused by implant technology and at least the large amount of animals to get significant results.

Denervated muscle and FES training

Skeletal muscle fibers are physiologically activated by motoneurons at the postsynaptic membrane of the motorunit. In the case of the denervated muscles no presynaptical action potential reaches the endplate. Stimulation can be achieved by the influence of special electric fields (Rattay, 1987). Therefore, at any point of the fiber an action potential has to be elicited, which will propagate across the muscle fiber in longitudinal and transversal directions (Adrian et al.,

1970). Due to this propagation, the whole fiber can be excited, and contraction occurs (Schmidt & Thews, 1987). The excitation process essentially depends on the electrical membrane and tissue properties and therefore the effective stimulation parameters vary in a wide range depending on the state of atrophy and training (Kern, 1995).

After 3-4 months of intensive training, the stimulation parameters can be changed to about 30ms pulse duration and 10ms break. At that stage, a stimulation frequency of 25Hz causes first tetanic contractions of the trained denervated muscles. From this stage, denervated muscles can be trained with a good adaptation of the intensity (=tetanic tension and muscle performance) to the stimulation. Only tetanic contraction can be the stimulus of hypertrophy.

There are several ways to measure the amount of hypertrophy and the increase of muscle performance, respectively. One way is to compare measurements (*Fig. 1*) from each patient In order to avoid areas with high current densities and to get a homogenous field distribution at the transition from the electrode to the skin, large conduction rubber electrodes covered by electrode gel are used. High current densities can cause temperature increase up to burnings of the skin and should be avoided, considering the bad cure process of denervated patients.

The second way is to determine the cross-section areas of CT-data. *Fig. 2* shows a middle cross-section of quadriceps femoris of a healthy (a) and a long-time denervated (b) patient. The large amount of fat in (b), will be reduced to normal percentage by building up the muscle mass at the same time. Atrophy of denervated muscle is clearly evident and the average of the amount of muscle mass compared to normal is about 40% after 2 years denervation.

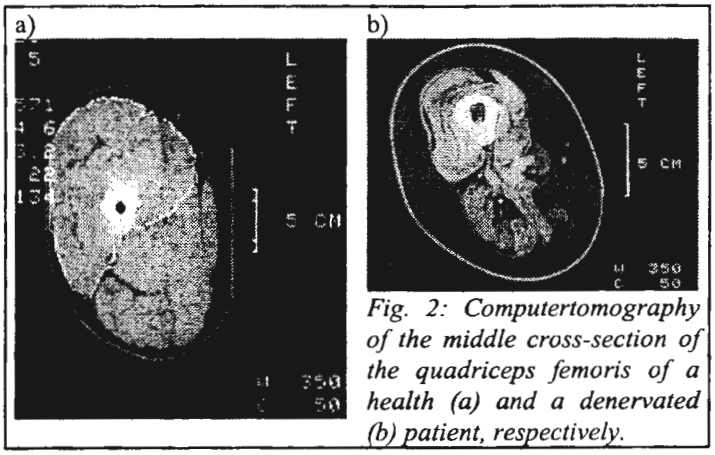

Fig. 2: Computertomography of the middle cross-section of the quadriceps femoris of a health (a) and a denervated (b) patient, respectively.

The electric field

For functional electric stimulation of denervated muscle a specific electric field around each muscle fiber is required, which is applied by a pair of electrodes and an appropriate stimulator. The differences between denervated and enervated muscles are not only the fact that no presynaptically action potential reaches the motorunit, but also that changes over the whole muscle and its surrounding tissue occur. The amount of the atrophy respectively the changes of the electrically and mechanically membrane and tissue properties are most important for the simulation. For the model of the electric field, atrophy essentially means that combined with the decrease of the muscle cross-section an increase of the muscle surrounding fat and intramuscularly fat will occur (Kern, 1995). All these facts make the stimulation more difficult, which means that big electrodes, covering almost the whole muscle, and sufficient currents are required to cause action potentials in nearly all regions of the muscle. To reach muscle fibers in deeper regions, current has to be strong enough but causes tissue damaging maximum current densities, which give a border of the system. A surface stimulator for denervated quadriceps femoris has to generate biphasic pulses of 10-200ms duration and 60-100V amplitude, applied by two large electrodes (200-250cm^2) arranged like shown in *Fig. 1*.

Fig. 3 shows a length-section of the thigh with two large skin electrodes. Furthermore, the equi-potental lines and areas of high current density (long arrows) are demonstrated. This arrangement of the electrodes is shown in *Fig. 1* as well (comp. Kern, 1995).

The stimulation pulses are biphasic rectangles of 30ms duration and ±80mV amplitude (Kern, 1995), therefore the calculation can be made under quasistationary conditions (Hofmann, 1974). This means that a system of linear elliptical differential equations has to be solved, where each different tissue has its own equation with its own parameters.

Fig. 3 was calculated with the help of the Matlab PDE-toolbox. From this solution the

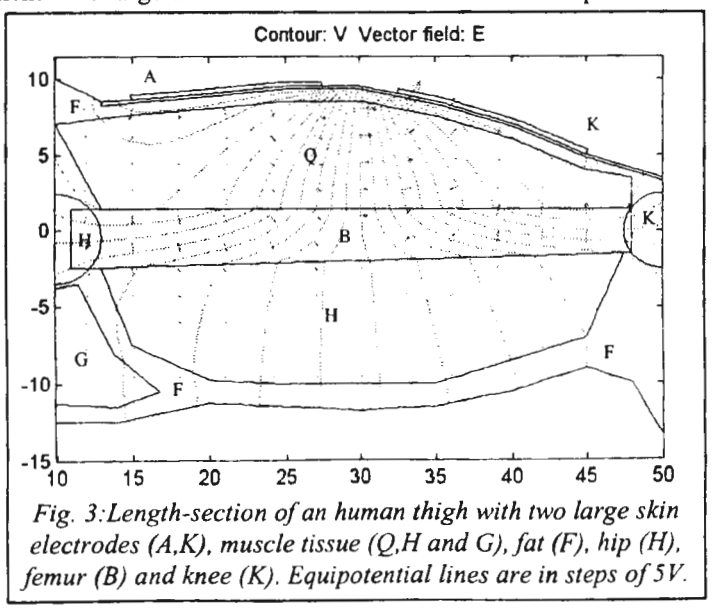

Fig. 3:Length-section of an human thigh with two large skin electrodes (A,K), muscle tissue (Q,H and G), fat (F), hip (H), femur (B) and knee (K). Equipotential lines are in steps of 5V.

electric field in the interesting muscle area can be determined.

The denervated muscle fiber

A muscle fiber is a cell of tubulary shape which essentially consists of the sarcolemma, the transverse tubular system, the myofibrils and the intracellular fluid. The sarcolemma is a membrane containing ionic channels. The ionic currents through the channels can be calculated by the method of Hodgkin & Huxley (1952). The proper parameters of different types of muscle fibers can be derived from in vitro experiments. From the data of 'voltage-clamp' experiments (Pappone, 1980) the Hodgkin & Huxley (HH) parameters can be determinated to calculate opening probabilities and time constants of the ionic channels dependent on membrane voltage V (Adrian et al., 1970). The HH-model considers the Na^+-channels and K^+-channels. The dynamic of ion channels can be described by the differential equation

$$\frac{dy}{dt} = \alpha(1-y) - \beta y \cdot \qquad (1)$$

y stands for the opening probability and the voltage dependent factors α and β describe the opening- and the closing-rate, respectively. For the description of the gating mechanism of the specific Na^+- and K^+-channels three parameters m, n and h corresponding

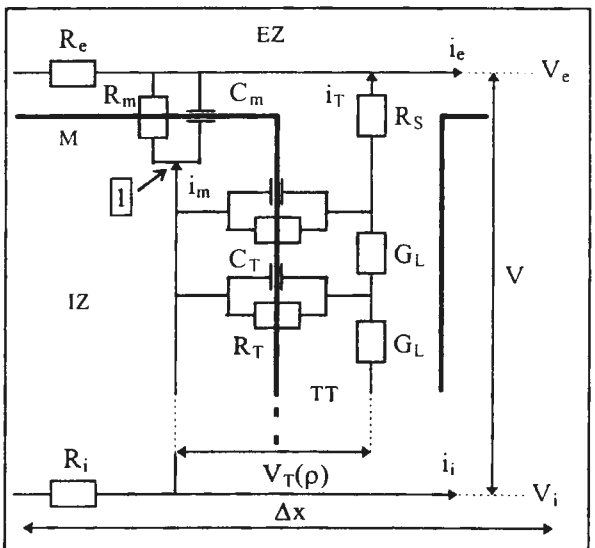

Fig. 4: Network section Δx of the muscle fiber, consisting of the sarcolemma (M), the T-system (TT), the extracellular (EZ) and the intracellular (IZ) space. The electric circuit for the sarcolemma and the T-system consists of the nonlinear HH-resistance R_m, the membrane capacity C_m and the nonlinear HH-resistance R_T, the capacity C_T connected by the lumen conductivity G_L, respectively. i_T denotes the current coming out of the T-system over the access resistance R_S. The extracellular potential is denoted V_e, the intracellular potential V_i and the tubular potential V_T. i_m describes the ionic current overt the sarcolemma. i_e and i_i are the extra- and intracellular current over the resistors R_e and R_i, respectively into the next compartment Δx.

to equation (1) are used. A hyperpolarization potential caused by the denervation gives a shift of the Na^+-channel characteristic m^3h towards hyperpolarization. Of course the opening- and closing-rate is required to calculate the dynamic of each parameter (m, n and h), which are functions of the membrane voltage (Rattay, 1990)

$$V = V_i - V_e - V_{rest} \cdot \qquad (2)$$

V_i is the intracellular potential, V_e the extracellular potential and V_{rest} the resting membrane potential of the muscle cell.

The description of the membrane current i_m is done by the sum of all currents in point 1 of *Fig. 4* and yields to

$$i_m = i_{ion} + i_T + C_m \frac{dV}{dt} \cdot \qquad (3)$$

The ionic current over the membrane resistance R_m consists of the sodium current i_{Na}, the potassium current i_K and the leakage current i_L.. This three nonlinear currents (R_m is extremely nonlinear) are described by Hodgkin & Huxely (1952).

The current flowing out of the transverse tubular system (T-system)

$$i_T = g_s\left(V - V_T(a)\right) \qquad (4)$$

results from the potential difference between the membrane potential V and the outermost (at radius a) tubular potential V_T(a), which causes a current over the access resistance R_S of the T-system. The tubular potential can be determined from the differential equation

$$G_{L,T}\left(\frac{\partial^2 V_T}{\partial \rho^2} + \frac{\partial V_T}{\rho \partial \rho}\right) = c_T \frac{dV_T}{dt} + i_{ion,T}, \qquad (5)$$

where C_T is the capacity of the T-system (*Fig. 4*). The calculation of the ionic currents of the T-system $i_{ion,T}$ over the resistance R_T (*Fig. 4*) is analogue to those of the sarcolemma with corresponding parameters. $G_{L,T}$ denotes the lumen conductivity of the T-system and ρ is the fiber radius.

The propagation of the action potential is determined by

$$\frac{d}{4\rho_i}\frac{\partial^2 V_i}{\partial x^2} = c_m \frac{\partial V}{\partial t} + i_{ion} + i_T \qquad (6)$$

(Adrian et al., 1970). Equation (6) is a nonlinear parabolic partial differential equation, where the right part is described by equation (3). The left part consists of the fiber diameter d, the intracellular conductivity ρ_i and the second derivation of the intracellular potential V_i respectively to the fiber length x.

Equation (6) can not be solved in an analytical way, thus the solution has to be found numerically. For example Adrian et al. (1969,1970) and Adrean & Peachey (1973) used Runge-Kutta and Henneberg & Roberge (1997) and Reichel et al. (1997) Crank-Nicolson, respectively. The Crank-Nicolson method (Moore et al., 1975) is an implicit method, which discretisizes in direction and time. The initial condi-

tions can be determined from the resting potential and the border conditions are derived from the neighbouring tissue (tendon).

Fig. 4 shows a network section of the muscle fiber, which consists of a system of electric circuits for the sarcolemma and the T-system (*Fig. 4*) connected by resistors (R_e, R_i).

The extracellular potential distribution $V_e(x)$ at the surface of the muscle fiber is very important for its stimulation. This potential distribution will be calculated as a function of the tissue depth z with the assumption that the fibers of the M. rectus femoris are parallel with the surface of the quadriceps and the fibers of the M. intermedius are parallel with the femur (*Fig. 3*).

The activating function follows to estimate the stimulating effect of the applied electric field as a function of x; i.e. rearranging equations (2) and (6) results in

$$\frac{d}{4\rho_i}\left(\frac{\partial^2 V}{\partial x^2}+\frac{\partial^2 V_e}{\partial x^2}\right)=\frac{\partial V}{\partial t}+i_{ion}+i_T \qquad (7)$$

and the influence by the extracellular potential $V_e(x)$ becomes

$$f=\frac{d}{4\rho_i}\cdot\frac{\partial^2 V_e}{\partial x^2}. \qquad (8)$$

$V_e(x)$ can be determined from the electrode placement and applied voltage. The activating function can be calculated from $V_e(x)$ and can be inserted in equation (7).

The activating function concept (Rattay, 1987) was used by many workers to calculate the recruitment of nerve fibers, and it is also useful to simulate the electrically stimulated muscle fiber.

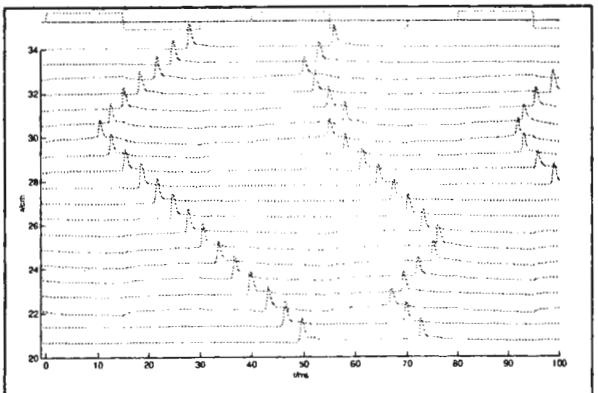

Fig. 5: Stimulated activity and propagation over the horizontal position x(Fig. 3) and time t of the action potential in one representative muscle fiber of a well trained M. rectus femoris by biphasic pulses (30ms, ±80V, 25Hz) applied to skin electrodes (Fig. 1).

Results & Discussion

Fig. 5 shows the propagation of the action potential, along one muscle fiber, elicited by the electric field in the M. rectus femoris. It can be observed that the fiber requires biphasic pulses shorter than 30ms to get elicited. The activating function is negative till about 27cm (horizontal position in *Fig. 3*)and positive afterwards. This causes the first action potential at 30cm and propagates in both directions from there. The second biphasic pulse activates the fiber also in the area of negative activating function, but propagation stops when the action potential crashes the propagation elicited from an other point of the fiber. The third pulse activates the fiber again at 30cm.

Pulse duration depends on state of training by FES after denervation. Three different states of training are considered. The first was a nearly physiological one (*Fig. 3*) and was calculated as 100%, the others were calculated with 80 and 60% of muscle mass and fiber diameter of the first. Simulations at this three different states of training showed that about 30ms (100%) to 160ms (60%) biphasic pulses are required to elicit all fibers in the whole M. quadriceps, respectively.

Since a 3-D model of the thigh has not been simulated, the activation of fibers in M. vastus lateralis and medialis has not been calculated. But stimulation parameter of three denervated patients show that the activating function must be equal to them in the M. rectus femoris to cause contraction simultaneously.

References

Adrian R.H. & Peachey L.D., 1973. Reconstruction of the action potential of frog sartorius muscle, J. Physiol. Lond. 235:103-131

Adrian R.H., Chandler W.K. & Hodgkin A.L., 1969. The kinetics of mechanical activation in frog muscle, J. Physiol. Lond. 204:207-230

Adrian R.H., Chandler W.K. & Hodgkin A.L., 1970. Voltage clamp experiment in striated muscle fibers, J. Physiol. Lond. 288:607-644

Henneberg K.A. & Roberge F.A., 1997. Simulation of propagation along an isolated skeletal muscle fiber in an isotropic volume conductor, Ann. Biomed. Eng. 25: 15-28

Hodgkin A.L. & Huxley A.F., 1952. A quantitative discription of membrane current and ist application to conduction and excitation in nerve, J. Physiol. Lond. 117:500-544

Hofmann H., 1974. Das elektromagnetische Feld (Theorie und grundlegende Anwendungen), Springer-Verlag/Wien

Kern H., 1995. Funktionelle Elektrostimulation paraplegischer Patienten, Österr. Z. Phys. Med. Heft 1, Supplementum

Moore J.W., Ramon F. & Joyner R.W., 1975. Axon voltage-clamp simulations (Cranck-Nicolson), Biophys. J. 15:11-24

Pappone P.A., 1980. Voltage-Clamp experiments in normal and denervated mammalian skeletal muscle fibers, J. Physiol. Lond. 306:377-410

Rattay F., 1987. Modelling and simulation of electrically stimulated nerve and muscle fibers, A. review. Math. Comput. in Simulation 29:357-366

Rattay F., 1990. Electric nerve stimulation (theory, experiments and applications), Springer-Verlag/Wien

Reichel M., Rattay F. & Mayr W., 1997. Modell einer extrazellulär elektrisch angeregten denervierten Skelettmuskelfaser, Österr. Z. Phys. Med. Rehabil. Suppl. 2:135-138

Schmidt R.F. & Thews G., 1987. Physiologie des Menschen, Springer-Verlag/Berlin

Address

Martin Reichel
Ins. f. biomed. Techn. & Physik
AKH-Wien, Ebene 4L
Währinger Gürtel 18-20, 1090 Wien
Tel: +43-1-40400-1972
Fax: +43-1-40400-3988
e-mail: m.reichel@bmtp.akh-wien.ac.at

ARGESIM

ARGE Simulation News (ARGESIM) ist eine gemeinnützige („non-profit") Arbeitsgruppe, die Infrastruktur für die Verwaltung und Durchführung von EUROSIM- und ASIM - Aktivitäten und anderer Aktivitäten im Bereich Modellbildung und Simulation bereitstellt und Publikation zu diesem Thema organisiert bzw. selbst in Form der *ARGESIM Reports* herausgibt.

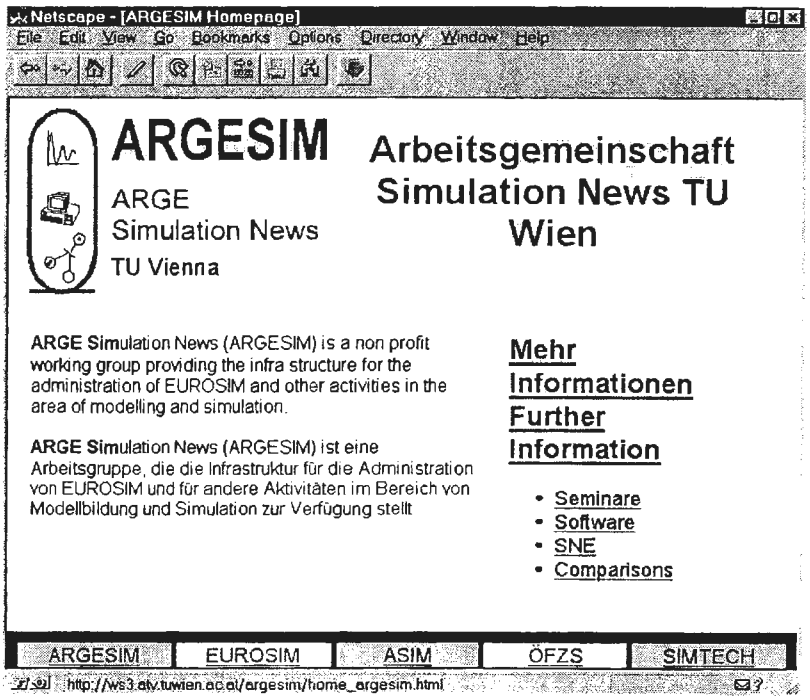

ARGESIM organisiert und stellt Infrastrukur zur Verfügung für:

- Herausgabe, Produktion, Druck, und Versand von *EUROSIM Simulation News Europe* (*SNE*), der Mitgliederzeitschrift von EUROSIM (Federation of European Simulation Societies)
- Mitgliederverwaltung von ASIM (deutschsprachige Simulationsvereinigung), Herausgabe des *ASIM Jahresberichtes* und Unterstützung bei der Herausgabe von *ASIM Mitteilungen* und der *ASIM Nachrichten*
- Herausgabe der *ARGESIM Reports*
- Definition, Durchführung, Verwaltung und Auswertung der EUROSIM Comparisons on Simulation Software and Simulation Techniques"
- Veranstaltung der Seminarreihe „Seminare über Modellbildung und Simulation" an der Technischen Univ. Wien (bisher 45 Seminare)
- Entwicklung von Simulationssoftware, z. B. mosis - kontinuierliche (parallele) Simulation
- Betreuung von MATLAB, ACSL und Computer Algebra Systemen an der Technischen Universität Wien
- Unterstützung der deutschsprachigen ACSL User Group
- Betrieb eines WWW-Servers für EUROSIM, ASIM, SNE, ARGESIM etc.:
  `http://www.argesim.org` (ARGESIM)
  `http://www.asim-gi.org` (ASIM)
  `http://www.eurosim.org` (EUROSIM)
  `http://simtech.tuwien.ac.at` (Abt. Simulationstechnik, Technische Univ. Wien)
- Herausgabe der ARGESIM Reports, und in Verbindung mit ASIM, der deutschsprachigen Simulationsvereinigung, Herausgabe der Reihe Fortschrittsberichte Simulation, die als eigener Reihenteil in den ARGESIM Reports erscheinen.

Information:

ARGESIM
c/o Prof. Dr. F. Breitenecker
Abt. Simulationstechnik, Techn. Universität Wien
Wiedner Hauptstraße 8-10, A-1040 Wien
Fax: +43-1-5056849, Email: info@argesim.org

JOURNAL *SNE - EUROSIM SIMULATION NEWS EUROPE*

EUROSIM Simulation News Europe (*SNE*) ist die Informationszeitschrift der europäischen Simulationsgesellschaften. *SNE* erscheint dreimal jährlich und wird den Mitgliedern der in EUROSIM zusammengeschlossenen Simulationsgesellschaften im Rahmen ihrer Mitgliedschaft zugestellt. Zudem wird SNE im Abonnement vertrieben und fungiert als Informationsträger auf Tagungen, für Firmen, etc.

Nähere Informationen sind am ARGESIM WWW- Server erhältlich: `http://www.argesim.org/sne`

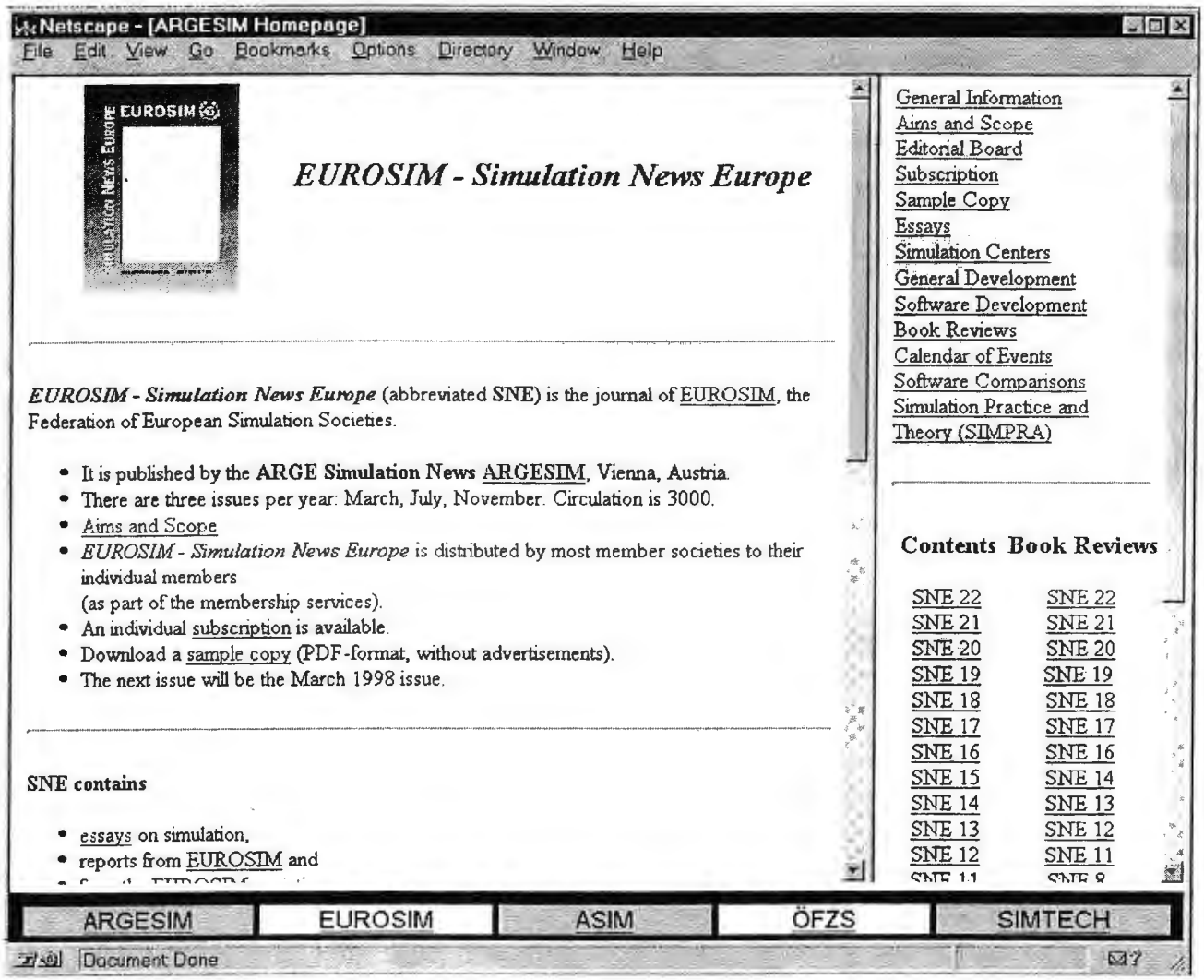

Im Informationsteil über Simulationsvereinigungen berichtet SNE über Neuigkeiten und Veranstaltungen von EUROSIM, der in EUROSIM zusammengefaßten nationalen und regionalen Simulationsvereinigungen und anderer Simulationsgesellschaften; weiters werden einzelne „Simulation Centers" vorgestellt.
Buchbesprechungen, Book News und Industry News runden diese Informationen ab. Den Serviceteil beendet ein umfangreicher Calendar of Events.

Allgemeine Trends, Entwicklungen und auch Grundlagen der Simulationstechnik werden in Essays veröffentlicht, die hohe Qualität haben. 1995 begann SNE mit dem neuen Corner „Development of Software" bzw. „Development in Simulation Technique", der über spezielle Entwicklungen auf diesen Gebieten berichtet und damit die Essays ergänzt.

Großen Erfolg hat SNE mit seiner Serie „Software Comparisons", wo zu 11 repräsentativen Simulationsaufgaben bisher etwa 150 Lösungen einlangten.

Bestellungen von Probeexemplaren bei ARGESIM (siehe vorige Seite)

ARGESIM REPORTS

Die *ARGESIM Reports* bieten ein Publikationsforum für:

- kurze Monographien über neuen Entwicklungen in Modellbildung und Simulation,
- Lehrunterlagen für Kurse,
- Proceedings kleinerer Tagungen,
- Berichte über State-of-the-Art in der Simulationstechnik etc.,.

Kurz nach Gründung dieser Reihe wurde der neue Verlag ARGESIM von ASIM, der deutschsprachigen Simulationsvereinigung, als Verleger für die ASIM - Buchreihe *Fortschrittsberichte Simulation* ausgewählt. Alle Bände erhalten eine ISBN - Nummer im Rahmen der Reihe *ARGESIM Reports*, die Bände der Reihe *Fortschrittsberichte Simulation* wird im A5-Format gedruckt, die *ARGESIM Reports* im Format A4.

Reihenherausgeber *ARGESIM Reports*: Prof. Dr. F. Breitenecker, Technische Univ. Wien

Reihenherausgeber *Fortschrittsberichte Simulation / ARGESIM Reports*: Dr. I. Bausch-Gall, München;
Prof. Dr. F. Breitenecker, TU Wien, Prof. Dr. G. Kampe, FHT Esslingen, Prof. Dr. SD.P.F. Möller, TU Clausthal

Rep. Nr.	*ARGESIM Reports*	ASIM-Mitglieder	Andere
1	Congress EUROSIM'95 - Late Paper Volume; F. Breitenecker, I. Husinsky (Hrsg.), ISBN 3-901608-01-X	DM 30.-	DM 40.-
2	Congress EUROSIM'95 - Session Software Products and Tools; F. Breitenecker, I. Husinsky (Hrsg.), ISBN 3-901608-02-8	DM 30.-	DM 40.-
3	EUROSIM'95 - Poster Book; F. Breitenecker, I. Husinsky (Hrsg.) ISBN-Nr.: 3-901608-03-6	DM 30.-	DM 40.-
4	Seminar Modellbildung und Simulation -Simulation in der Didaktik; F. Breitenecker, I. Husinsky, M. Salzmann (Hrsg.), ISBN 3-901608-04-4	DM 30.-	DM 40.-
5	Seminar Modellbildung und Simulation -COMETT - Course 'Fuzzy Logic'; D. Murray-Smith, D.P.F. Moeller, F. Breitenecker, ISBN 3-901608-05-2	DM 30.-	DM 40.-
6	Seminar Modellbildung und Simulation -COMETT - Course 'Object-Oriented Discrete Simulation; N. Kraus, F. Breitenecker, ISBN 3-901608-06-0	DM 30.-	DM 40.-
7	EUROSIM Comparison 1 - Solutions and Results; F. Breitenecker, I. Husinsky (Hrsg.), ISBN 3-901608-07-9	DM 30.-	DM 40.-
8	EUROSIM Comparison 2 - Solutions and Results; F. Breitenecker, I. Husinski (Hrsg.), ISBN 3-901608-08-7	DM 30.-	DM 40.-
9	Bericht zum Treffen der ASIM -FGs „Simulationssoftware und -Hardware", „Simulation und Künstliche Intelligenz" und „Simulation in Biologie, Medizin und Ökologie", Ebernburg, ISBN 3-901608-09-5	in Vorbereitung	
10	Proceedings TU-BioMed Symposium 1998 „Brain Modelling", F. Rattay (Hrsg.) ISBN 3-901608-10-9	DM 15.-	DM 30.-
11	Proceedings 2nd MATHMOD Conference, I. Troch, F. Breitenecker (Hrsg.) ISBN 3-901608-11-7	DM 90.-	DM 120.-

Rep. Nr.	Bd Nr.	Fortschrittsberichte Simulation / ARGESIM Reports	ASIM-Mitglieder	Andere
51	1	C. Westerkamp: Anwendung der Mehrgrößen-Parameterschätzung zur Simulation von lineraren passiven Netzwerken; 1996; ISBN 3-901 608-51-6	DM 30.-	DM 40.-
52	2	M. Salzmann: Genetische Algorithmen in diskreter Simulation; 1996; ISBN 3-901 608-52-4	DM 30.-	DM 40.-
53	3	J. Plank: State Events in Continuous Modelling and Simulation - Concepts, Implementation and New Methodology; 1997; ISBN 3-901 608-53-2	DM 30.-	DM 40.-
54	4	P. Acel: Methode zur Durchführung betrieblicher Simulationen - Effiziente Optimierung der diskreten Simulation; 1997; ISBN 3-901 608-54-0	DM 30.-	DM 40.-
55	5	M. Kinder: Stochastische Simulation biotechnischer Prozesse - Entwurf von Filtern und Reglern; 1997; ISBN 3-901 608-55-9	DM 30.-	DM 40.-

Vertrieben werden beide Publikationen sowohl von ASIM (Büro Dr. I. Bausch-Gall, München) und der ARGESIM (TU Wien). Bestellungen bei

Dr. Ingrid Bausch-Gall, BAUSCH-GALL GmbH, Wohlfartstraße 21b, D-80939 München,
Fax: +49-89 3231063

oder bei ARGESIM, c/o Prof. Dr. F. Breitenecker, Abt. Simulationstechnik, Techn. Universität Wien,
Wiedner Hauptstraße 8-10, A-1040 Wien, Fax:+43-1-5056849